10. SITE 1016[1]

Shipboard Scientific Party[2]

HOLE 1016A

Date occupied: 13 May 1996

Date departed: 17 May 1996

Time on hole: 3 days, 9 hr, 30 min

Position: 34°32.415′N, 122°16.594′W

Drill pipe measurement from rig floor to seafloor (m): 3845.4

Distance between rig floor and sea level (m): 11.1

Water depth (drill pipe measurement from sea level, m): 3834.3

Total depth (from rig floor, m): 4161.9

Penetration (m): 316.5

Number of cores (including cores having no recovery): 36

Total length of cored section (m): 316.5

Total core recovered (m): 303.7

Core recovery (%): 95

Oldest sediment cored:
Depth (mbsf): 316.5
Nature: Porcellanite and chert
Age: late Miocene

Measured velocity (km/s): 3.826 at Section 35X-1, 6 cm

Comments: Camera survey of the ocean bottom was conducted before spudding.

HOLE 1016B

Date occupied: 17 May 1996

Date departed: 18 May 1996

Time on hole: 1 day, 2 hr, 30 min

Position: 34°32.314′N, 112°16.577′W

Drill pipe measurement from rig floor to seafloor (m): 3847.7

Distance between rig floor and sea level (m): 11.1

Water depth (drill pipe measurement from sea level, m): 3836.6

Total depth (from rig floor, m): 4058.5

Penetration (m): 210.8

Number of cores (including cores having no recovery): 23

Total length of cored section (m): 210.8

Total core recovered (m): 218.1

Core recovery (%): 103.0

Oldest sediment cored:
Depth (mbsf): 210.8
Nature: Diatom clay, nannofossil ooze with diatoms, and diatom ooze
Age: late Miocene

HOLE 1016C

Date occupied: 18 May 1996

Date departed: 18 May 1996

Time on hole: 2 hr, 15 min

Position: 34°32.292′N, 122°16.591′W

Drill pipe measurement from rig floor to seafloor (m): 3846.3

Distance between rig floor and sea level (m): 11.1

Water depth (drill pipe measurement from sea level, m): 3835.2

Total depth (from rig floor, m): 3865.0

Penetration (m): 18.7

Number of cores (including cores having no recovery): 2

Total length of cored section (m): 18.7

Total core recovered (m): 18.8

Core recovery (%): 100.0

Oldest sediment cored:
Depth (mbsf): 18.7
Nature: N/A
Age: Quaternary

Comments: Cores were not split on ship

HOLE 1016D

Date occupied: 18 May 1996

Date departed: 19 May 1996

Time on hole: 19 hr, 30 min

Position: 34°32.306′N, 122°16.585′W

Drill pipe measurement from rig floor to seafloor (m): 3845.5

Distance between rig floor and sea level (m): 11.1

Water depth (drill pipe measurement from sea level, m): 3834.4

Total depth (from rig floor, m): 3996.0

Penetration (m): 150.5

Number of cores (including cores having no recovery): 16

Total length of cored section (m): 150.5

Total core recovered (m): 154.2

Core recovery (%): 102.0

Oldest sediment cored:
Depth (mbsf): 150.5

[1]Lyle, M., Koizumi, I., Richter, C., et al., 1997. *Proc. ODP, Init. Repts.,* 167: College Station, TX (Ocean Drilling Program).
[2]Shipboard Scientific Party is given in the list preceding the Table of Contents.

Nature: Nannofossil ooze with diatoms and foraminifers
Age: late Pliocene

Principal results: Site 1016 is located about 150 km west of Point Conception and forms the deep-water drill site (water depth 3834 mbsl) on the Conception Transect (35°N). The site was chosen to provide material to investigate the longer term Neogene record as well as to assess paleoceanographic conditions near the core of the California Current. Site 1016 occupies an important transitional zone for modern flora and fauna and provides a good opportunity to develop a chronology for the biostratigraphy. Geochemical indices of paleoproductivity and microfossil assemblages obtained from this site will provide important data on nutrients carried by the California Current. Organic carbon deposition should be relatively high compared to typical pelagic sedimentary sections in relatively deep water. This environment provides one of the end-members needed to study preservation of bulk organic matter and of specific organic molecules.

Four holes were cored with the APC/XCB at Site 1016 to a maximum depth of 316.5 mbsf, recovering an apparently continuous interval of Quaternary to upper Miocene sediments (Fig. 1). Hole 1016A was cored with the APC to 93.1 mbsf and extended with the XCB to 315.5 mbsf. Slow drilling and poor recovery were encountered in massive chert and porcellanite layers starting at 298 mbsf. One core was taken with the Motor Driven Core Barrel down to 316.5 mbsf. The hole was logged with the density-porosity combination tool (density, neutron porosity, resistivity, and natural gamma ray), the GHMT magnetic tool, and the sonic-Formation MicroScanner. Hole 1016B was cored with the APC to 210.8 mbsf. Two APC cores were taken at Hole 1016C down to 18.7 mbsf and Hole 1016D was cored with the APC to 150.5 mbsf. Detailed comparisons between the magnetic susceptibility and GRAPE density records generated on the MST, and high-resolution color reflectance measured with the Oregon State University system, demonstrated complete recovery of the sedimentary sequence down to 245 meters composite depth (mcd), with the exception of a core gap at 172.6 mcd, which could not be covered by overlap.

Sediments are dominated by decimeter- to meter-scale alternations of carbonate, diatomaceous, and siliciclastic layers. Several fine-grained sand layers and volcanic ash bands, each up to several centimeters thick, occur in the upper two-thirds of the sequence. The sedimentary section begins with approximately 70 m of clay and diatom oozes of Quaternary to late Pliocene age (Fig. 1). It continues downward with a 92-m late Pliocene to early Pliocene sequence of interbedded nannofossil and diatom ooze. The underlying lower Pliocene to upper Miocene unit (150 m thick) is dominated by diatomite and diatom clay and contains several volcanic ash layers and blebs of solid bitumen. The base of this unit consists of poorly recovered porcellanite and chert resulting from diagenesis of the diatomaceous sediments. The base of this unit is late Miocene age (<7 Ma). Sedimentation rates are high, averaging 50 m/m.y. from the Quaternary to the upper Pliocene, and are drastically lower during the early to middle Pliocene (10–15 m/m.y.), and average 30 m/m.y. in the late Miocene.

A well-constrained biostratigraphy and chronology are provided by a combination of calcareous nannofossil, planktonic foraminifer, diatom, and radiolarian datums for the upper Pliocene and Quaternary. The upper Miocene to lower Pliocene (below 154 mbsf) is dated by calcareous nannofossils, diatoms, and radiolarians. Diatom and radiolarian assemblages suggest two major episodes of strong upwelling during the late Miocene and the late Pliocene through early Quaternary. These two episodes are separated by an interval marked by decreased vertical advection of deep waters during the Pliocene, resulting in a relatively low sedimentation rate. Cooling at thermocline depths is suggested after 3.0 Ma by Arctic radiolarian assemblages. This was followed at 2.5 Ma by major surface-water cooling. Lower bathyal benthic foraminifer assemblages appear to change little throughout the late Pliocene and Quaternary, including between glacial and interglacial episodes.

Magnetic intensities were below the noise level of the magnetometer and precluded the establishment of a magnetic polarity stratigraphy aboard ship.

Calcium carbonate values vary from 1 to 62 wt%. Organic carbon concentrations are high (average 0.93 wt%) compared to normal open ocean environments. According to total organic carbon/total nitrogen ratios, the organic material is mainly of marine origin. Chemical gradients in the interstitial waters reflect organic matter diagenesis, the dissolution of biogenic opal and calcium carbonate, the diffusive influence of reactions in the underlying basalt, and the influence of authigenic mineral precipitation.

Highs in *P*-wave velocity and GRAPE density correspond well with reflections on the 3.5 kHz PDR site survey record. The impedance contrasts, which generate the reflections, correspond to sandy turbidite layers in the upper 70 mbsf of the section. The average thermal conductivity of 0.838 W/(m·K) and the thermal gradient of 105°C/km yield a heat-flow estimate of 88 mW/m^2.

The log physical properties data closely matched the measured core density, porosity, and magnetic susceptibility over the core-log data overlap. Initial core-log comparisons suggest that decimeter-scale variations in lithology are reliably recorded by the logging tools. This provides the opportunity to assess the degree of rebound and deformation of the core material and will be especially useful for putting together continuous records even where material is missing at core gaps.

BACKGROUND AND OBJECTIVES

General Description

Site 1016 is located about 150 km west of Point Conception and forms the deep water drill site on the Conception Transect (Fig. 2). The site is located on an abyssal hill that trends northeast and rises 50–100 m above the surrounding seafloor. It is also located about 70 km west of the toe of the continental slope in water 3835 m deep. On a regional scale, the site is surrounded by major submarine fans, although the abyssal hill is covered with hemipelagic sediments. Just to the north, lobes of the Monterey Fan fill low-lying topography, while to the south the Arguello Fan extends from Arguello Canyon, near Point Conception. Basement is 22.5 Ma oceanic basalt, based on magnetic anomalies (Anomaly 6B; Atwater and Severinghaus, 1989). The site was surveyed in detail with the *Maurice Ewing* on cruise EW9504 in 1995 (Lyle et al., 1995a, 1995b; Fig. 3). The survey was designed to locate a good drilling target within hemipelagic sediments outside of an abandoned chemical munitions dumping area at the toe of the continental slope. The site was located about 10 km west of the dump boundary.

The sediment column from the seismic reflection profile (Fig. 3) can be divided into upper and lower sedimentary sections. The upper part of the sediment column has few reflectors and is vaguely layered. The lower section, in contrast, is marked by strong acoustic reflectors that obscure basement in some parts of the survey area. These strong reflectors may mark cherts. The depth to the transition is 350 ms TWT, or about 275–280 mbsf. Basement can be distinguished by a strong but scattered return 520 ms TWT below the seafloor, or about 420–440 mbsf. Site 1016 was chosen for drilling because the lower sediment section had somewhat lower amplitude reflectors than elsewhere in the survey area (i.e., the site probably has fewer cherts than average) and because basement was well imaged.

Site Objective

Site 1016 is situated in deep water and has a relatively slow pelagic sedimentation rate (average of about 19 m/m.y. for the total sediment column) compared to other Leg 167 drill sites. It was drilled to study the longer term Neogene record as well as to assess paleoceanographic conditions near the core of the California Current. We also hoped to develop a correlation between Neogene biostratigraphic data from the northeastern Pacific and the paleomagnetic chronostratigraphy. Because subtropic and subarctic flora and fauna mix along the coast of California, the detailed biostratigraphy fits imper-

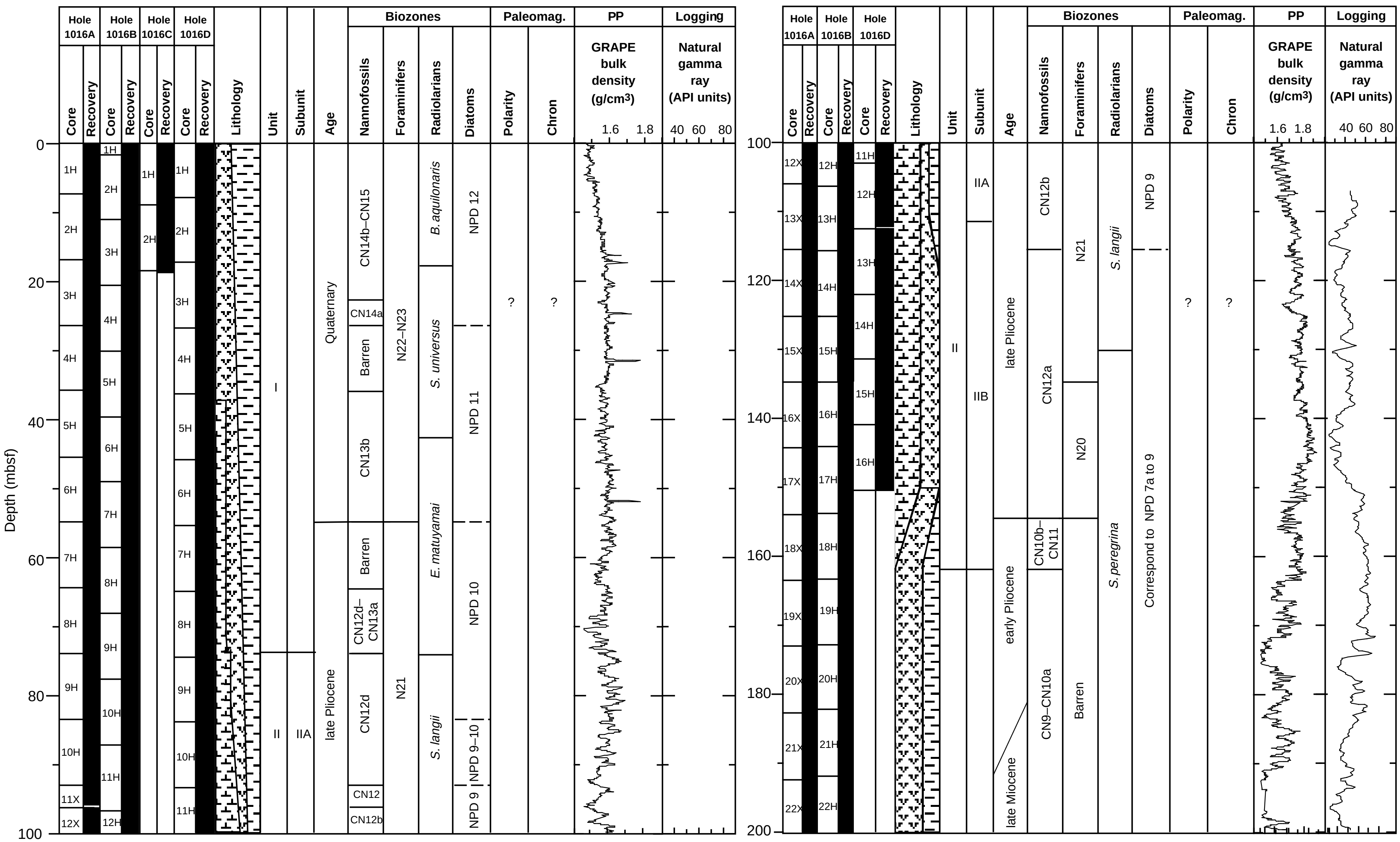

Figure 1. Site 1016 master column.

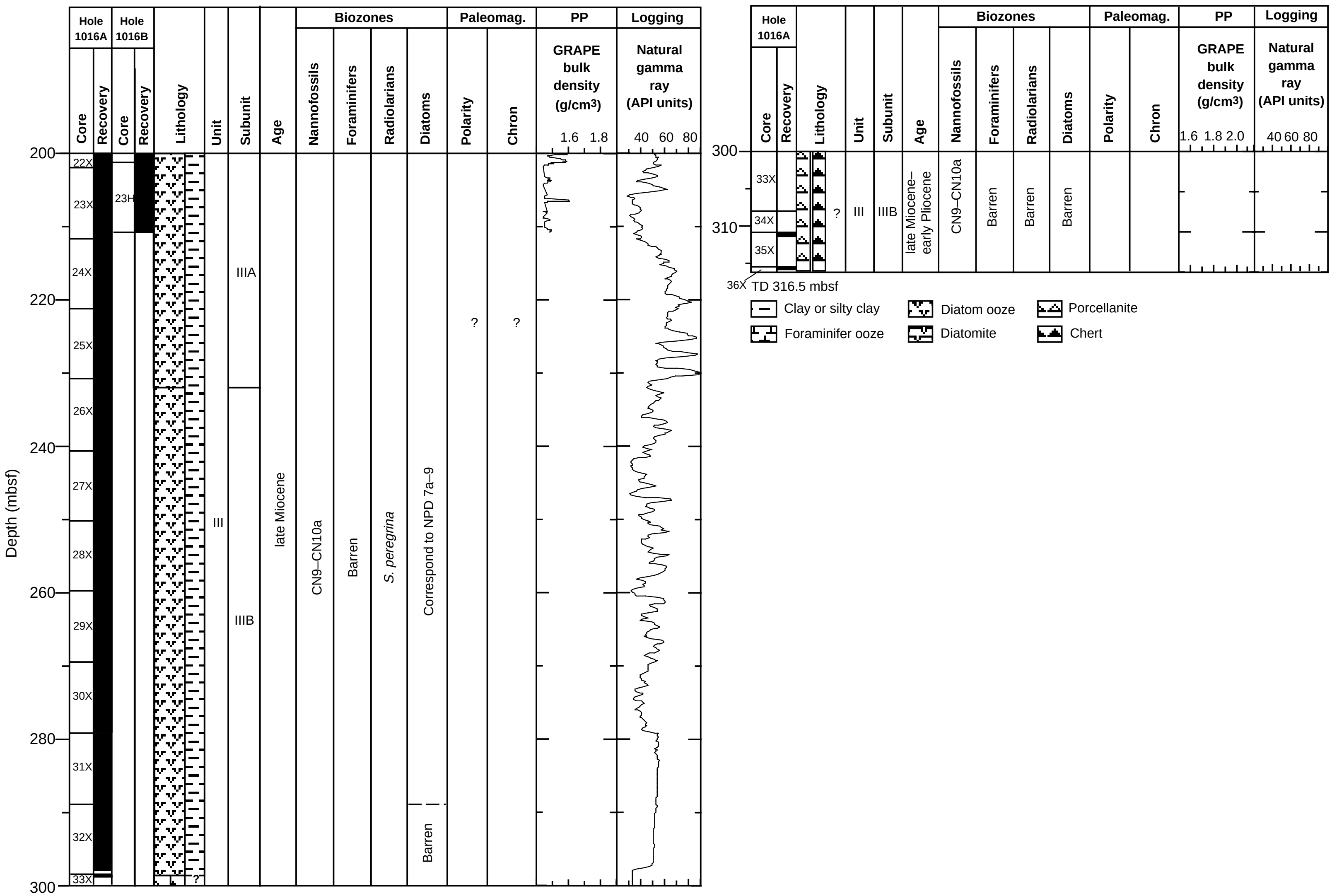

Figure 1 (continued).

fectly with schema developed for either the tropics or the subarctic North Pacific. Site 1016 occupies an important transitional zone for modern flora and fauna and provides a good opportunity to develop a biostratigraphic chronology.

Site 1016 will also assess the paleoceanographic conditions within the central region of the California Current. In the modern oceans, an important transition between subtropical and subarctic fauna occurs just south of the drill site (Roessler and Chelton, 1987). Site 1016 should therefore be sensitive to changes in California Current strength. Because all the deep-water drill sites on Leg 167 penetrate a large proportion of the Neogene, they will monitor the long-term evolution of the California Current system. Older studies from rotary-cored DSDP drill sites and land sections indicate that significant shifts in the strength, or at least the temperature, of the California Current have occurred in the past (Ingle, 1973), and Leg 167 drilling will improve our ability to resolve these events. Geochemical indices of paleoproductivity and microfossil assemblages obtained from Site 1016 will also provide important data on nutrients carried by the California Current.

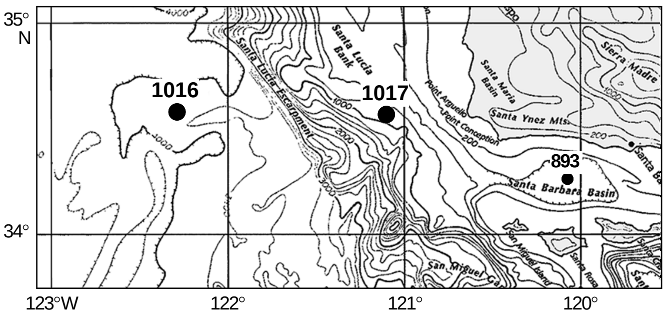

Figure 2. Location map for Site 1016. The drill site is located on 22.5 Ma oceanic crust about 70 km from the toe of the continental slope and about 150 km west of Point Arguello.

Site 1016 has important geochemical objectives. Organic carbon deposition is relatively high compared to typical pelagic sedimentary sections, yet the sedimentation rate is relatively low and the site is in deep water. This environment provides one of the end-members needed to study preservation of bulk organic matter and of specific organic molecules.

OPERATIONS

Transit from Site 1015 to Site 1016

The 190.0-nmi transit from Site 1015 to Site 1016 was accomplished in 16.75 hr at an average speed of 11.3 kt. A rendezvous with a small vessel from University of California at Santa Barbara (UCSB) took place at 1045 hr on 13 May in the Santa Barbara channel. Five boxes of samples were off-loaded to the rendezvous boat for transport to UCSB. The *JOIDES Resolution* continued on and arrived at Site 1016 at 2230 hr on 13 May.

Hole 1016A

Site 1016 is located approximately 7 nmi outside of a former chemical munitions dumping area. A subsea camera survey of the seafloor was conducted for safety reasons within a 50-m perimeter of the positioning beacon. The results of the camera survey were nega-

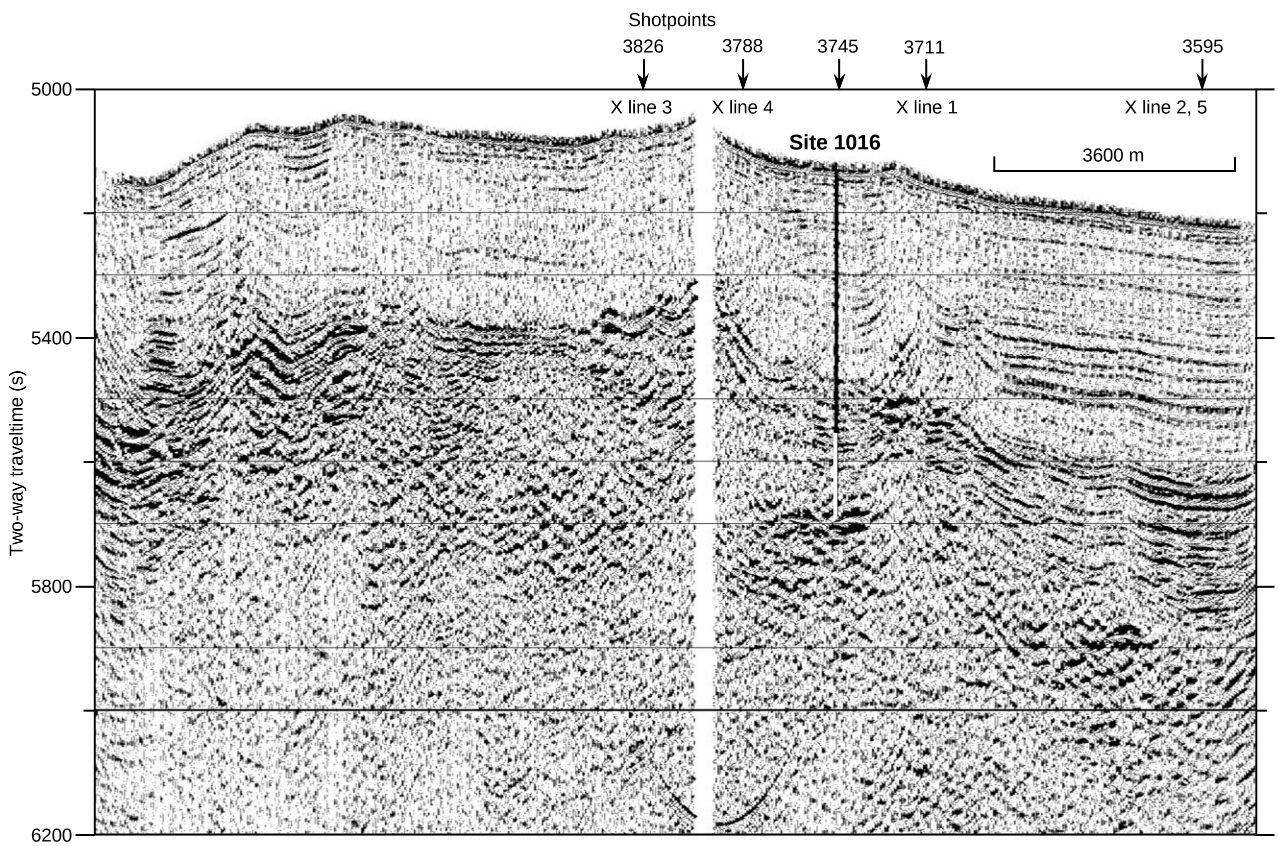

Figure 3. Seismic reflection profile through Site 1016 (Line EW9504 CA11-7; Lyle et al., 1995a, 1995b). The summed 4-channel data were filtered between 30 and 200 Hz, with predictive deconvolution and Stolt F-K migration applied. On y-axis, (s) = milliseconds.

Table 1. Coring summary for Site 1016.

Core	Date (May 1996)	Time	Top (mbsf)	Bottom (mbsf)	Length cored (m)	Length recovered (m)	Recovery
167-1016A-							
1H	14	2320	0.0	7.6	7.6	7.56	99.5
2H	15	0015	7.6	17.1	9.5	9.93	104.0
3H	15	0100	17.1	26.6	9.5	9.93	104.0
4H	15	0200	26.6	36.1	9.5	10.08	106.1
5H	15	0245	36.1	45.6	9.5	9.69	102.0
6H	15	0355	45.6	55.1	9.5	9.92	104.0
7H	15	0430	55.1	64.6	9.5	9.70	102.0
8H	15	0530	64.6	74.1	9.5	10.13	106.6
9H	15	0610	74.1	83.6	9.5	10.10	106.3
10H	15	0700	83.6	93.1	9.5	10.08	106.1
11X	15	1000	93.1	96.3	3.2	2.82	88.1
12X	15	1050	96.3	106.0	9.7	9.13	94.1
13X	15	1145	106.0	115.6	9.6	9.68	101.0
14X	15	1235	115.6	125.2	9.6	9.75	101.0
15X	15	1330	125.2	134.8	9.6	9.57	99.7
16X	15	1420	134.8	144.4	9.6	9.72	101.0
17X	15	1510	144.4	154.0	9.6	9.64	100.0
18X	15	1610	154.0	163.6	9.6	9.69	101.0
19X	15	1700	163.6	173.2	9.6	9.65	100.0
20X	15	1750	173.2	182.8	9.6	9.73	101.0
21X	15	1935	182.8	192.5	9.7	9.69	99.9
22X	15	2030	192.5	202.1	9.6	9.68	101.0
23X	15	2120	202.1	211.7	9.6	9.75	101.0
24X	15	2205	211.7	221.3	9.6	9.72	101.0
25X	15	2300	221.3	230.9	9.6	9.82	102.0
26X	15	2345	230.9	240.6	9.7	9.77	101.0
27X	16	0030	240.6	250.2	9.6	9.85	102.0
28X	16	0125	250.2	259.8	9.6	9.83	102.0
29X	16	0210	259.8	269.5	9.7	9.82	101.0
30X	16	0300	269.5	279.2	9.7	9.43	97.2
31X	16	0355	279.2	288.8	9.6	9.71	101.0
32X	16	0515	288.8	298.4	9.6	8.94	93.1
33X	16	0650	298.4	308.0	9.6	0.30	3.1
34X	16	0900	308.0	311.0	3.0	0.00	0.0
35X	16	1230	311.0	315.5	4.5	0.40	8.9
36N	16	1515	315.5	316.5	1.0	0.44	44.0
167-1016B-							
1H	17	1735	0.0	1.8	1.8	1.82	101.0
2H	17	1830	1.8	11.3	9.5	9.98	105.0
3H	17	2050	11.3	20.8	9.5	9.74	102.0
4H	17	2140	20.8	30.3	9.5	9.86	104.0
5H	17	2230	30.3	39.8	9.5	9.85	103.0
6H	17	2310	39.8	49.3	9.5	9.59	101.0
7H	18	0000	49.3	58.8	9.5	9.85	103.0
8H	18	0130	58.8	68.3	9.5	9.86	104.0
9H	18	0215	68.3	77.8	9.5	9.28	97.7
10H	18	0310	77.8	87.3	9.5	9.85	103.0
11H	18	0400	87.3	96.8	9.5	10.00	105.2
12H	18	0510	96.8	106.3	9.5	9.87	104.0
13H	18	0600	106.3	115.8	9.5	9.82	103.0
14H	18	0650	115.8	125.3	9.5	9.94	104.0
15H	18	0740	125.3	134.8	9.5	9.35	98.4
16H	18	0830	134.8	144.3	9.5	10.08	106.1
17H	18	1000	144.3	153.8	9.5	9.86	104.0
18H	18	1050	153.8	163.3	9.5	9.88	104.0
19H	18	1140	163.3	172.8	9.5	9.84	103.0
20H	18	1235	172.8	182.3	9.5	9.93	104.0
21H	18	1330	182.3	191.8	9.5	9.96	105.0
22H	18	1420	191.8	201.3	9.5	9.98	105.0
23H	18	1545	201.3	210.8	9.5	9.91	104.0
167-1016C-							
1H	18	1900	0.0	9.2	9.2	9.16	99.5
2H	18	1945	9.2	18.7	9.5	9.60	101.0
167-1016D-							
1H	18	2035	0.0	8.0	8.0	7.98	99.7
2H	18	2115	8.0	17.5	9.5	9.89	104.0
3H	18	2200	17.5	27.0	9.5	8.90	93.7
4H	18	2245	27.0	36.5	9.5	9.98	105.0
5H	18	2330	36.5	46.0	9.5	9.36	98.5
6H	19	0010	46.0	55.5	9.5	9.81	103.0
7H	19	0100	55.5	65.0	9.5	10.00	105.2
8H	19	0145	65.0	74.5	9.5	9.77	103.0
9H	19	0230	74.5	84.0	9.5	9.66	101.0
10H	19	0320	84.0	93.5	9.5	9.98	105.0
11H	19	0405	93.5	103.0	9.5	9.70	102.0
12H	19	0440	103.0	112.5	9.5	9.28	97.7
13H	19	0530	112.5	122.0	9.5	10.00	105.2
14H	19	0620	122.0	131.5	9.5	9.74	102.0
15H	19	0710	131.5	141.0	9.5	10.14	106.7
16H	19	0800	141.0	150.5	9.5	9.97	105.0

Note: Table 2, on the CD-ROM in the back pocket, this volume, is a more detailed coring summary.

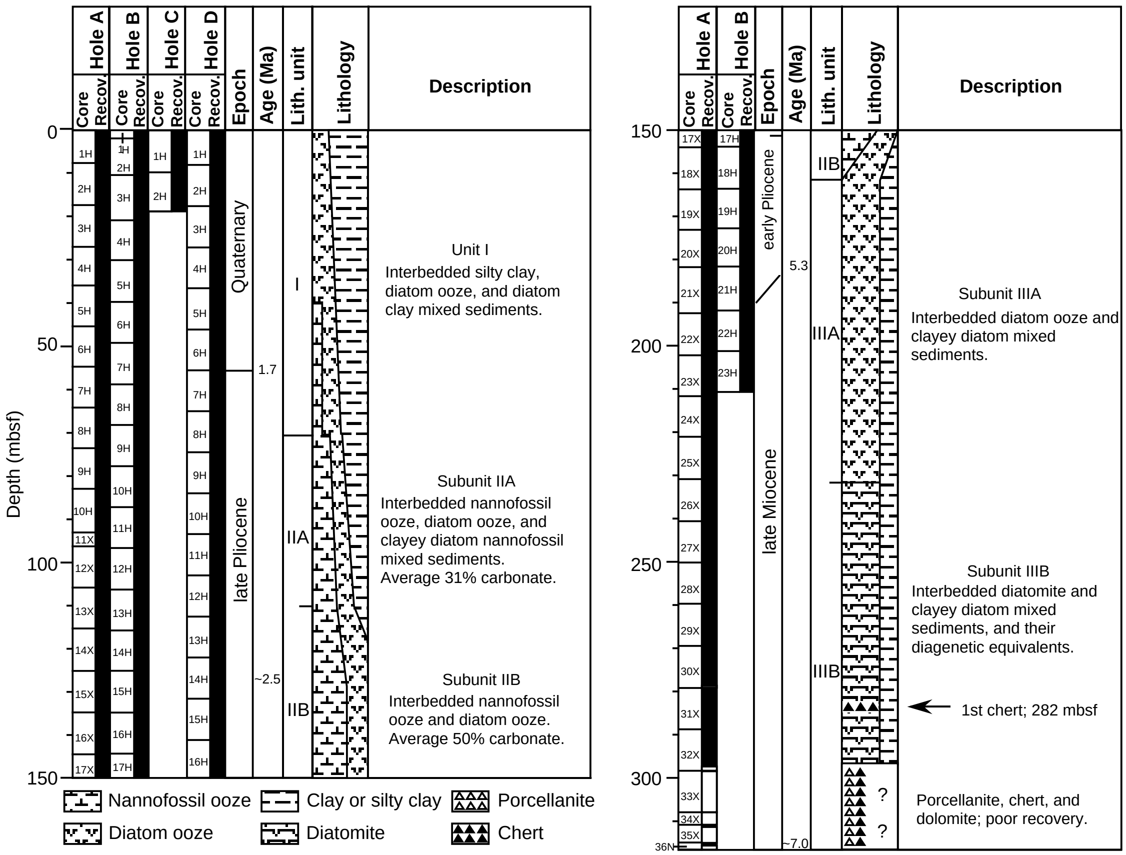

Figure 4. Site 1016 lithostratigraphic summary (0 to 316.5 mbsf).

tive and Hole 1016A was spudded at 1600 hr on 14 May. APC Cores 167-1016A-1H through 10H were taken from 0 to 93.1 mbsf with 104.3% recovery (Table 1; see Table 2 on CD-ROM in the back pocket of this volume for a more detailed coring summary). Cores 1H and 2H were run through the multisensor track and then split open to search for artifacts. The search results were negative and APC coring proceeded. Adara temperature measurements were taken on Cores 4H, 6H, and 8H (see “Physical Properties” section, this chapter). XCB Cores 167-1016A-11X through 35X were taken down to 315.5 mbsf with 92.5% recovery. Slow drilling was encountered in a massive chert and porcellanite layer starting at approximately 298 mbsf. One MDCB core, Core 167-1016A-36N, was taken down to 316.5 mbsf with 1 m of advancement and 0.44 m of chert recovered. Because of the slow progress from 298 to 316 mbsf with only fragments of chert recovered, the decision was made to stop coring at 316 mbsf and log the hole before reaching the planned depth of 440 mbsf. Hole 1016A was logged with the sonic-Formation MicroScanner, and the GHMT toolstrings from 313 to 60 mbsf with good results.

HOLE 1016B

The vessel was offset 10 m to the west and Hole 1016B was spudded at 0800 hr on 17 May. APC Cores 167-1016B-1H through 23H were taken from 0 to 210.8 mbsf with 103.5% recovery (Table 1). Oriented cores were obtained starting with Core 167-1016B-3H.

HOLE 1016C

The vessel was offset 10 m to the west and Hole 1016C was spudded at 1140 hr on 18 May. APC Cores 167-1016C-1H and 2H were taken down to 18.7 mbsf with 100.3% recovery (Table 1).

Hole 1016D

Hole 1016D was spudded at 1315 hr on 18 May. APC Cores 167-1016D-1H through 16H were taken down to 150.5 mbsf with 102.8% recovery (Table 1). The drill string was tripped back to the surface and secured for the 5-hr transit to Site 1017 by 0815 hr on 19 May.

LITHOSTRATIGRAPHY

Introduction

A nearly continuous 316.5-m-thick Quaternary to upper Miocene (0 to ~7 Ma) sequence of sediments was recovered at Site 1016. Three lithostratigraphic units are identified based on visual core description and sediment composition from smear-slide analysis. Unit I and Unit III are each dominated by diatomaceous and siliciclastic components interbedded on a decimeter to meter scale, although containing different proportions of the two. They are separated by Unit II, which is dominated by calcareous nannofossils and is divided into two subunits at a level where carbonate content increases. Unit III is also divided into two subunits based on the diagenetic transformation from diatom ooze to diatomite, and by the occurrence of porcellanite and chert near the base of the sequence (Fig. 4). Fine-grained siliciclastic sand layers occur intermittently through Unit I, and several volcanic ash bands, up to several centimeters thick, occur in Unit II and Unit III.

Description of Units

Unit I

Hole 1016A, intervals 167-1016A-1H-1 through 8H; 0–74.1 mbsf;

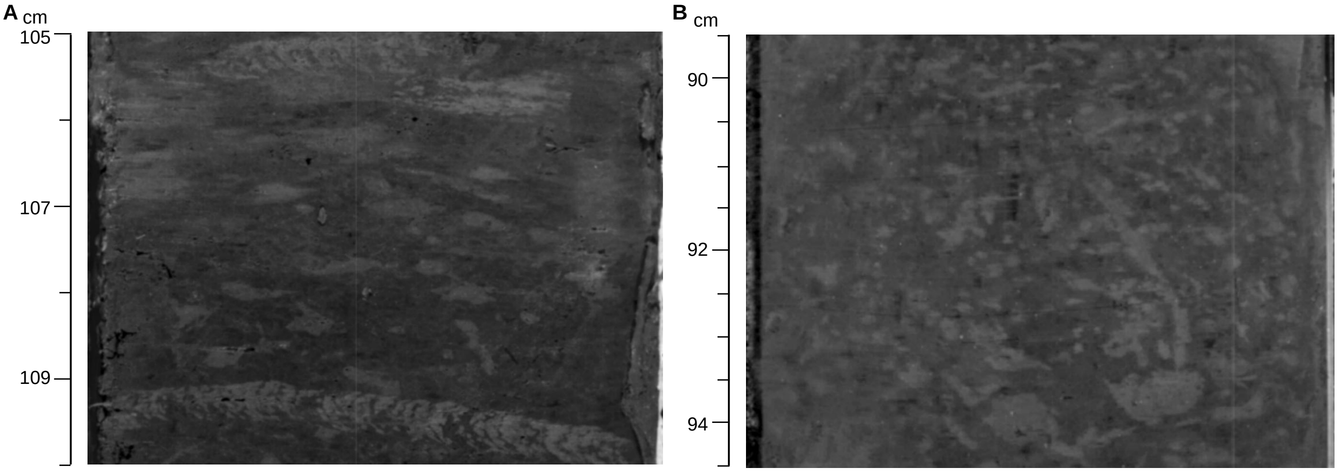

Figure 5. Styles of bioturbation at Site 1016. **A.** Cross-cutting *Zoophycos* in Subunit IIB (Sample 167-1016A-17X-4, 105–110). **B.** *Chondrites* in Unit III (Sample 167-1016B-19H-5, 89.5–94.5 cm).

Hole 1016B, intervals 167-1016B-1H-1 through 8H; 0–68.3 mbsf;
Hole 1016C, intervals 167-1016C-1H-1 through 2H; 0–18.7 mbsf (base of hole);
Hole 1016D, intervals 167-1016D-1H-1 through 8H; 0–74.5 mbsf.
Age: Quaternary to late Pliocene, 0 to 2.1 Ma.

Unit I consists of gradationally interbedded dark gray to dark greenish gray (5Y 5/1 to 5GY 4/1) diatom ooze with clay, grayish olive (10Y 4/1) diatom clay and clayey diatom ooze, and light greenish yellow to light olive gray (10Y 4/2 to 10Y 5/2) diatom nannofossil ooze with clay. Interbedding is on a decimeter to meter scale. From smear-slide analysis, siliciclastic components (clay, quartz and feldspar) compose an average of 43% (5%–95%) of Unit I, and carbonate grains compose 8%. Nannofossils and foraminifers are minor components.

Six centimeter-scale, normally graded, dark gray (N3) sand beds have sharp basal contacts upon scoured surfaces. The sand is fine to very fine grained and contains quartz and feldspar and up to 5% amphibole. Bioturbation occasionally results in redistribution of sand up to 50 cm below sand beds.

Overall, Unit I is highly bioturbated and includes abundant *Zoophycos*, *Chondrites* and less common *Skolithos* and *Planolites* trace fossils.

Unit II

Hole 1016A, intervals 167-1016A-9H through 18X-CC; 74.1–163.6 mbsf;
Hole 1016B, intervals 167-1016B-9H through 18H-CC; 68.3–163.3 mbsf;
Hole 1016D, intervals 167-1016D-9H through 16H-CC; 74.5–150.5 mbsf (base of hole).
Age: late to early Pliocene, 2.1 to 5.0 Ma.

Unit II predominantly consists of nannofossil ooze gradationally interbedded with diatomaceous sediments on a decimeter-to-meter scale. From smear-slide analysis, clay forms an average of 15% of the sediment (0%–78%), and quartz and feldspar occur in minor amounts. Unit II is divided into two subunits based on smear-slide estimates of carbonate content. The contact between these subunits is gradational.

Subunit IIA

Hole 1016A, intervals 167-1016A-9H through 13X-4; 74.1–112.0 mbsf;
Hole 1016B, intervals 167-1016B-9H through 13H-4, 120 cm; 68.3–112 mbsf;
Hole 1016D, intervals 167-1016D-9H through 12H-CC; 74.5–112.5 mbsf.
Age: late Pliocene, 2.1 to 2.8 Ma.

Subunit IIA consists of interbedded olive gray to light greenish gray (10Y 5/2 to 10Y 7/1) diatom nannofossil ooze, olive to olive gray (5Y 5/3 to 5Y 4/2) foraminifer or clayey diatom ooze with nannofossils and grayish olive to dark gray (10Y 4/1 to 5Y 3/1) diatom clay. Color and compositional changes between these lithologies are gradational. From smear-slide analysis, Subunit IIA has an average of 31% (0%–84%) biogenic carbonate (also see "Organic Geochemistry" section, this chapter). Clay contents decrease downward.

Subunit IIB

Hole 1016A, intervals 167-1016A-13X-5 through 18X; 112.0–163.6 mbsf;
Hole 1016B, intervals 167-1016B-13H-4, 120 cm through 18H-CC; 112.0–163.3 mbsf;
Hole 1016D, intervals 167-1016D-13H through 16H-CC; 112.5–150.5 mbsf (base of core).
Age: late to early Pliocene; 2.8 to 5.0 Ma.

Subunit IIB consists of gradationally interbedded olive gray to light greenish gray (5Y 6/2 to 10Y 7/1) nannofossil ooze with diatoms or foraminifers, light gray to greenish gray (5Y 7/2 to10Y 6/1) nannofossil ooze, and gray to greenish gray (5Y 5/1 to 5GY 5/1) nannofossil diatom ooze. The contact with Subunit IIA is gradational. Carbonate content averages ~50% from smear-slide estimates. Four discrete, centimeter-scale, normally graded, light gray (N6) vitric ash layers occur at 133, 134, 135, and 139 mbsf (Fig. 5).

Unit III

Hole 1016A, intervals 167-1016A-19X-1 through 36X; 163.6–316.5 mbsf (base of hole);
Hole 1016B, intervals 167-1016B-19H-1 through 23H; 163.3–210.8 mbsf (base of hole).
Age: early Pliocene to late Miocene; 5.0–~7.0 Ma.

Unit III consists of gradationally interbedded diatom ooze, nannofossil ooze, and diatom clay, resembling those of Unit I, except that the siliceous microfossil content is higher, whereas carbonate and siliciclastic components are reduced. The contact of Unit II with Unit III is gradational and characterized by a downward decrease in biogenic component. Unit III is heavily bioturbated, and some burrows show well-developed reduction haloes. The appearance of porcellanite and chert at the base of Unit III marks the onset of silica diagenesis.

Subunit IIIA

Hole 1016A, intervals 167-1016A-19X-1 through 25X; 163.6–230.9 mbsf;
Hole 1016B, intervals 167-1016B-19H-1 through 23H; 163.3–210.8 mbsf (base of hole).
Age: late Miocene, 5.0–6.4 Ma.

Subunit IIIA consists of gradationally interbedded grayish olive (10Y 4/2) diatom ooze with clay, dark grayish olive to olive gray (10Y 4/1 to 5Y 4/2) diatom clay, pale olive to light olive gray (10Y 6/2 to 5Y 4/2) diatom nannofossil ooze and grayish olive to dark olive gray (10Y 4/1 to 5Y 3/2) clayey diatom ooze. Clay content ranges from 0% to 60% (average 20%). A gray (N4) vitric ash is present at interval 1016A-23X-5, 130–135 cm. The sediments are moderately bioturbated, with *Zoophycos* trace fossils being quite abundant, but extensive coring-related fracturing makes observation of surface features difficult.

Subunit IIIB

Hole 1016A, intervals 167-1016A-26X-1 through 36X; 230.9–316.5 mbsf (base of core).
Age: late Miocene, 6.4 to ~7 Ma.

Subunit IIIB consists of gradationally interbedded olive to olive gray (5Y 4/3 to 5Y 4/2) diatomite, grayish olive (10Y 4/1) clayey diatomite, light grayish olive (10Y 5/1) clayey nannofossil chalk with diatoms and greenish gray (5GY 4/1) to olive gray diatomite with nannofossils or clay. The contact of Subunit IIIA with Subunit IIIB is gradational and characterized by the presence of lithified siliceous strata.

Four centimeter-scale layers of white (N8) vitric ash, a pale olive (10Y 6/2) dolomite clay with nannofossils, and four thin beds of dark gray chert and porcellanite occur in the basal part of Subunit IIIB. Bioturbation is observed on the fractured surfaces of porcellanite and chert, mainly *Chondrites* and *Zoophycos.*

Depositional History

At Site 1016 diatomaceous sediments accumulated rapidly (66 m/m.y.) during the late Miocene (~7.0–5.0 Ma; see “Composite Depths and Sedimentation Rates” section, this chapter). These sediments are indicative of high primary productivity. At the base of the sedimentary succession, the formation of porcellanite and chert reflects the silica diagenesis of upper Miocene diatomites.

After a 1–2 Ma depositional hiatus from the latest Miocene to the lowermost Pliocene (see “Biostratigraphy” section, this chapter), the sedimentation rate was deposited at 33 m/m.y. During the Pliocene (5.0–2.1 Ma), sedimentation was dominated by calcareous nannofossils, but at about 2.4 Ma terrigenous input began increasing.

From the latest Pliocene through the Quaternary (~2.4–0 Ma) terrigenous clay-rich sediments continued to accumulate at a rate of 33 m/m.y. (see “Composite Depths and Sedimentation Rates” section, this chapter). This indicates either an increased terrigenous sediment influx, low primary productivity, or a combination of these two processes.

BIOSTRATIGRAPHY

The sedimentary sequence recovered from the four holes at Site 1016 consists of a well-dated, apparently continuous, 308-m-thick interval ranging from the upper Miocene to the Quaternary. A well-constrained biostratigraphy and chronology for all holes of Site 1016 is provided by a combination of calcareous nannofossil, planktonic foraminifer, diatom, and radiolarian datums for the upper Pliocene and Quaternary. The upper Miocene to lower Pliocene (below 154 mbsf) is dated by calcareous nannofossils, diatoms, and radiolarians. The base of the sequence is upper Miocene (less than 7 Ma) in age. The Pliocene/Pleistocene boundary is placed between 55.1 and 55.8 mbsf, the lower/upper Pliocene boundary between 154.5 and 157.45 mbsf, and the upper Miocene/lower Pliocene boundary between 182.8 and 192.3 mbsf.

Age/depth plots for Hole 1016A and Hole 1016B (Figs. 6, 7) show high sedimentation rates from the Quaternary to the upper Pliocene and for the upper Miocene. Sedimentation rates were drastically lower during the lower to middle Pliocene.

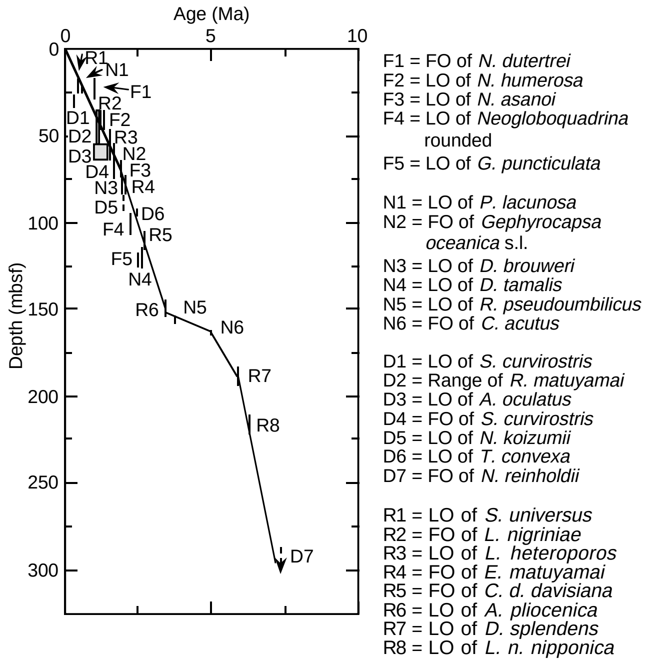

Figure 6. Age/depth plot for Hole 1016A.

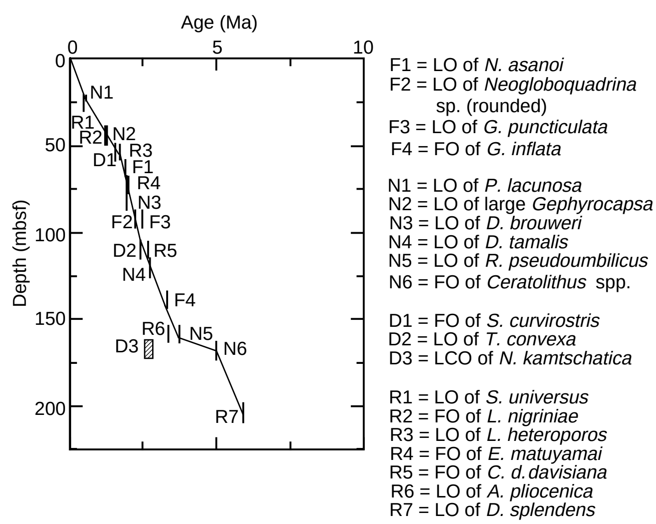

Figure 7. Age/depth plot for Hole 1016B.

The late Pliocene through the Quaternary (0–154 mbsf) contains common to abundant well-preserved calcareous nannofossils, planktonic foraminifers, diatoms, and radiolarians. In the lower part of the sequence (154 to 308 mbsf), planktonic foraminifers are absent, while nannofossils, radiolarians, and diatoms are abundant and moderately to well preserved.

Site 1016 offers much potential for paleoceanographic/paleoclimatic studies from about 6 Ma through the Quaternary. Diatom and radiolarian assemblages suggest two major episodes of strong upwelling during the upper Miocene and upper Pliocene through lower Quaternary. These two episodes are separated by an interval marked by decreased vertical advection of deep waters during the lower to middle Pliocene, resulting in a relatively low sedimentation rate.

Cooling at thermocline depths is suggested after 3.0 Ma by Arctic radiolarian assemblages. This was followed at 2.5 Ma by major surface-water cooling indicated by the first common appearance of dominant, sinistrally coiled *Neogloboquadrina pachyderma.* Lower bathyal benthic foraminifer assemblages appear to change little throughout the upper Pliocene and Quaternary, including between glacial and interglacial episodes.

Planktonic Foraminifers

Site 1016 contains a moderate to good planktonic foraminifer sequence in the upper 154 m (from Samples 167-1016A-17X-CC and 167-1016B-18X-CC to the top of sequence) that extends from the early late Pliocene (~2.9 Ma) through the Quaternary. Episodes of intense dissolution of planktonic foraminifers are conspicuous in the Quaternary and latest Pliocene. These are most frequent in Hole 1016B. Below 154 mbsf in Hole 1016A (Table 3) and 163 mbsf in Hole 1016B, the sequence is completely barren of planktonic foraminifers. The assemblages are common to abundant throughout much of the section and are moderate to well preserved. Benthic foraminifers are generally common and well preserved throughout the upper 154 m in Hole 1016A and 163 m in Hole 1016B, but are rare and of low diversity at greater depths.

The sequence of planktonic foraminifer biostratigraphic datums is similar to that of Site 1014 of Tanner Basin for the lower upper Pliocene through the Quaternary. However, the stratigraphic resolution of the datums is not as well constrained in Site 1016 using the core catchers because of the lower sedimentation rates at this site as compared with Site 1014. As in Site 1014, we place the base of the Quaternary (between Samples 167-1016A-7H-CC and 6H-CC) within the upper range of *Neogloboquadrina humerosa* in the interval above the LO of *Neogloboquadrina asanoi.* We recognize a sequence of five datum levels in the Quaternary and upper Pliocene as follows: FO of *Neogloboquadrina dutertrei* at 1.0 Ma (Sample 167-1016A-2H-CC); LO of *N. humerosa* at 1.2 Ma (Sample 167-1016A-5H-CC); LO of *N. asanoi* at 1.9 Ma (Sample 167-1016A-8H-CC); LO of *Neogloboquadrina* sp. (rounded) at 2.25 Ma (Sample 167-1016A-12X-CC); and LO of *Globorotalia puncticulata* at 2.50 Ma (Sample 167-1016A-14X-CC). As at Site 1014, the FO of consistent and often abundant *Neogloboquadrina pachyderma* (sinistral) coincides with the LO of *G. puncticulata* at 2.5 Ma (Table 4). Climatic conditions suggested by these changes in planktonic foraminifers at Site 1016 are similar to that of Site 1014. As in that section, conspicuous and large-scale cooling of surface waters occurred at ~2.5 Ma.

Benthic foraminifers in the lower upper Pliocene to Quaternary (154 mbsf to the top of sequence) are typical lower bathyal assemblages from the deep sea, and include forms such as *Uvigerina peregrina, Pyrgo, Oridorsalis, Gyroidina, Cibicidoides, Hoeglundina, Melonis, Globobulimina, Chilostomella,* and *Laticarinina.* The faunas appear to change little throughout the upper Pliocene and Quaternary, including during glacial to interglacial oscillations. Below 154 mbsf, the diversity of benthic foraminifers is considerably reduced and assemblages are usually dominated by a few robust species of nodosarids including *Dentalina* and *Nodosaria.* Agglutinated forms are also conspicuous such as *Eggerella* and *Martinottiella.* These faunas have probably resulted from extreme calcium carbonate dissolution.

Hole 1016B

In Hole 1016B, using core-catcher samples, we were unable to place the positions of the FO of *Neogloboquadrina dutertrei* and the LO of *Neogloboquadrina humerosa,* as in Hole 1016A, because of strong foraminifer dissolution in the upper part of the sequence. The LO of *Neogloboquadrina asanoi* at 1.9 Ma occurs in Sample 167-1016B-8H-CC; the LO of *Neogloboquadrina* sp. (rounded) at 2.25 Ma is in Sample 167-1016B-11H-CC; and the LO of *Globorotalia puncticulata* at 2.50 Ma is in Sample 167-1016B-11H-CC. In Hole 1016B, the FO of *Globorotalia inflata* at 3.3 Ma is well defined in Sample 167-1016B-15H-CC. As at Site 1014, in Tanner Basin, the FO of *G. inflata* is immediately underlain by a distinct but short range zone marked by the appearance of *Globorotalia* cf. *conomiozea.* The FO of conspicuous populations of sinistral *Neogloboquadrina pachyderma* is in Sample 167-1016B-11H-CC, which is close to the level exhibited in Hole 1016A.

Calcareous Nannofossils

Calcareous nannofossils are generally common to abundant and well preserved through the Quaternary and upper Pliocene in Holes 1016A and 1016D. In the upper Miocene/lower Pliocene, calcareous nannofossils are absent to common and preservation is poor. Specimens often are broken and identification is difficult (Table 5). In Hole 1016B calcareous nannofossils are absent to common and poorly preserved through the Quaternary and the upper upper Pliocene. In the middle upper Pliocene and upper Miocene/lower Pliocene they are few to abundant and well preserved. An interval spanning the upper Miocene/lower Pliocene Zone CN10a-CN9 to the upper Pleistocene Zone CN15 was recognized in Holes 1016A and 1016B. Hole 1016D represents an interval ranging from the upper Pliocene Zone CN12a to upper Pleistocene CN15-CN14a.

In the Quaternary, calcareous nannofossil assemblages are marked by the presence of *Emiliania huxleyi, Pseudoemiliania lacunosa, Calcidiscus leptoporus, Helicosphaera carteri, Helicosphaera sellii,* and several morphotypes of *Gephyrocapsa* spp. and *Ceratolithoides.*

The FO of *Gephyrocapsa oceanica* s.l. places the Pliocene/Pleistocene boundary at 55.10 mbsf (Sample 167-1016A-6H-CC) in Hole 1016A, at 55.80 mbsf (Sample 167-1016B-7H-CC) in Hole 1016B, and at 55.50 mbsf (Sample 167-1016D-6H-CC) in Hole 1016D.

Pliocene nannofossil assemblages are marked by an association of *Helicosphaera carteri, Discoaster brouweri, D. tamalis, D. pentaradiatus, D. surculus, Amaurolithis delicatus, A. primus,* and several morphotypes of *Reticulofenestra* and *Ceratolithus.* The lower/upper Pliocene boundary is recognized between 154.50 mbsf (Sample 167-1016A-18X-1, 45 cm) and 157.45 mbsf (Sample 167-1016A-18X-3, 45 cm) in Hole 1016A, and between 153.80 mbsf (Sample 167-1016D-17H-CC) and 163.30 mbsf (Sample 167-1016D-18H-CC) in Hole 1016D, using the LO of *Reticulofenestra pseudoumbilicus,* which marks the base of Zone CN12a. The presence of *Amaurolithus* spp. and *Ceratolithus* spp. in Samples 167-1016A-18X-5, 45 cm, to 18X-6, 50 cm, and in Sample 167-1016D-18H-CC allows assignment of this interval to the lower Pliocene Zone CN11/CN10b. The FO of *Ceratolithus acutus* that occurs between Sample 167-1016A-18X-6, 50 cm, and Sample 167-1016A-18X-7, 42 cm, marks the base of the lower Pliocene Zone CN10b. From Samples 167-1016A-18X-7, 42 cm, to 167-1016A-33X-CC and from Samples 167-1016D-18H-CC to 167-1016D-22H-CC, calcareous nannofossil assemblages contain *Amaurolithus* spp., which indicates the lower Pliocene–upper Miocene Zones CN10a and CN9. However, the absence of *Dis-*

Table 3. Distribution and relative abundances of planktonic foraminifers in Hole 1016A.

Zone	Core, section, interval	Depth (mbsf)	Abundance	Preservation	*Neogloboquadrina dutertrei*	*Globorotalia inflata*	*Globorotalia puncticulata*	*Neogloboquadrina asanoi*	*Neogloboquadrina* sp. "rounded"	*Neogloboquadrina humerosa*	*Neogloboquadrina pachyderma* dex.	*Neogloboquadrina pachyderma* sin.	*Globigerina bulloides*	*Orbulina universa*	*Globigerinoides conglobatus*	*Globigerinoides ruber*	*Globorotaloides hexagona*	*Globigerina quadrilatera*	*Globorotalia scitula*	*Hastigerina aequilateralis*	*Globigerina umbilicata*	*Beella digitata*	*Globigerina apertura*	*Globigerina quinqueloba*
	167-1016A-																							
	1H-CC	7.6	A	G	A	A					A		A	C		R	R		C	R				
	2H-CC	17.1	C	G	R						F	A	A											
	3H-CC	26.6	A	G		R					C	A	A				R		R		A			
N22/23	4H-CC	36.1	C	M								A	A											
	5H-CC	45.6	A	G		A				A	A		A	F					R			R		
	6H-CC	55.1	C	M		A				A	A		C	F	R	R								
	7H-CC	64.6	B																					
	8H-CC	74.1	A	G				A		A		A	A	F										
	9H-CC	84.0	A	M		R		A			C	A	A	R							A			A
	10H-CC	93.0	C	M				A		C		A	C											
	11X-CC	96.0	F	P		C		A		C	F		R								A			
N21	12X-CC	106.0	A	G		F		A	A	F	C		A	F					R		A			
	13X-CC	116.0	A	G		F		A	C	A		A	A	F							A		F	
	14X-CC	125.0	A	G		F	C	A			A		A	F					R		C	F		
	15X-CC	135.0	A	M/G		C	F	A	A	C	F		F	C				F	R		F			
	16X-CC	144.0	A	G		F		A		R			A	C		R						R		
	17X-CC	154.0	R	P				R																
	18X-CC	164.0	B																					
	19X-CC	173.0	B																					
	20X-CC	183.0	B																					
	21X-CC	192.0	B																					
	22X-CC	202.0	B																					
	23X-CC	212.0	B																					
?	24X-CC	221.0	B																					
	25X-CC	231.0	B																					
	26X-CC	241.0	B																					
	27X-CC	250.0	B																					
	28X-CC	260.0	B																					
	29X-CC	279.0	B																					
	30X-CC	289.0	B																					
	31X-CC	298.0	B																					
	32X-CC	308.0	B																					

Note: See "Explanatory Notes" chapter for abbreviations.

Table 4. Coiling dominance of *Neogloboquadrina pachyderma* in the upper Pliocene through Quaternary of Hole 1016B.

Core, section, interval	Depth (mbsf)	*Neogloboquadrina pachyderma* coiling dominance
167-1016B-		
1H-CC	1.8	Sinistral
2H-CC	11.3	Sinistral/Dextral
3H-CC	20.8	Sinistral/Dextral
4H-CC	30.3	Sinistral
5H-CC	39.8	Dextral
6H-CC	49.3	Dextral
7H-CC	58.8	—
8H-CC	68.3	—
9H-CC	77.8	—
10H-CC	87.3	Sinistral/Dextral
11H-CC	96.8	Sinistral/Dextral
12H-CC	106.3	Dextral
13H-CC	115.3	Dextral
14H-CC	125.3	Dextral
15H-CC	134.8	Dextral
16H-CC	144.3	Dextral
17H-CC	153.8	—
18H-CC	163.3	—
19H-CC	172.8	Barren

Note: — = inadequate number of specimens for analysis.

coaster quinqueramus/berggrenii (Zone CN9) does not allow certain assignment of the latest Miocene age for this interval.

Diatoms

Diatoms are generally common to abundant and poorly to well preserved in the upper Miocene through Pleistocene section above 290 mbsf at Site 1016.

Two kinds of the diatom zonal schemes were used to date this late Neogene through Quaternary sequence. Three zones of the north Pacific diatom zonation were recognized in the Pleistocene assemblages and standard north Pacific diatom datums were useful in dating the interval from the late Pleistocene *Neodenticula seminae* Zone (NPD 12) to the late Pliocene *Actinocyclus oculatus* Zone (NPD 10). The latest Miocene through Pliocene diatom assemblages are considered within a local biostratigraphic framework that reflects a transitional provincialism of the diatom flora, extending along the eastern rim temperate north Pacific.

In contrast to Sites 1011 through 1015, typical Quaternary assemblages are well preserved and easily zoned from Cores 167-1016A-1H through 10H (Table 6). The LO of the *Simonseniella (Rhizosolenia) curvirostris* (0.30 Ma) falls between Samples 167-1016A-3H-CC and 4H-CC, where it differentiates the *N. seminae* Zone (NPD 12) from the underlying *S. curvirostris* Zone (NPD 11). The zonal boundary between the NPD 12/11 Zones is also determined at Holes 1016B and 1016D (Table 7).

Table 5. Distribution and relative abundances of calcareous nannofossils at Site 1016.

Zone	Core, section, interval (cm)	Depth (mbsf)	Preservation	Abundance	*Emiliania huxleyi*	*Pseudoemiliania lacunosa*	*Helicosphaera carteri*	*Helicosphaera sellii*	*Gephyrocapsa oceanica* s.l.	*Gephyrocapsa* sp. 3	*Gephyrocapsa* small	*Gephyrocapsa* large	*Discoaster brouweri*	*Discoaster triradiatus*	*Discoaster pentaradiatus*	*Discoaster surculus*	*Discoaster tamalis*	*Discoaster asymmetricus*	*Sphenolithus* spp.	*Reticulofenestra pseudoumbilicus*	*Ceratolithus* spp.	*Ceratolithus telesmus*	*Ceratolithus acutus*	*Amaurolithus primus*	*Amaurolithus* spp.	*Coccolithus pelagicus*	*Calcidiscus macintyrei* >11 µm	*Calcidiscus leptoporus*
	167-1016A-																											
CN15	1H-CC	7.60	G	C	P		F		P	C/F	F/C										R					F		R
CN15–CN14b	2H-6, 100	16.10	P	F							P																	
	2H-7, 14	16.74		B																								
CN15–CN14b	2H-CC	17.10	M/G	C			R		R		C/A										R					F		R
CN15–CN14b	3H-1, 95	18.05	P	RR																						C		
CN15–CN14b	3H-2, 95	19.55	P	RR					P																			
CN15–CN14b	3H-3, 95	21.05	G	A			C				A											R						
CN15–CN14b	3H-4, 118	22.78	G	A					P		C																	
CN14a	3H-5, 118	24.28	G	A		R	R		C																			F
CN14a	3H-6, 40	25.00	M	C/A		C																						
CN14a	3H-7, 40	26.50	M/G	A		P			P		C																	
CN14a	3H-CC	26.60	G	A		R/F			P		A																	R
	4H-CC	36.10		B																								
CN13b	5H-CC	45.60	M	C		A	R				P															C		P
	167-1016B-																											
CN13b	6H-CC	55.10	M	C		C	R	R	P																			C
	167-1016A-																											
	7H-CC	64.60		B																								
CN13a–CN12d	8H-CC	74.10	P	F/C		R	R						RR														P	P
CN12d	9H-CC	83.60	P	F/C		P	R						R														P	P
CN12d	10H-CC	93.10	G	A		C		P					F								R							
CN12	11X-CC	96.30	P	R/F		P	R																					
CN12b	12X-CC	106.00	P	F		C									P	P												
CN12b	13X-CC	115.60	G	A											F	C					F						C	
CN12a	14X-CC	125.20	G	C/A		C									C	P	C										P	
CN12a	15X-CC	134.80	M/G	A											C	C										C	C	
CN12a	16X-CC	144.40	G	A		R							R			R	F										C	R
CN12a	17X-4, 41	150.81	G	A		C							C		R	R	F		P							P	C	
CN12a	17X-CC	154.00	P	R													P	P	P									
CN12a	18X-1, 45	154.45	G	A																							P	
CN10b–CN12a	18X-2, 45	155.95	G	A		R	R	F												F/R	F				P			
CN10b–CN11	18X-3, 45	157.45	G	A																P								
CN10b–CN11	18X-4, 44	158.94	G	A		P		C							C	P	P				P							
CN10b–CN11	18X-5, 45	160.45	G	A		R		C												P			P		P			
CN10b–CN11	18X-6, 50	162.00	P	F		R									C					C			R		P			
CN9–CN10a	18X-7, 42	163.42	P/M	C																A					C			
CN9–CN10a	18X-CC	163.60	P	R/F		R									P					F				cf	R		P	
CN9–CN10a	19X-1, 63	164.23	G	A																A					F		C	
CN9–CN10a	19X-2, 53	165.63	G	A											P					A				R	P		C	
CN9–CN10a	19X-3, 48	167.08	P	R																P								
CN9–CN10a	19X-CC	173.20	M	A									C		P	P				C				R	P		P	
CN9–CN10a	20X-CC	182.60	P	C									P		P					R				R	R			
CN9–CN10a	21X-CC	192.30	M	F															R	R				R	F		R	
CN9–CN10a	22X-CC	201.10	G	C																C					R			
	23X-CC	211.70		B																								
	24X-CC	221.30		B																								
	25X-CC	230.90		B																								
	26X-CC	240.60		B																								
CN9–CN10a	27X-CC	250.20	P	F											P					C								
CN9–CN10a	28X-CC	259.80	P	RR																P								
CN9–CN10a	29X-CC	269.50	P	R/F											R					R					R			
CN9–CN10a	30X-CC	279.20	P	RR																P								
	31X-CC	288.80		B																								
CN9–CN10a	32X-CC	298.40	P	RR																								
CN9–CN10a	33X-CC	308.00	P	RR																								
CN9–CN10a	35X-CC	315.50	P	RR																					P			
	167-1016B-																											
CN15–CN14b	1H-CC	1.80	P	R/F					P																	P		
	2H-CC	11.30		B																								
CN15–CN14b	3H-CC	20.80	G	A			R		C	R	A															C		
CN15–CN14b?	4H-1, 136	22.16	P	R					P		P																	
CN14a	4H-2, 60	22.90	M/G	C		F/C			F/R		A																	
CN14a	4H-2, 136	23.66	G	C		F/R	F		P		C/A																	
CN14a	4H-3, 114	24.94	G	C/A		F/R	R		C		A																	
CN14a	4H-4, 74	26.04	M	F		P	R				P																	
	4H-5, 95	27.75		B																								
CN14a	4H-6, 56	28.86	M	F		P				R	C																	
	4H-7, 65	30.45		B																								
	4H-CC	30.30		B																								
CN14a	5H-CC	39.80	P/M	R		P			P	R																		
CN13b	6H-CC	49.30	P	R		R		R				R									R							R
CN13b	7H-CC	58.80	P	RR					R			RR																
CN13a	8H-CC	68.30	P	C		C	R	R																			P	R
CN13a–CN12d	9H-CC	77.80	P	F									RR														P	
CN12d	10H-CC	87.30	P	C		F							F	R												C	C	F

Table 5 (continued).

Zone	Core, section, interval (cm)	Depth (mbsf)	Preservation	Abundance	*Emiliania huxleyi*	*Pseudoemiliania lacunosa*	*Helicosphaera carteri*	*Helicosphaera sellii*	*Gephyrocapsa oceanica* s.l.	*Gephyrocapsa* sp. 3	*Gephyrocapsa* small	*Gephyrocapsa* large	*Discoaster brouweri*	*Discoaster triradiatus*	*Discoaster pentaradiatus*	*Discoaster surculus*	*Discoaster tamalis*	*Discoaster asymmetricus*	*Sphenolithus* spp.	*Reticulofenestra pseudoumbilicus*	*Ceratolithus* spp.	*Ceratolithus telesmus*	*Ceratolithus acutus*	*Amaurolithus primus*	*Amaurolithus* spp.	*Coccolithus pelagicus*	*Calcidiscus macintyrei* >11 µm	*Calcidiscus leptoporus*
CN12c?	11H-CC	96.80	M	A		R	R	C					RR		R						R					F	P	P
CN12b	12H-CC	106.30	M	C		C									R	C										F		
CN12b	13H-CC	115.30	G	A		P							R		R/F	C										F		R
CN12b	14H-CC	125.30	G	A											R	C	R				R					C/F	F	F
CN12a	15H-CC	134.80	G	A		R							C			P	R/F				R						R	C
CN12a	16H-CC	144.30	M/G	A		P									R	P	C/F										C	C
CN12a	17H-CC	153.80	P/M	F/C		R		R					P		R		RR				R						C	C
CN11–CN10b	18H-CC	163.30	P	F			R								C				R	C	R			R	F	C	C	
CN10a–CN9	19H-CC	172.80	P	F											R	R				P					P			F
CN10a–CN9	20H-CC	182.30	M/G	A									P		P										P			
CN10a–CN9	21H-CC	191.80	M/G	A												R				RR							C	F
CN10a–CN9	22H-CC	201.30	G	A												P									R		P	P
	23H-CC	210.80		B																								
	167-1016C-																											
CN15–CN14b	1H-CC	8.00	M/G	C							A															P		
CN15–CN14b	2H-CC	17.50	G	C					C		A																	
	167-1016D-																											
CN15–CN14b	1H-CC	8.00	G	F/C			R				A															C		
CN15–CN14b	2H-CC	17.50	G	A			F		C	F	A											F				F		R
CN14a	3H-CC	27.00	M	C		P			P		A															P		R
	4H-CC	36.50	P	RR		P																						P
	5H-CC	46.00	P	R		P																				P		P
CN13b	6H-CC	55.50	P/M	C		C			F																			R
	7H-CC	65.00		B																								
CN13a	8H-CC	74.50	G	A		C	C	P																			C	P
CN13a?	9H-CC	84.00	M/P	C		C																				C	P	R
CN13a?	10H-CC	93.50	G	C		P		F																		C	F	F
CN12b	11H-CC	103.50	M/P	A		P							R			F										C	C	
CN12b	12H-CC	112.50	M/G	A									F		R	C											P	
CN12a	13H-CC	121.00	G	A		P	F							F	F/C	C	F/C	P			R					C		
CN12a	14H-CC	130.50	G	A		F	F								C	P	C				R						C	F
CN12a	15H-CC	141.00	G	A		P							R			C										P	P	F
CN12a	16H-CC	150.50	P	F									P			P	F/R									F	P	

Note: See “Explanatory Notes” chapter for abbreviations.

A rare occurrence of *Rhizosolenia matuyamai* in Sample 167-1016A-5H-CC is dated as 1.04 to 1.12 Ma and indicates a tight correlation with a short interval spanning the normal-polarity Jaramillo subchron (Barron, 1980; Barron and Gladenkov, 1995). Both the FO of *S. curvirostris* in Sample 167-1016A-6H-CC and the last rare occurrence of *A. oculatus* in Sample 167-1016A-7H-CC have been used to tentatively place the boundary between the *S. curvirostris* and *A. oculatus* Zones (NPD 11/10).

Following Koizumi (1992), the base of the *A. oculatus* Zone (NPD 10) and top of the underlying *Neodenticula koizumii* Zone (NPD 9) are defined by the LO of *N. koizumii* (2.0 Ma). The LO of *Thalassiosira convexa* (2.4 Ma) occurs just below the LO of *N. koizumii* (Barron and Gladenkov, 1995). These latest Pliocene events were documented in Samples 167-1016A-12X-CC through 10X-CC, but occurrences of these species are too sparse to provide high stratigraphic reliability at Site 1016. In spite of an abundance of diatoms in sediments between Samples 167-1016A-14X-CC (125.2 mbsf) and 31X-CC (288.8 mbsf), the following three zones of the late Pliocene through latest Miocene age: the *N. koizumii* Zone (NPD 9), the underlying *N. koizumii-N. kamtschatica* Zone (NPD 8) and the lowest *N. kamtschatica* Zone (NPD 7) could not be defined because of the absence of zonal marker species *N. koizumii* and *N. kamtschatica.* Barron and Baldauf (1986) reported that it is inappropriate to use the *N. kamtschatica* Zone (NPD 7) in California and substituted two zones defined by Barron (1981): the *Nitzschia reinholdii* Zone and the overlying *Thalassiosira oestrupii* Zone.

The 160-m-thick diatomaceous interval from 125.2 to 288.8 mbsf at Site 1016 includes abundant representatives of *Coscinodiscus marginatus*, *Rhizosolenia barboi*, and *Thalassiothrix* spp., which are characteristic of oceanic-to-marginal upwelling systems and are indicative of high coastal productivity. The diatom assemblages contain scattered and consistent representatives of *Hemidiscus cuneiformis*, *Thalassiosira convexa*, *Azpeitia nodulifer*, and *N. reinholdii* (Tables 6, 7). These assemblages are typical of neither the subarctic north Pacific nor the equatorial eastern Pacific, but rather the relatively warm-temperate surface waters that extend along the northeastern Pacific rim off California.

The presence of *N. reinholdii* in Sample 167-1016A-31X-CC (288.8 mbsf) indicates that the base of the diatomaceous interval in Hole 1016A may be younger than 7.3 Ma.

Surface waters at Site 1016 have maintained intermediate properties between subarctic cold waters and subtropical warm waters during the latest Miocene through Pliocene. Oceanic-to-marginal upwelling caused high diatom productivity between both fronts. An almost continuous absence of cold-water *Neodenticula* spp. suggests warm conditions during the late Miocene through early Pliocene.

Radiolarians

Radiolarians are common to abundant and moderately to well preserved in Holes 1016A and 1016B. Sample 167-1016A-33X-CC, above the chert layer (308 mbsf), is barren.

Consistent occurrence of *Eucyrtidium matuyamai* and the LO of *Lamprocyrtis heteroporos* permits location of the Pliocene/Pleistocene boundary between 45.6 and 55.1 mbsf in Hole 1016A and between 49.3 and 58.8 mbsf in Hole 1014B (Tables 8, 9). The Miocene/

Table 6. Diatoms in Hole 1016A.

Geologic age	North Pacific diatom zone	Numeric age (Ma)	Core, section, interval	Depth (mbsf)	Abundance	Preservation	Upwelling	*Actinocyclus oculatus* (fragment)	*Actinocyclus ehrenbergii*	*Actinocyclus ellipticus* cf. *lanceolata*	*Actinocyclus ingens*	*Actinocyclus ingens nodus*	*Actinoptychus senarius*	*Coscinodiscus asteromphalus*	*Coscinodiscus marginatus*	*Coscinodiscus* cf. *marginatus*	*Azpeitia (Coscinodiscus) nodulifer*	*Coscinodiscus radiatus*	*Coscinodiscus* sp.	*Crucidenticula nicobarica*	*Denticulopsis dimorpha*	*Denticulopsis hustedtii*	*Denticulopsis hyalina*	*Denticulopsis lauta*	*Denticulopsis lauta* s.l.	*Denticulopsis* sp.	*Hemidiscus cuneiformis*	*Navicula* sp.	*Neodenticula* cf. *seminae*	*Neodenticula kamtschatica*	*Neodenticula* cf. *kamtschatica*	*Neodenticula koizumii*	*Neodenticula* cf. *koizumii*	*Neodenticula seminae*	*Neodenticula seminae* (sensu Akiba)	*Neodenticula* sp.
			167-1016A-																																	
Quaternary	NPD 12	0	1H-CC	7.6	P	P																												P		
			2H-CC	17.1	R	P																			T									P		
		0.3	3H-CC	26.6	F	P																			R									F		
	NPD 11		4H-CC	36.1	F	P									P										P			P						F		
			5H-CC	45.6	F	P/M																												F		
		1.44	6H-CC	55.1	C	P/M					P														P									F		
Pliocene	NPD 10		7H-CC	64.6	C	P/M		P																			F							C		
			8H-CC	74.1	C	M						P											P											F	P	
		2?	9H-CC	83.6	C	P														P					P		P									
	NPD 9/10	2.4?	10H-CC	93.1	A	P/M									A										P											
	NPD 9	2.7?	11X-CC	96.3	A	P/M									A																					
			12X-CC	106.0	A	M	Up								A												P					P		P		
			13X-CC	115.6	A	M	Up			R					A																				R	
			14X-CC	125.2	F	P									P				P				P				P									
			15X-CC	134.8	R	P									C								P	P			F						P			
			16X-CC	144.4	R	P									F											R										
			17X-CC	154.0	F	P/M	Up								F						P			P												P
			18X-CC	163.6	R	P		P														P	P		P		P									
			19X-CC	173.2	F	P/M									R							P														
	NPD 9 to NPD 7a		20X-CC	182.8	A	P/M	Up								C															P	P	P	P			P
			21X-CC	192.3	C	P									F																					
			22X-CC	202.1	A	P/M	Up						R		A		C										F		R							
			23X-CC	211.7	A	M/G	Up								C		A	R									R									
			24X-CC	221.3	A	P	Up																													
			25X-CC	230.9	A	P	Up		P																											
			26X-CC	240.6	A	P/M	Up								A												R			P						
			27X-CC	250.2	A	P	Up								C	F			R				R													
			28X-CC	259.8	A	M	Up								C																					
			29X-CC	259.8	A	P	Up				P																									
			30X-CC	279.2	A	M/G	Up							P	P																					
late Miocene		7.2?	31X-CC	288.2	A	P/M	Up																													
			32X-CC	298.4	B																															
			33X-CC	308.0	B																															
			34X-CC	311.0	No sample																															
			35X-CC	315.5	B																															
			36N-CC	316.5	No sample																															

Table 6 (continued).

Geologic age	North Pacific diatom zone	Numeric age (Ma)	Core, section, interval	Depth (mbsf)	Abundance	Preservation	Upwelling	*Neodenticula* sp. (*N. rolandii*)	*Nitzschia* cf. *jouseana*	*Nitzschia marina*	*Nitzschia reinholdii*	*Nitzschia rolandii*	*Paralia sulcata*	*Rhizosolenia barboi*	*Simonseniella* (*Rhizosolenia*) *curvirostris*	*Rhizosolenia matuyamai*	*Rhizosolenia* sp.	*Stephanopyxis turris*	*Synedra* sp.	*Thalassionema nitzschioides*	*Thalassionema nitzschioides parva*	*Thalassionema schraderi*	*Thalassiosira antiqua*	*Thalassiosira convexa*	*Thalassiosira eccentrica*	*Thalassiosira hyalinopsis*	*Thalassiosira leptopus*	*Thalassiosira nativa*	*Thalassiosira oestrupii*	*Thalassiosira plicata*	*Thalassiosira* sp.	*Thalassiosira* spp. (*nativa* type)	*Thalassiothrix longissima*	*Thalassiothrix* spp.	Sponge spicules
			167-1016A-																																
		0	1H-CC	7.6	P	P														P							P								
	NPD 12		2H-CC	17.1	R	P							P																						
Quaternary		0.3	3H-CC	26.6	F	P								P																					
			4H-CC	36.1	F	P								P	P																		P		
	NPD 11		5H-CC	45.6	F	P/M				R		R		C		R																			
		1.44	6H-CC	55.1	C	P/M				P					F			P		P													P		
			7H-CC	64.6	C	P/M				P	R			F																					
	NPD 10		8H-CC	74.1	C	M				P	F			F						P															
		2?	9H-CC	83.6	C	P				R	P			C						F											P		C		
	NPD 9/10	2.4?	10H-CC	93.1	A	P/M					R			A				P															R	A	
		2.7?	11X-CC	96.3	A	P/M								A				P						A											
	NPD 9		12X-CC	106.0	A	M	Up							A								P											P	C	
			13X-CC	115.6	A	M	Up							A										C									F		
			14X-CC	125.2	F	P								P																			P		
			15X-CC	134.8	R	P			P					C							P	P		P											
			16X-CC	144.4	R	P								F																	R		F		
			17X-CC	154.0	F	P/M	Up							C																			F		
Pliocene			18X-CC	163.6	R	P								F							P												F	P	A
			19X-CC	173.2	F	P/M							R									P									P				F
	NPD 9		20X-CC	182.8	A	P/M	Up	P						F																			F	F	
			21X-CC	192.3	C	P														F													F		
	to		22X-CC	202.1	A	P/M	Up										R		R							R						R			
			23X-CC	211.7	A	M/G	Up			F	F	R		C				P		R			F		F			R							
	NPD 7a		24X-CC	221.3	A	P	Up													P			P		P			P	P						
			25X-CC	230.9	A	P	Up							F									F					R					P		
			26X-CC	240.6	A	P/M	Up			R		P																R	R						
			27X-CC	250.2	A	P	Up							R						R									F						
			28X-CC	259.8	A	M	Up				F									A								F	R				C		
			29X-CC	259.8	A	P	Up												F		R		R						R						
			30X-CC	279.2	A	M/G	Up											P		P				P						P					
late Miocene		7.2?	31X-CC	288.2	A	P/M	Up				P												P	P											
			32X-CC	298.4	B																														
			33X-CC	308.0	B																														
			34X-CC	311.0	No sample																														
			35X-CC	315.5	B																														
			36N-CC	316.5	No sample																														

Notes: P = present; more detailed abundance information not available. See "Explanatory Notes" chapter for other abbreviations.

Table 7. Diatoms in Holes 1016B, 1016C, and 1016D.

Geologic age	North Pacific diatom zone	Numeric age (Ma)	Core, section, interval	Sample depth (mbsf)	Abundance	Preservation	Upwelling	*Actinocyclus curvatulus*	*Actinocyclus ingens*	*Actinocyclus ingens nodus*	*Actinocyclus oculatus*	*Actinocyclus oculatus* (fragment)	*Actinocyclus tsugaruensis*	*Actinoptychus senarius*	*Cocconeis californica*	*Coscinodiscus marginatus*	*Azpeitia* (*Coscinodiscus*) *nodulifer*	*Coscinodiscus oculus iridis*	*Coscinodiscus radiatus*	*Coscinodiscus* sp.	*Denticulopsis hustedtii*	*Denticulopsis hyalina*	*Denticulopsis lauta*	*Denticulopsis lauta* s.l.	*Grammatophora* sp.	*Hemiaulus polymorphus*	*Hemidiscus cuneiformis*	*Neodenticula kamtschatica*	*Neodenticula* cf. *kamtschatica*	*Neodenticula koizumii*	*Neodenticula* cf. *koizumii*	*Neodenticula seminae*	*Nitzschia marina*	*Nitzschia reinholdii*	*Nitzschia rolandii*	*Nitzschia* sp.
			167-1016B-																																	
			1H-CC	1.8	T	P			P																											
			2H-CC	11.3	T	P														F																
Quaternary	NPD 12		3H-CC	20.8	T	P														T																
			4H-CC	30.3	T	P																														
		0.3?	5H-CC	39.8	T	P						R				T					T	T		T								F		R		
			6H-CC	49.3	R	P					T					T						T	T			T						R				
	NPD 11/10	1.58?	7H-CC	51.8	A	M/G	Up																										F	C		
			8H-CC	68.3	A	M/G	Up												R													F	R	R		
	NPD 9	2.0?	9H-CC	77.8	C	P	Up									F														T		F		F		
			10H-CC	87.3	C	P	Up	T							R										R							T	F	T		T
			11H-CC	96.8	A	M/G	Up									C				R							F									
			12H-CC	106.3	A	M	Up	R								A							T									F	R			
	NPD 9	2.4?	13H-CC	115.8	C	P	Up		T							A														T						
			14H-CC	125.3	F	P/M															T	R	T											R		
Pliocene			15H-CC	134.8	C	P										C											R									
			16H-CC	144.3	F	P										F									R											
			17H-CC	153.8	C	P/M	Up									C																				
		2.63?	18H-CC	163.3	F	P			T													T														
	NPD 8/7b	2.73?	19H-CC	172.8	A	M/G	Up			T						F												F	R		T				T	
			20H-CC	182.3	F	P										F	R																			
			21H-CC	191.8	A	M/G	Up									A		R											T							
			22H-CC	201.3	A	M/G	Up									A																				
			23H-CC	210.8	A	M/G	Up	R								A											R									
			167-1016C-																																	
			1H-CC	9.2	T	P																														
			2H-CC	18.7	T	P																														
			167-1016D-																																	
			1H-CC	8.0	R	P							T																			F				
	NPD 12		2H-CC	17.5	T	P																T														
Quaternary		0.3?	3H-CC	27.0	T	P																										T				
		1.44	4H-CC	36.5	F	P/M										R																C				
	NPD 11		5H-CC	46.0	F	P								T								T										F	F	F		
		1.58	6H-CC	55.5	F	P													T													F				
			7H-CC	65.0	R	P																										R				
			8H-CC	74.5	A	M/G	Up		T							R					T											F		R		
	NPD 10/9		9H-CC	84.0	A	P/M	Up								R	R																				
			10H-CC	93.5	A	P/M	Up	R								F			R															R		
Pliocene		2.4?	11H-CC	103.0	A	M	Up									A																C				
		2.7?	12H-CC	112.5	C	P/M										C												T			T	C	R			
	NPD 8		13H-CC	121.0	C	P/M										C											R					C				
			14H-CC	130.5	R	P										C												R								
	NPD 8/7a		15H-CC	141.0	T	P																														
			16H-CC	150.5	A	M/G	Up									F											R									

Note: See "Explanatory Notes" chapter for abbreviations.

Table 7 (continued).

Geologic age	North Pacific diatom zone	Numeric age (Ma)	Core, section, interval	Sample depth (mbsf)	Abundance	Preservation	Upwelling	*Paralia sulcata*	*Rhizosolenia barboi*	*Simonseniella (Rhizosolenia) curvirostris*	*Rhizosolenia* sp.	*Stephanopyxis schenckii*	*Stephanopyxis turris*	*Synedra jouseana*	*Thalassionema nitzschioides*	*Thalassiosira antiqua*	*Thalassiosira convexa*	*Thalassiosira eccentrica*	*Thalassiosira nativa*	*Thalassiosira oestrupii*	*Thalassiosira* spp.	*Thalassiosira* sp. (*convexa* type)	*Thalassiosira* spp. (*nativa* type)	*Thalassiothrix longissima*	*Thalassiothrix* spp.	Diatom fragment (bands)	Diatom fragments	Sponge spicules
			167-1016B-																									
			1H-CC	1.8	T	P																					R	R
			2H-CC	11.3	T	P																		F				C
	NPD 12		3H-CC	20.8	T	P																					R	F
Quaternary			4H-CC	30.3	T	P		T					T		T									T			F	
		0.3?	5H-CC	39.8	T	P		R							R													
			6H-CC	49.3	R	P				T				T	T							F						
	NPD 11/10	1.58?	7H-CC	51.8	A	M/G	Up		C				C		C									A	A	A		
			8H-CC	68.3	A	M/G	Up		C				F											C	A			
	NPD 9	2.0?	9H-CC	77.8	C	P	Up				F		F												F			
			10H-CC	87.3	C	P	Up	R	C				T		R					R								
			11H-CC	96.8	A	M/G	Up		C				C											C				
			12H-CC	106.3	A	M	Up						T		F					F				C				
	NPD 9	2.4?	13H-CC	115.8	C	P	Up		C							T	F											
			14H-CC	125.3	F	P/M			C						R		C											
Pliocene			15H-CC	134.8	C	P			F								C							F	R			
			16H-CC	144.3	F	P																		R				
			17H-CC	153.8	C	P/M	Up		C								F							C				
		2.63?	18H-CC	163.3	F	P			F														R	T				
	NPD 8/7b	2.73?	19H-CC	172.8	A	M/G	Up								R			T	T		F		F					
			20H-CC	182.3	F	P		T	R															R				
			21H-CC	191.8	A	M/G	Up								C	R		F	C					F	A			
			22H-CC	201.3	A	M/G	Up								F	R								C	C			
			23H-CC	210.8	A	M/G	Up		R						F										A			
			167-1016C-																									
			1H-CC	9.2	T	P															T						R	R
			2H-CC	18.7	T	P										T											T	R
			167-1016D-																									
			1H-CC	8.0	R	P		F																				
	NPD 12		2H-CC	17.5	T	P																				R	R	
Quaternary		0.3?	3H-CC	27.0	T	P									T													
		1.44	4H-CC	36.5	F	P/M			F	T			T				T				R			C				
	NPD 11		5H-CC	46.0	F	P			F				F															
		1.58	6H-CC	55.5	F	P			T	T														T				F
			7H-CC	65.0	R	P			T			T	F															
			8H-CC	74.5	A	M/G	Up		R															C	A			
	NPD 10/9		9H-CC	84.0	A	P/M	Up	R	R															C				
			10H-CC	93.5	A	P/M	Up		A				F					R	R						A			
Pliocene		2.4?	11H-CC	103.0	A	M	Up		A												R			C	A			
		2.7?	12H-CC	112.5	C	P/M											R											
	NPD 8		13H-CC	121.0	C	P/M			C				F				F							C				
			14H-CC	130.5	R	P			R								R							F				
	NPD 8/7a		15H-CC	141.0	T	P			R															R				
			16H-CC	150.5	A	M/G	Up		F							T	R							C	A			

Table 8. Radiolarians in Hole 1016.

Zone	Core, section, interval	Depth (mbsf)	Abundance	Preservation	*Acrosphaera murrayana*	*Actinomma popofskii*	*Anthocyrtidium pliocenica*	*Botryostrobus aquilonaris*	*Botryostrobus praetumidulus*	*Botryostrobus tumidulus*	*Ceratospyris hyperborea*	*Clathrocyclas bicornis*	*Cycladophora bicincta*	*Cycladophora davisiana davisiana*	*Dictyophimus crisiae*	*Dictyophimus splendens*	*Eucyrtidium acuminatum*	*Eucyrtidium calvertense*	*Eucyrtidium erythromystax*	*Eucyrtidium matuyamai*	*Eucyrtidium teuscheri*	*Gondwanaria dogeli*	*Lamprocyclas hadros*	*Lamprocyclas hannai*	*Lamprocyclas junonis*	*Lamprocyrtis daniellae*	*Lamprocyrtis heteroporos*	*Lamprocyrtis neoheteroporos*	*Lamprocyrtis nigriniae*	*Lithostrobus hexagonalis*
	167-1016A																													
	1H-CC	7.6	C	G	R			R		R			R		R			R				R			F				C	
B. aquilonaris	2H-CC	17.7	A	G	R	F		C					C	A	R			R				R			C				A	
	3H-CC	26.6	A	G	R			F		F	T		C	A				R			T	T						R	A	T
S. universus	4H-CC	36.1	A	G		F		C		C		R	A	A	R		T				T							A	A	T
	5H-CC	45.6	A	G						R	T	F		A			R	R		R					F			A		T
	6H-CC	55.1	C	G				C		C			C	A				R		F		R			R		T	A		
E. matuyamai	7H-CC	64.5	A	G					F	A		C		A						C	R	R	T				R	A		
	8H-CC	74.1	A	G						A	R	C			R					F							C	A		
	9H-CC	83.6	A	G		R		A	C		F	C		A	R		T	R				R			F		A	C		
S. langii	10H-CC	93.1	A	G					R			C		A	R			R							F		F	C		
	11X-CC	96.3	A	G	R			R			F			C			T		T		T						A	F		
	12X-CC	106.0	A	G						C		A		C	R			R									A			
	13X-CC	115.6	A	G	T	R						A			R			R			T						R	A		
	14X-CC	125.2	C	G					R			R					T	R									R	F		
	15X-CC	134.8	A	G					R			C					C	R					C		R		C	A		
	16X-CC	144.4	C	G		T			C			R							T									A		
	17X-CC	154.0	C	G			R		R			R															R			
	18X-CC	163.6	R	M			R					R																		
	19X-CC	173.2	F	G			C																		T	T	R			
	20X-CC	182.8	A	G			C		C			R						R				T			F		A			
	21X-CC	192.3	A	G			R		F			R				T	T	R									A			
S. peregrina	22X-CC	202.1	C	G								C															R			
	23X-CC	211.7	F	G								C															R			
	24X-CC	221.3	C	G			R					F						R									R			
	25X-CC	230.9	C	G					R			C												F						
	26X-CC	240.6	F	G								C				F														
	27X-CC	250.2	R	G					R																					
	28X-CC	259.8	F	G			C		C			C				R														
	29X-CC	269.5	F	G			C		C			R																		
	30X-CC	279.2	C	G			C		C			R				F	R							R						
	31X-CC	288.8	A	G			A									A					R		T	F						
	32X-CC	298.4	R	M																										
	33X-CC	308.0	B																											

Note: See "Explanatory Notes" chapter for abbreviations.

Pliocene boundary is located above the top of *Dictyophimus splendens* between Samples 167-1016A-20X-CC and 21X-CC (Table 8).

The main radiolarian events are summarized in Table 10. Abundant and well-preserved assemblages contain species that are indicative of upwelling conditions throughout all the sequence. Persistent occurrence of many subtropical species in assemblages below Samples 167-1016A-13X-CC (115.6 mbsf) and 167-1016B-13H-CC (115.8 mbsf) suggest warmer conditions during the late Miocene through early Pliocene and an age slightly younger than 3 Ma for the beginning of major thermocline-water cooling at Site 1016.

PALEOMAGNETISM

We made magnetic measurements on the archive halves of APC cores from Holes 1016A and 1016B with the pass-through cryogenic magnetometer. After measuring the natural remanent magnetization (NRM), 10 cores from Hole 1016A were demagnetized with a peak alternating field (AF) of 25 mT. We measured six APC cores from Hole 1016B after AF demagnetization at 20 mT. The NRM intensity of Cores 167-1016A-1H to 10H ranged between 1 and 10 mA/m, and after the AF cleaning it was reduced to values around 0.3 mA/m (Fig. 8). After AF demagnetization, the magnetization of most sections was lower than the sensitivity of the magnetometer (<1 mA/m). We did not find an interval of negative inclination (reverse polarity) in either Hole 1016A or 1016B, although the biostratigraphic data suggest that the top of the Matuyama Chron (C1r) should be located approximately in Core 167-1016A-5H (see "Biostratigraphy" section, this chapter).

A significant drop of the remanence intensity was observed between 0 and 2 mbsf with a decrease in magnetic susceptibility in the same interval. A similar strong decrease was reported at Site 1011, representing diagenetic dissolution of magnetic minerals (see "Paleomagnetism" section, "Site 1011" chapter, this volume). The pelagic sediment of Site 1016 is characterized by magnetic susceptibilities smaller than the ones of Site 1011 (see "Physical Properties" section, this chapter). Reduction diagenesis of the diluted magnetic grains probably leads to the weak intensity of remanent magnetization, which is too low for measurement by the shipboard magnetometer.

COMPOSITE DEPTHS AND SEDIMENTATION RATES

Multisensor track (MST) data collected at 4-cm intervals from Holes 1016A through 1016D, and color reflectance data collected at

Table 8 (continued).

Zone	Core, section, interval	Depth (mbsf)	Abundance	Preservation	*Lychnocanoma nipponica sakai*	*Lychnocanoma nipponica nipponica*	*Phormostichoartus crustula*	*Phormostichoartus fistula*	*Phormostichoartus intermedium*	*Pseudocubus warreni*	*Pterocanium auritum*	*Pterocanium korotnevi*	*Pterocorys clausus*	*Pterocorys zancleus*	*Rhizosphaera antarctica*	*Rhopalastrum profunda*	*Siphocampe modeloensis*	*Sphaeropyle langii*	*Sphaeropyle robusta*	*Spongotrochus glacialis*	*Stauroxiphos communis*	*Stichocorys delmontensis*	*Stichocorys peregrina*	*Stylacontarium acquilonium*	*Stylatractus universus*	*Stylochlamidium venustum*	*Stylodictya validispina*	*Theocorys redondoensis*
	167-1016A																											
	1H-CC	7.6	C	G			T				R		F	F	F			F								R	R	
B. aquilonaris	2H-CC	17.7	A	G	R		R			R	R	F	C		C	R		C		R				R			R	
	3H-CC	26.6	A	G	F						R	R	A		F	R		C		R				C	F	F		
S. universus	4H-CC	36.1	A	G	F		R				R			R		R		C						F	R		F	
	5H-CC	45.6	A	G						R	F		F	C	F										F	R	R	
	6H-CC	55.1	C	G	F								R			R								C	F	R		
E. matuyamai	7H-CC	64.5	A	G					R						C	F								R	R		R	
	8H-CC	74.1	A	G						T				R		R		C		R				R	R	A	C	
	9H-CC	83.6	A	G	R				R		R				F									F	C	A	A	
S. langii	10H-CC	93.1	A	G						R		R			F			C								F	C	
	11X-CC	96.3	A	G					F	T					C			F									F	
	12X-CC	106.0	A	G						R		R			R	R									R	R	R	
	13X-CC	115.6	A	G	T		T									T							F	R	R	C	F	
	14X-CC	125.2	C	G			T		R							T			T				C			F	F	
	15X-CC	134.8	A	G	R				C						R	R			T						C	R		
	16X-CC	144.4	C	G	R		R									R								R	C	C		
	17X-CC	154.0	C	G			F									R							C			C	C	
	18X-CC	163.6	R	M																				R	R			
	19X-CC	173.2	F	G											R		T						R			R	R	
	20X-CC	182.8	A	G						R										R			A		R		R	
	21X-CC	192.3	A	G											R								R	R	R		R	
S. peregrina	22X-CC	202.1	C	G				T		T					F													
	23X-CC	211.7	F	G			T			R					F												F	
	24X-CC	221.3	C	G		R				R	R												F		R	F	R	T
	25X-CC	230.9	C	G						F					R					T			C		R	R	R	
	26X-CC	240.6	F	G						C													R					T
	27X-CC	250.2	R	G											R								R		R			
	28X-CC	259.8	F	G		T									R		R					R	A					
	29X-CC	269.5	F	G																		R	A		R		C	
	30X-CC	279.2	C	G		R				R						R									R		R	
	31X-CC	288.8	A	G		F									A						A		R		R	R	C	
	32X-CC	298.4	R	M																		R	R					
	33X-CC	308.0	R	B																								

6- to 10-cm intervals from Holes 1016A, 1016B, and 1016D were used to determine depth offsets in the composite section. On the composite depth scale (expressed as mcd, meters composite depth), features of the plotted MST and color reflectance data present in adjacent holes are aligned so that they occur at approximately the same depth. Working from the top of the sedimentary sequence, a constant was added to the mbsf (meters below sea floor) depth for each core in each hole to arrive at a mcd depth for that core. The depths offsets that compose the composite depth section are given in Table 11, also on CD-ROM, back pocket. Except for a core gap of unknown length at 172.6 mcd, continuity of the sedimentary sequence was documented for the upper 245 mcd.

GRAPE and color reflectance measurements were the primary parameters used for interhole correlation purposes. Magnetic susceptibility measurements were used in a few intervals to provide additional support for composite construction although, in general, these measurements were not as useful because of the low variability of the signal. Natural gamma-ray activity measurements were made throughout the entire section in Holes 1016A and 1016B, but the sampling interval of 12 cm was insufficient for interhole correlation.

The GRAPE, color reflectance, and magnetic susceptibility records used to verify core overlap for Site 1016 are shown on a composite depth scale in Figures 9, 10, and 11, respectively. The GRAPE data were used to identify intervals of voids and highly disturbed sediments (values less than 1.45 g/cm^3), and all MST and color reflectance data were culled from these intervals. The cores from Holes 1016A, 1016B, and 1016D provide nearly continuous overlap to about 245 mcd. There is a core gap of unknown length beginning at 172.6 mcd (between the bottom of Core 167-1016B-17H and the top of Core 167-1016A-18X). Although cores from Holes 1016A and 1016B were placed into composite depths over the interval from 173.2 to 244.8 mcd, the correlation between cores was poor in many cases (e.g., see the interval from 180–200 mcd in Fig. 9). The composite records suggest that up to 2.5 m of material may be missing between cores down to about 245 mcd, although the average gap is less than one meter. As there are no data to fill possible core gaps below 245 mcd, an assessment of core gap length below this depth is not possible.

Following construction of the composite depth section for Site 1016, a single spliced record was assembled from the aligned cores. Cores from Hole 1016B were used as the backbone of the sampling splice. Cores from Holes 1016A were used to splice across core gaps in Hole 1016B from 0 to 100 mcd and 160 to 245 mcd, and cores from Hole 1016D were used to splice across core gaps in Hole 1016B between 100 and 160 mcd. The composite depths were aligned so that tie points between adjacent holes occurred at exactly the same depths in meters composite depth. Intervals having significant disturbance or distortion were avoided if possible. The Site 1016 splice (Table 12,

Table 9. Radiolarians in Hole 1016B.

Zone	Core, section, interval	Depth (mbsf)	Abundance	Preservation	*Actinomma popofski*	*Anthocyrtidium pliocenica*	*Botryostrobus aquilonaris*	*Botryostrobus praetumidulus*	*Botryostrobus tumidulus*	*Clathrocyclas bicornis*	*Cycladophora bicincta*	*Cycladophora davisiana davisiana*	*Dictyophimus crisiae*	*Dictyophimus splendens*	*Eucyrtidium calvertense*	*Eucyrtidium erythromystax*	*Eucyrtidium matuyamai*	*Lamprocyclas hadros*	*Lamprocyrtis heteroporos*	*Lamprocyrtis neoheteroporos*	*Lamprocyrtis nigriniae*	*Lychnocanoma n. sakai*	*Phormostichoartus crustula*	*Pseudocubus warreni*	*Pterocanium auritum*	*Sphaeropyle langii*	*Sphaeropyle robusta*	*Stichocorys delmontensis*	*Stichocorys peregrina*	*Stylacontarium acquilonium*	*Stylatractus universus*
	167-1016B-																														
	1H-CC	1.8	C	M	A		A		C		A	A	R							T					F						
B. aquilonaris	2H-CC	11.3	A	G	A				C		A	A	C		F						A	R	T			R					
	3H-CC	20.8	R	M							R		R							T											
	4H-CC	30.3	A	G			C				A	A	F								A				R	A					C
S. universus	5H-CC	39.8	C	M			C	C				A	R					T			T	R		R		R					
	6H-CC	49.3	A	G				F		A	C	A	R				R			C					R	R	T				R
E. matuyamai	7H-CC	58.8	A	G	C		C			C	C	A	F				C	R	F	A		F			F	R				F	R
	8H-CC	68.3	A	G	C			C				A	R				R		R	A						R					R
	9H-CC	77.8	A	G						C	R	A							A	R					R	R					R
	10H-CC	87.3	A	G	A		F					A	R			R			A	A			F			R					F
S. langii	11H-CC	96.8	A	G				R		C		A	R			T			A	C		T	T	T			R				R
	12H-CC	106.3	A	G	A					A		A			R	R			R	C		R		R			C				F
	13H-CC	115.8	C	M						C				T	T				R	A											F
	14H-CC	125.3	C	M				C		C					C				F	A				R		R			R		A
	15H-CC	134.8	A	G	C			C		C			T		R			C	C				R						R		C
	16H-CC	144.3	A	G						C					C				A	A		R			R		R		R		
	17H-CC	153.8	A	G	C					C			T		C	T			C			R	R				R				C
	18H-CC	162.3	F	M		R				C									R									T	R		
S. peregrina	19H-CC	172.8	A	G		F													A			T		T			T		F		F
	20H-CC	182.3	C	G		C				F									C					T					R		
	21H-CC	191.8	C	G		R				C									C			R							R		
	22H-CC	201.3	F	G		R								T					A										C		
	23H-CC	210.8	F	G		R				C				T					A										R		

Note: See “Explanatory Notes” chapter for abbreviations.

Table 10. Radiolarian events in Holes 1016A and 1016B.

Event	Hole 1016A Top (mbsf)	Hole 1016A Base (mbsf)	Hole 1016B Top (mbsf)	Hole 1016B Base (mbsf)
LO *S. universus*	17.7	26.6	20.8	30.3
FO *L. nigriniae*	36.1	45.6	39.8	49.3
LO *L. heteroporos*	45.6	55.1	49.3	58.8
LO *E. matuyamai*	36.1	45.6	39.8	49.3
FO *E. matuyamai*	74.1	83.6	68.3	77.8
FO *C. d. davisiana*	106.0	115.6	106.3	115.8
LO *A. pliocenica*	144.4	154.0	153.8	162.3
LO *D. splendens*	182.8	192.3	191.8	201.3
LO *L. n. nipponica*	211.7	221.3		

Note: LO = last occurrence, FO = first occurrence.

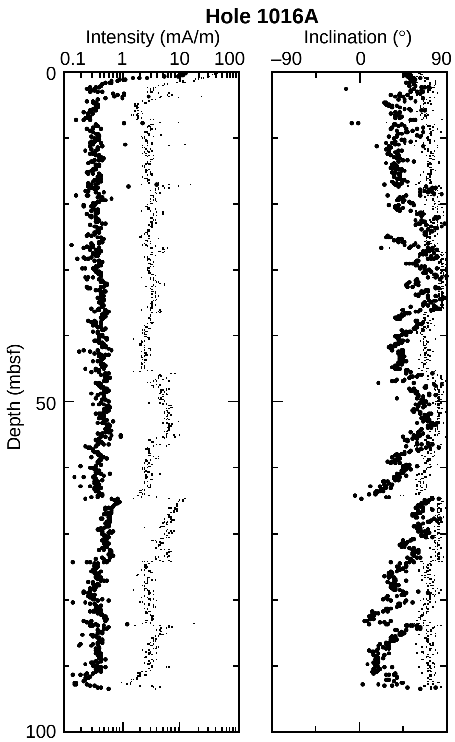

Figure 8. Plots of magnetic intensity and inclination of APC cores from Hole 1016A. Small and large dots represent magnetic intensity and inclination before and after AF demagnetization at 25 mT, respectively. The measurements of the upper 6 cores from Hole 1016B confirmed the results from Hole 1016A.

also on CD-ROM, back pocket) can be used as a sampling guide to recover a single continuous sedimentary sequence between 0 and 245 mcd (with the exception of a core gap at 172.6 mcd).

A preliminary age model (Table 13) was constructed to estimate sedimentation rates (Fig. 12). The age model was applied to the spliced records of GRAPE bulk density, magnetic susceptibility, and color reflectance shown in Figure 13.

INORGANIC GEOCHEMISTRY

We collected 14 interstitial water samples from Hole 1016A at depths ranging from 4.45 to 273.95 mbsf, with samples covering the three lithostratigraphic units defined at this site (see “Lithostratigraphy” section, this chapter). Chemical gradients in the interstitial waters at this site (Table 14) reflect organic matter diagenesis, the dissolution of biogenic opal and calcium carbonate, the diffusive influence

Table 11. Site 1016 composite depth section.

Core, section	Depth (mbsf)	Offset (m)	Depth (mcd)
167-1016A-			
1H-1	0.00	0.00	0.00
2H-1	7.60	0.48	8.08
3H-1	17.10	1.20	18.30
4H-1	26.60	1.60	28.20
5H-1	36.10	2.52	38.62
6H-1	45.60	2.74	48.34
7H-1	55.10	3.24	58.34
8H-1	64.60	4.54	69.14
9H-1	74.10	5.00	79.10
10H-1	83.60	6.62	90.22
11X-1	93.10	9.24	102.34
12X-1	96.30	9.78	106.08
13X-1	106.00	9.54	115.54
14X-1	115.60	12.43	128.03
15X-1	125.20	14.31	139.51
16X-1	134.80	17.15	151.95
17X-1	144.40	19.05	163.45
18X-1	154.00	19.05	173.05
19X-1	163.60	21.20	184.80
20X-1	173.20	23.96	197.16
21X-1	182.80	25.70	208.50
22X-1	192.50	28.56	221.06
23X-1	202.10	29.70	231.80
24X-1	211.70	29.70	241.40
25X-1	221.30	28.40	249.70
26X-1	230.90	28.40	259.30
27X-1	240.60	28.40	269.00
28X-1	250.20	28.40	278.60
29X-1	259.80	28.40	288.20
30X-1	269.50	28.40	297.90
31X-1	279.20	28.40	307.60
32X-1	288.80	28.40	317.20
167-1016B-			
1H-1	0.00	0.00	0.00
2H-1	1.80	1.90	3.70
3H-1	11.30	2.86	14.16
4H-1	20.80	2.94	23.74
5H-1	30.30	4.22	34.52
6H-1	39.80	5.14	44.94
7H-1	49.30	5.76	55.06
8H-1	58.80	6.28	65.08
9H-1	68.30	7.40	75.70
10H-1	77.80	7.88	85.68
11H-1	87.30	8.18	95.48
12H-1	96.80	9.24	106.04
13H-1	106.30	9.56	115.86
14H-1	115.80	12.26	128.06
15H-1	125.30	15.28	140.58
16H-1	134.80	16.97	151.77
17H-1	144.30	18.76	163.06
18H-1	153.81	22.92	176.73
19H-1	163.31	24.61	187.92
20H-1	172.81	26.78	199.59
21H-1	182.31	29.56	211.87
22H-1	191.81	32.34	224.15
23H-1	201.31	33.92	235.23
167-1016C-			
1H-1	0.00	–0.32	–0.32
2H-1	9.20	1.20	10.40
167-1016D-			
1H-1	0.00	0.00	0.00
2H-1	8.00	0.28	8.28
3H-1	17.50	1.12	18.62
4H-1	27.00	1.80	28.80
5H-1	36.50	3.26	39.76
6H-1	46.00	3.84	49.84
7H-1	55.50	4.66	60.16
8H-1	65.00	5.40	70.40
9H-1	74.50	5.40	79.90
10H-1	84.01	7.00	91.01
11H-1	93.51	7.02	100.53
12H-2	104.51	7.78	112.29
13H-1	112.51	10.72	123.23
14H-1	122.01	11.78	133.79
15H-1	131.51	12.61	144.12
16H-1	141.01	16.35	157.36

Note: This table is also on CD-ROM, back pocket, this volume.

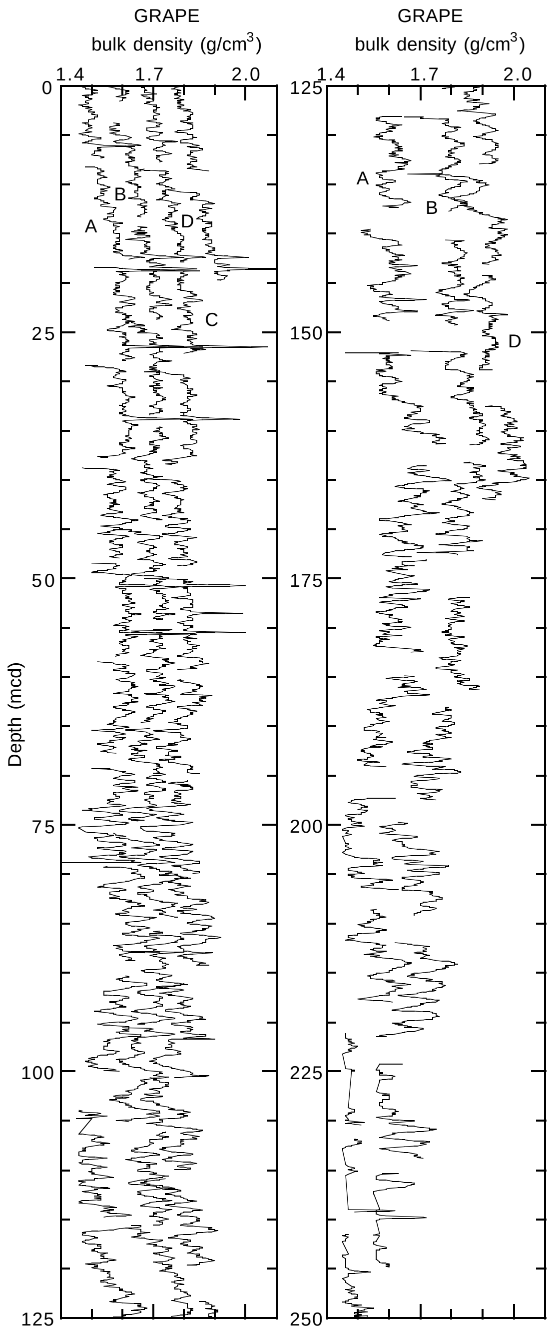

Figure 9. Smoothed (15-cm Gaussian) GRAPE bulk density data for the upper 250 m from Site 1016 on the mcd scale. Holes 1016A, 1016B, 1016D, and 1016C are offset from each other by a constant (0.1 g/cm^3).

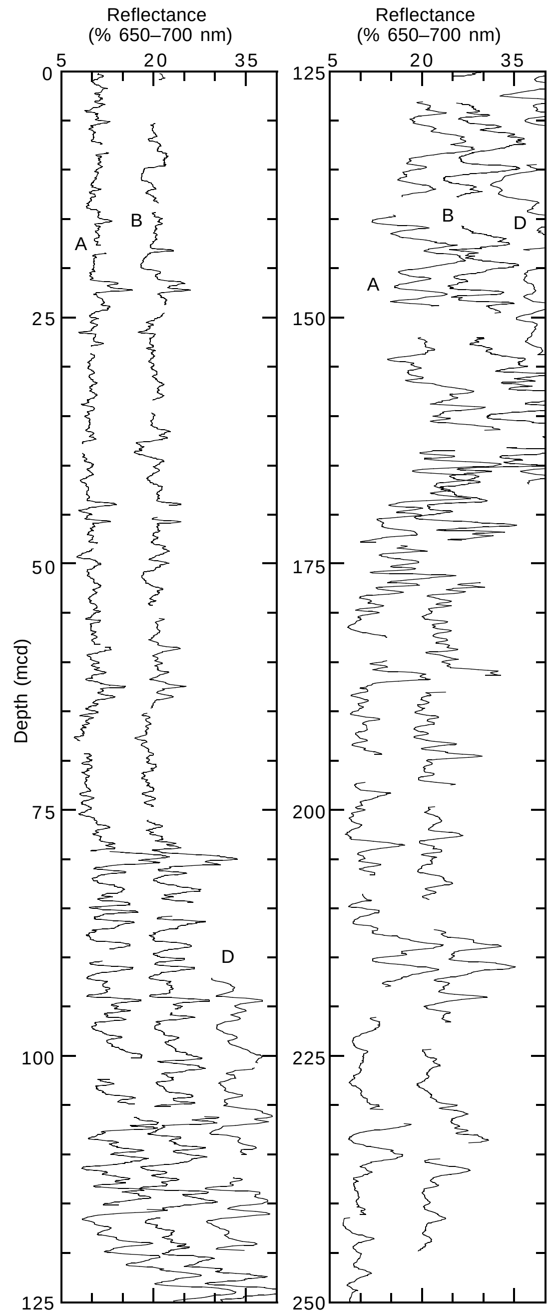

Figure 10. Smoothed (5-point running mean) color reflectance (% 650−700 nm band) data for the upper 250 m from Site 1016 on the mcd scale. Holes 1016A, 1016B, and 1016D are offset from each other by a constant (10%).

of reactions in underlying basalt, and the influence of authigenic mineral precipitation.

Chlorinity increases by 1.3% to a broad plateau from 31.05 to 100.75 mbsf, then decreases to values similar to those in the shallowest two samples by 129.65 mbsf (Fig. 14). Salinity, measured refractively as total dissolved solids, ranges from 31.5 to 35. Sodium concentrations measured by flame emission spectrophotometry were on average <4% higher than those estimated by charge balance (Table 14).

Alkalinity increases to peak values >17 mM from 40.55 to 50.05 mbsf, then decreases to 11.2 mM by 129.65 mbsf, with a further decrease to 6.8 mM at 273.95 mbsf (Fig. 14). Sulfate concentrations decrease to values below the detection limit (approximately 1 mM) by 78.55 mbsf. The two deepest samples at 245.05 and 273.95 mbsf have sulfate concentrations exceeding the detection limit, but these may be caused by slight contamination with drilling fluid. Phosphate concentrations increase to a maximum of 57 µM at 31.05–40.55 mbsf, then decrease steeply with increasing depth to 6 µM by 129.65 mbsf, with values of 2–3 µM at greater depth. The highest phosphate

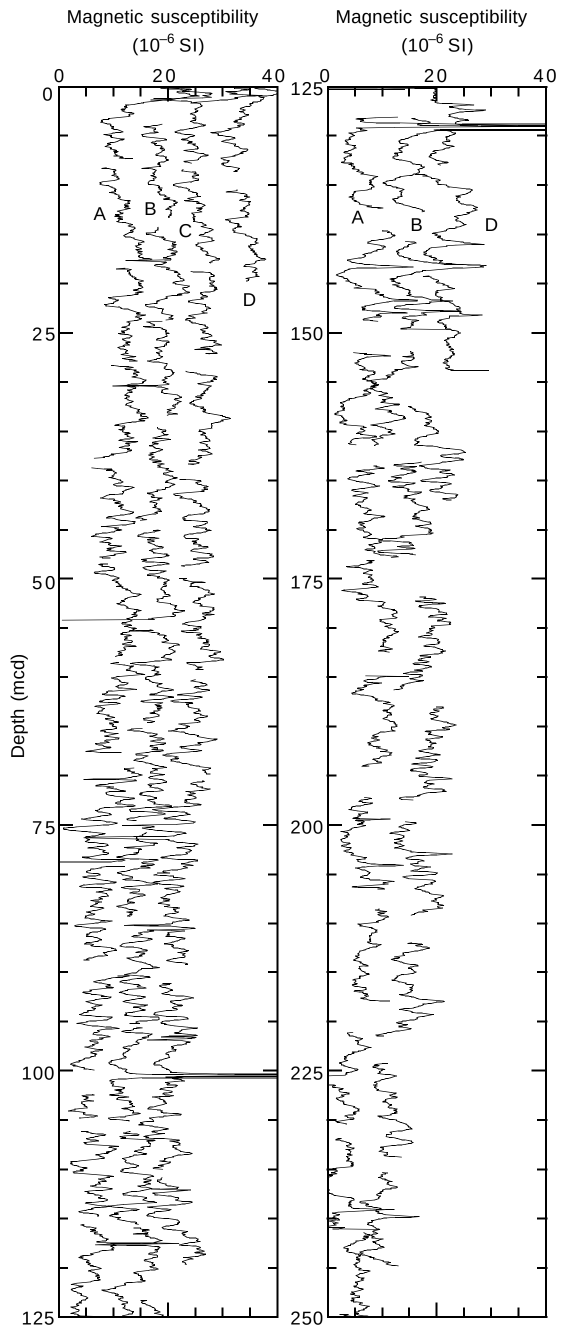

Figure 11. Smoothed (15-cm Gaussian) magnetic susceptibility data for the upper 250 m from Site 1016 on the mcd scale. Holes 1016A, 1016B, 1016C, and 1016D are offset from each other by a constant (10×10^{-6} SI).

concentrations are found just shallower than or coincident with the alkalinity maximum, with the steep declines in alkalinity and phosphate occurring over similar depth ranges. Ammonium concentrations increase with increasing depth to an average of 2.3 mM from 78.55 to 273.95 mbsf. Dissolved manganese concentrations are above the detection limit (2 µM) in only the four shallowest samples, decreasing from 18 µM at 4.45–12.05 mbsf to 8 µM at 21.55 mbsf and 4 µM at 31.05 mbsf, consistent with suboxic organic carbon diagenesis shallow in the section.

Dissolved silicate concentrations are relatively high (>800 µM) in the shallowest samples and increase with depth to values ≥1000 µM by 78.55 mbsf (Fig. 14), indicative of the dissolution of biogenic opal. Strontium concentrations increase with depth to >160 µM by 129.65 mbsf, consistent with the influence of the dissolution and/or recrystallization of calcium carbonate especially in the relatively calcium carbonate−rich lithostratigraphic Unit II.

Calcium concentrations decrease to 5.2 mM at 78.55 mbsf, with this minimum just below the zone of maximum alkalinity values, then increase with increasing depth to 13.2 mM in the deepest sample at 273.95 mbsf (Fig. 14), with an overall gradient of +4.1 mM/100 m. Magnesium concentrations decrease throughout the section to 26.1 mM at 273.95 mbsf, with an overall gradient of –8.9 mM/100 m. From 78.55 mbsf and deeper, the decrease in magnesium is linearly correlated with the increase in calcium, with a $\Delta Ca/\Delta Mg$ value of –0.80 ($R^2 = 0.92$), suggesting conservative behavior of these elements reflecting the diffusive influence of reactions in the underlying basalt. The decrease in dissolved calcium in the upper sediment, with a weaker positive correlation of calcium and magnesium decreases in this interval, indicates that authigenic mineral precipitation is significant in influencing the Ca profile in this depth range. Potassium decreases from values of around 11.0 mM in the shallowest samples to 8.6 mM at 273.95 mbsf (Table 14). Lithium concentrations increase with depth to 100 µM or greater from 158.45 to 273.95 mbsf (Fig. 14).

ORGANIC GEOCHEMISTRY

The organic geochemistry analyses performed at Site 1016 include measurements of elemental composition and volatile hydrocarbons (for methods see “Organic Geochemistry” section, “Explanatory Notes” chapter, this volume).

Volatile Hydrocarbons

As a part of the shipboard safety and pollution program, volatile hydrocarbons (methane, ethane, and propane) were routinely measured by gas chromatography in the sediments at Site 1016. Results are presented in Table 15. Headspace methane concentrations were near the limit of detection within the entire hole. Higher weight molecular hydrocarbons were not observed. The overall low methane content in these sediments indicates that environmental conditions were not favorable for methanogenesis.

Elemental Analysis

At Site 1016, 109 sediment samples were analyzed for total carbon, inorganic carbon, total nitrogen, and total sulfur (Table 16, also on CD-ROM, back pocket; Fig. 15).

The percentage of calcium carbonate ($CaCO_3$) was calculated from the inorganic carbon concentrations by assuming that all carbonate occurs in the form of calcite. $CaCO_3$ content varies between ~1 and 62 wt%, depending on the lithology (see “Lithostratigraphy” section, this chapter; Fig. 15). Lithostratigraphic Unit I (top–70 mbsf) and Unit III (165–299 mbsf) show low $CaCO_3$ content, while Unit II (70–165 mbsf) is characterized by higher content (15–60 wt%). Within the Pliocene section (Unit II), the carbonate is mainly composed of nannofossils and foraminifers. In this interval, the fluctuation of the carbonate record is probably caused by extensive dissolution of calcareous microfossils (see “Biostratigraphy” section, this chapter).

Total organic carbon (TOC) content varies between 0.20 and 2.79 wt% with high-amplitude fluctuation (Table 16; Fig. 15). The aver-

Table 12. Site 1016 splice tie points.

Hole, core, section, interval (cm)	Depth (mbsf)	Depth (mcd)		Hole, core, section, interval (cm)	Depth (mbsf)	Depth (mcd)
1016A-1H-5, 65	5.15	5.15	tie to	1016B-2H-1, 145	3.25	5.15
1016B-2H-6, 133	10.63	12.53	tie to	1016A-2H-3, 145	12.05	12.53
1016A-2H-7, 13	16.73	17.21	tie to	1016B-3H-3, 6	14.36	17.21
1016B-3H-7, 5	20.35	23.21	tie to	1016A-3H-4, 41	22.01	23.21
1016A-3H-6, 49	25.09	26.29	tie to	1016B-4H-2, 105	23.35	26.29
1016B-4H-6, 93	29.23	32.17	tie to	1016A-4H-3, 97	30.37	32.17
1016A-4H-6, 63	34.75	36.35	tie to	1016B-5H-2, 33	32.13	36.35
1016B-5H-7, 17	39.47	43.69	tie to	1016A-5H-4, 57	41.17	43.12
1016A-5H-5, 101	43.11	45.63	tie to	1016B-6H-1, 69	40.49	45.63
1016B-6H-6, 133	48.63	53.77	tie to	1016A-6H-4, 93	51.13	53.77
1016A-6H-6, 56	53.65	56.41	tie to	1016B-7H-1, 135	50.65	56.41
1016B-7H-6, 107	57.87	63.63	tie to	1016A-7H-4, 79	60.39	63.63
1016A-7H-5, 117	62.27	65.51	tie to	1016B-8H-1, 43	59.23	65.31
1016B-8H-6, 137	67.67	73.95	tie to	1016A-8H-4, 31	69.41	73.95
1016A-8H-6, 5	72.15	76.69	tie to	1016B-9H-1, 99	69.29	76.69
1016B-9H-6, 29	76.09	83.49	tie to	1016A-9H-3, 139	78.59	83.49
1016A-9H-6, 5	81.65	86.65	tie to	1016B-10H-1, 97	78.77	86.65
1016B-10H-7, 9	86.89	94.77	tie to	1016A-10H-4, 15	88.15	94.77
1016A-10H-5, 137	90.97	97.59	tie to	1016B-11H-2, 61	89.41	97.59
1016B-11H-7, 5	96.35	104.53	tie to	1016D-11H-3, 101	97.51	104.53
1016D-11H-5, 88	100.37	107.39	tie to	1016B-12H-1, 135	98.15	107.39
1016B-12H-6, 65	104.95	114.19	tie to	1016D-12H-3, 41	106.41	114.19
1016D-12H-5, 15	109.15	116.93	tie to	1016B-13H-1, 107	107.27	116.93
1016B-13H-6, 101	114.81	124.37	tie to	1016D-13H-1, 115	113.65	124.37
1016D-13H-5, 35	118.85	129.57	tie to	1016B-14H-2, 1	117.31	129.57
1016B-14H-6, 5	123.35	135.61	tie to	1016D-14H-2, 33	123.83	135.61
1016D-14H-6, 35	129.85	141.63	tie to	1016B-15H-1, 105	126.35	141.63
1016B-15H-5, 137	132.67	147.95	tie to	1016D-15H-3, 84	135.34	147.95
1016D-15H-6, 115	140.15	152.76	tie to	1016B-16H-1, 99	165.78	152.76
1016B-16H-6, 105	143.35	160.32	tie to	1016D-16H-2, 147	143.97	160.32
1016D-16H-5, 15	147.15	163.50	tie to	1016B-17H-1, 44	144.74	163.50
1016B-17H-7, 49	153.79	172.55	append	1016A-18X-1, 0	154.00	173.05
1016A-18X-4, 47	158.97	178.02	tie to	1016B-18H-1, 130	155.10	178.02
1016B-18H-6, 143	162.73	185.65	tie to	1016A-19X-1, 110	164.70	185.65
1016A-19X-4, 131	169.41	190.36	tie to	1016B-19H-2, 95	165.75	190.36
1016B-19H-7, 11	172.41	197.02	tie to	1016A-20X-1, 89	174.09	197.02
1016A-20X-5, 101	180.21	203.14	tie to	1016B-20H-3, 56	179.36	203.14
1016B-20H-7, 47	182.27	209.05	tie to	1016A-21X-1, 55	183.35	209.05
1016A-21X-4, 107	188.37	214.07	tie to	1016B-21H-2, 70	184.51	214.07
1016B-21H-7, 53	191.83	221.39	tie to	1016A-22X-1, 33	192.83	221.39
1016A-22X-7, 11	201.61	230.17	tie to	1016B-22H-5, 3	197.83	230.17
1016B-22H-7, 59	201.39	233.73	tie to	1016A-23X-1, 34	202.45	233.73
1016A-23X-3, 77	205.87	237.15	tie to	1016B-23H-2, 43	203.23	237.15
1016B-23H-7, 62	210.92	244.84				

Note: This table is also on CD-ROM, back pocket, this volume.

Table 13. Site 1016 sedimentation rate age control points.

Event	Composite depth (mcd)	Age (Ma)
T *P. lacunosa*	24.523	0.460
T *R. matuyamai*	43.370	0.975
B *G. oceanica*	69.770	1.690
T *D. brouweri*	84.765	1.960
T *T. convexa*	117.340	2.400
T *A. pliocenica*	174.610	3.360
T *R. pseudoumbilicus*	178.235	3.790
B *Ceratolithus* spp.	192.660	5.025
T *D. splendens*	221.070	5.900
T *L. n. nipponica*	246.200	6.250

Note: T = top, B = bottom.

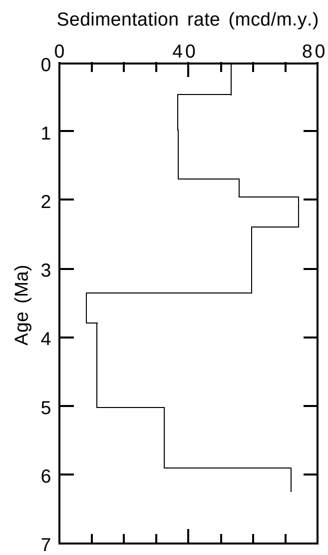

Figure 12. Sedimentation rate vs. age at Site 1016 based on the age control points from Table 13.

age value of TOC at this site is 0.93 wt%, which is much higher than that of normal open ocean sediment (~0.3 wt%). The high TOC value at 154 mbsf is attributed to a high proportion of terrigenous organic matter, based on its relatively high TOC/TN ratio (Table 16). In contrast, the organic matter in the high TOC interval between 36 and 93 mbsf shows low TOC/TN ratio, indicating a predominantly marine origin (Bordovskiy, 1965; Emerson and Hedges, 1988).

Total nitrogen contents vary between 0.07 and 0.39 wt%. Total sulfur content ranges from 0 to ~2.02 wt% (Table 16). To characterize the type of organic matter in the sediments, total organic carbon/total nitrogen (TOC/TN) ratios were used. Most of the TOC/TN ra-

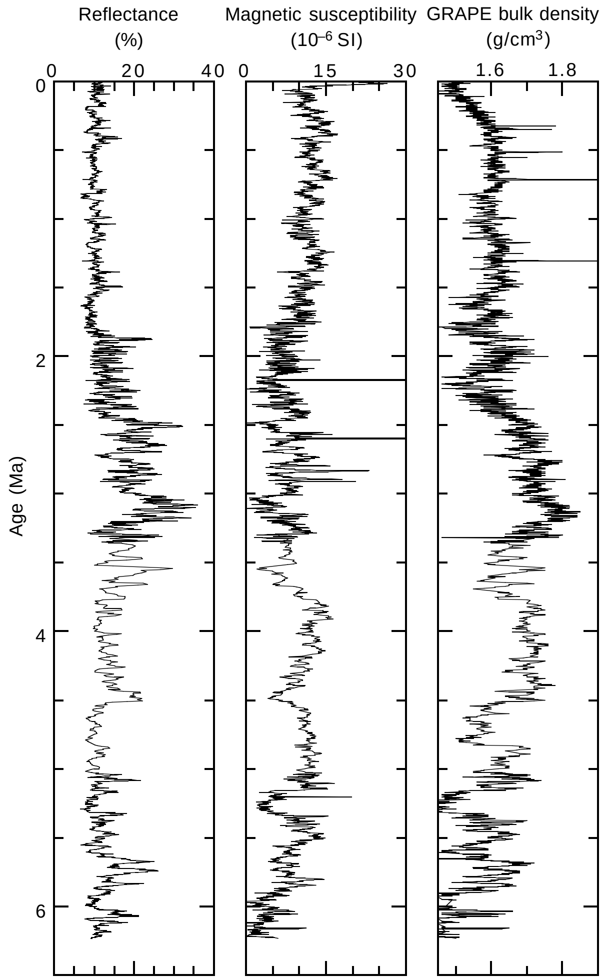

Figure 13. Spliced records of Site 1016 color reflectance, magnetic susceptibility, and GRAPE bulk density vs. age based on age control points from Table 13.

tios range between 3 and 10, which indicates a predominantly marine origin of the organic material (Bordovskiy, 1965; Emerson and Hedges, 1988). However, the downcore increasing fluctuation of the TOC/TN values likely points to a more heterogeneous organic matter composition.

PHYSICAL PROPERTIES

Multisensor Track Measurements

The shipboard physical properties program at Site 1016 included nondestructive measurements of bulk density, magnetic susceptibility, *P*-wave velocity, and natural gamma-ray activity on whole sections of all cores using the MST. Magnetic susceptibility was measured at 4-cm intervals at low sensitivity (1-s measuring time) on all Site 1016 cores. GRAPE bulk density measurements were made at 4-cm intervals on all Site 1016 cores. PWL velocity measurements were made at 4-cm intervals on cores from Holes 1016A through 1016C. The PWL was not run on cores from Hole 1016D. Natural gamma-ray activity was measured with a 15-s count every 12 cm on cores from Holes 1016A through 1016C but not run on cores from Hole 1016D.

High values of PWL velocity and GRAPE density correspond well with reflections from the 3.5-kHz precision depth recorder (PDR) profile acquired aboard *JOIDES Resolution* during the Site 1016 survey (Fig. 16). Abrupt changes in PWL velocity and GRAPE density (Fig. 16), which correspond to some nannofossil-rich zones and several sandy turbidite layers (see “Lithostratigraphy” section, this chapter), appear to generate the reflectors seen in the 3.5-kHz PDR site-survey record.

Index Properties

Index properties measurements were made at one sample per working section from Hole 1016A and every 4 cm throughout Core 167-1016B-17H. Index properties of bulk density and the index properties void ratio, porosity, water-content, dry bulk density, and grain density were determined by the gravimetric Method C (see “Physical Properties” section, “Explanatory Notes” chapter, this volume) and are presented in Figure 17 (Table 17 on CD-ROM in the back pocket of this volume). At about 140 mbsf there is a marked increase in GRAPE density (Fig. 18B) that corresponds to an increase in calcium carbonate content. At about 180 mbsf density and magnetic susceptibility values begin fluctuating because of the interbedded diatomaceous and nannofossil-rich sediments (see “Lithostratigraphy” section, this chapter). To better determine the validity and cause of the geophysical signals measured by the MST, Core 167-1016B-17H was sampled for index properties every 4 cm (Table 17) at the intervals chosen to coincide with GRAPE density and magnetic susceptibility measurements. This core was chosen because it corresponds to a depth interval that displays a great range in amplitude in many physical properties. There is an excellent correlation between GRAPE and index property bulk density and between porosity and intensity of color CIELAB L* (Fig. 19).

Compressional-Wave Velocity

Discrete *P*-wave velocity measurements were made in each section of Hole 1016A cores to approximately 33 mbsf and three per core from 33 mbsf to the base of the hole. The digital sound velocimeter was used to measure sonic velocity parallel to bedding in the first four cores of Hole 1016A by using both the insertable probes (T2, in the y-direction) and the Hamilton Frame (T3, in the z-direction). Velocity values from T2 measurements range from 1494 to 1524 m/s, averaging 1509 m/s, whereas velocity measurements from T3 range from 1510 to 1548 m/s, averaging 1531 m/s (Table 18 on CD-ROM in the back pocket of this volume). Average velocity values measured using the Hamilton Frame (T3) are more than 20 m/s higher than those from the T2 probes. This increase is most likely due to sediment compression from applying pressure between the transducers and sediment in order to achieve the contact necessary to propagate energy.

Heat Flow

Thermal conductivity was measured to 91.85 mbsf in Hole 1016A (Table 19 on CD-ROM in the back pocket of this volume). Three downhole temperature measurements were taken with the APC Adara temperature tool in Hole 1016A: 4.9°C at 36.1 mbsf, 7.0°C at 55.1 mbsf, and 9.0°C at 74.1 mbsf in Cores 167-1016A-4H, 6H, and 8H, respectively (Fig. 20). Bottom-water temperature was measured on all runs, indicating a bottom-water temperature of 1.3°C ± 0.1°C. The four data points yield a thermal gradient of 105°C/km (Fig. 21). Using an average measured thermal conductivity of 0.838 W/(m·K) provides a heat-flow estimate of 88 mW/m^2 at Site 1016.

Color Reflectance

Reflectance measurements were made at 4- to 6-cm intervals in Holes 1016A, 1016B, and 1016D. Using band averages of reflectance, we were able to simulate the lithostratigraphic units (see

Table 14. Interstitial water geochemical data, Hole 1016A.

Core, section, interval (cm)	Depth (mbsf)	pH	Alkalinity (mM)	Salinity	Cl^- (mM)	Na^+ (mM)	SO_4^{2-} (mM)	HPO_4^{2-} (μM)	NH_4^+ (mM)	H_4SiO_4 (μM)	Ca^{2+} (mM)	Mg^{2+} (mM)	Sr^{2+} (μM)	Li^+ (μM)	K^+ (mM)
167-1016A-															
1H-4, 135–140	4.45	7.53	6.41	34.5	553	479	25.7	27	0.34	804	10.0	50.4	84	23	10.8
2H-3, 145–150	12.05	7.46	10.6	35.0	549	473	19.8	53	0.81	848	8.93	48.8	89	24	11.0
3H-3, 145–150	21.55	7.60	13.7	34.0	555	480	14.7	51	1.23	858	7.26	46.6	94	27	10.8
4H-3, 145–150	31.05	7.53	15.9	34.0	558	482	10.3	57	1.45	875	6.64	44.3	98	27	10.6
5H-3, 145–150	40.55	7.66	17.1	34.0	558	481	7.1	57	1.68	949	6.02	42.9	108	30	10.3
6H-3, 145–150	50.05	7.70	17.3	33.0	554	478	4.9	49	1.78	993	5.55	41.1	112	34	10.2
9H-3, 145–150	78.55	7.30	15.5	32.0	558	480	<1	26	2.20	1000	5.15	36.7	136	49	10.3
12X-3, 145–150	100.75	7.25	13.8	32.0	556	481	<1	15	2.33	1033	6.38	33.3	154	68	9.6
15X-3, 145–150	129.65	7.13	11.2	32.0	554	478	<1	6	2.41	1125	7.81	30.7	164	87	9.9
18X-3, 145–150	158.45	7.26	10.3	32.0	548	473	<1	3	2.29	1174	8.84	29.4	164	99	9.1
21X-3, 145–150	187.25	7.24	9.51	31.5	553	475	<1	3	2.40	1174	10.2	29.0	164	103	9.2
24X-3, 145–150	216.15	7.33	9.66	32.0	547	469	<1	4	2.16	1318	11.8	27.6	168	104	9.0
27X-3, 145–150	245.05	7.43	8.88	32.0	552	475	1.3	3	2.38	1433	12.8	26.8	168	100	9.0
30X-3, 145–150	273.95	7.30	6.84	35.0	547	470	1.5	3	2.30	1482	13.2	26.1	173	98	8.6

"Lithostratigraphy" section, this chapter). A summary for the 450–500 nm (blue) band from Hole 1016A is given in Figure 22A. In lithostratigraphic Unit I, which consists of interbedded silty clay, diatom ooze, and diatom clay mixed sediments, color reflectance is generally low. As lithostratigraphic Unit I grades into Unit II, the proportion of nannofossils increases, and so does percent reflectance. Lithostratigraphic Subunit IIB, which is predominantly nannofossil ooze interbedded with diatom ooze, has the highest color reflectance of any stratigraphic unit at Site 1016. The signal of lithostratigraphic Subunit IIB is variable, however, with high reflectance values generally matching nannofossil-enriched layers and low values matching more diatomaceous zones. In lithostratigraphic Unit III, diatoms replace nannofossils as the dominant microfossil component, and color reflectance is low. The dark color of the diatom oozes and diatomites appears related to organic matter/pigmentation.

As at Site 1011, an attempt was made to predict opal content using a multiple linear regression equation generated from Leg 167 site-survey color reflectance and opal data. Unlike Site 1011, the results from the opal prediction are not consistent with the major lithostratigraphic units. This is most likely caused by the different spectra of diatomaceous sediments at the two sites. At Site 1011, diatomites show an absorbance peak near 650 nm and a steep positive reflectance slope in the red to infrared range (Fig. 30C, "Site 1011" chapter, this volume). The diatomites in lithostratigraphic Subunit IIIB at Site 1016, although displaying a subtle absorbance peak at 650 nm, have a much weaker positive reflectance slope in the longer wavelengths (Fig. 23C) than at Site 1011. Interbedded diatom nannofossil chalks of lithostratigraphic Subunit IIIB have a spectra with a negative slope and a curved pattern at wavelengths shorter than 600 nm (Fig. 23B).

In an effort to better quantify diatom-rich zones at Site 1016, we created a ratio using the 850–900-nm band (near-infrared) and the 450–500-nm (blue) band (Fig. 22B). This is analogous to the ratio between the near-infrared and 650–700-nm (red) bands used to detect diatomaceous sediments in the eastern equatorial Pacific (Mix et al., 1992). We chose to use near-infrared/blue at Site 1016 because it showed greater variance (mean = 1.13, standard deviation = 0.18) than near-infrared/red (mean = 0.99, standard deviation = 0.06). The near-infrared/blue ratio is generally greater where the diatom content is greatest (e.g., in lithostratigraphic Subunit IIA and Unit III). In lithostratigraphic Unit I and Subunit IIB, where clays and nannofossils predominate, the near-infrared/blue ratio is low. From 240 to 260 mbsf, the near-infrared/blue values correlate well with the compositional trends of interbedded diatomite and diatom nannofossil chalk (Fig. 23A). This result shows that color reflectance is sensitive to the spectral character of diatom-rich sediments or a sedimentary component that covaries with the diatom content at Site 1016.

The near-infrared/blue ratio therefore provides a means by which the frequency and relative intensity of the opal signal can be determined. To quantitatively predict opal content will require a calibration data set spanning a broad range of opal values, similar to the calcium carbonate data used for the calcite predictions at Sites 1012, 1013, and 1014.

Digital Color Video

All Site 1016 cores were also imaged with the ODP color digital imaging system 20-cm intervals, providing a 0.25-mm pixel. The video images from Holes 1016A, 1016B, and 1016D show (Fig. 24) hole-to-hole correlation of dark and light sediment color CIELAB L* (see "Physical Properties" section, "Explanatory Notes" chapter, this volume).

DOWNHOLE MEASUREMENTS

Logging Operations and Log Quality

Hole 1016A was logged with the density-porosity combination tool string, sonic-FMS, and GHMT tool strings after the hole was flushed of debris with a sepiolite pill and the drill pipe was set at 70 mbsf (Table 20). One full pass (pass 1: 109–313 mbsf) and two repeat passes (pass 2: 158–310 mbsf; pass 3: 0–195 mbsf) of the density-porosity combination tool string, one full pass of the FMS-sonic tool string (75–292 mbsf), and two passes of the GHMT tool string (pass 1: 65–285 mbsf; pass 2: 47–282 mbsf) were conducted (Table 20). Sea-state conditions were strong (3-m swells), and the wireline heave compensator was used on all passes.

Borehole caliper measurements conducted during the density-porosity combination and FMS-sonic passes indicate that the borehole was significantly washed out from the bottom of the hole to about 230 mbsf and moderately washed out from 230 to about 210 mbsf (Fig. 25). Overall log quality at this site is good, with the exception of the FMS data in the washed-out section below about 220 mbsf.

The TLT was run with the density-porosity combination tool string. The temperature logs were linked to the actual logging depths using the time-depth log recorded at the logging unit. The raw TLT results show a minimum downhole thermal gradient of 27.5°C/km (Fig. 26); this is an underestimate because of the cooling effect of seawater circulation. In situ temperature measurements using the Adara probe indicate a thermal gradient near 105°C/km at this site (see "Physical Properties" section, this chapter).

Lithology

A decrease in density and increase in porosity downhole, starting at about 150 mbsf, mark the transition from the more carbonate-rich sediments of lithostratigraphic Subunit IIB to the less carbonate-rich sediments of Subunit IIIA (Fig. 25; see "Lithostratigraphy" section, this chapter). The lowest density and highest porosity values occur

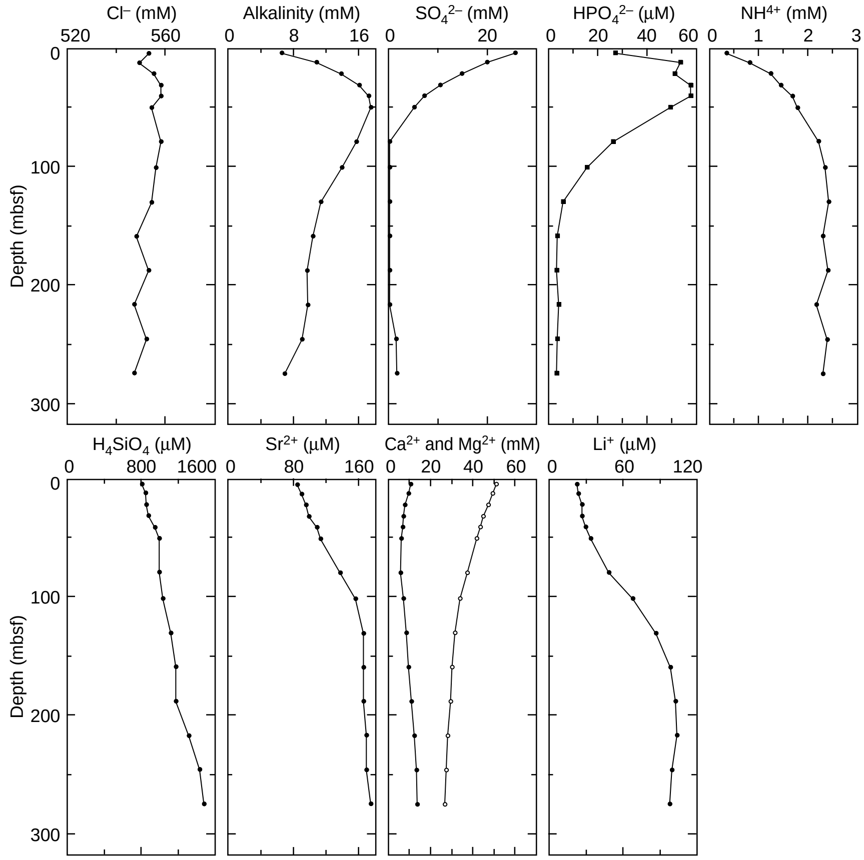

Figure 14. Interstitial water geochemical data, Site 1016. Solid circles = Ca, open circles = Mg.

Table 15. Concentrations of methane (C_1) obtained by the headspace technique from Hole 1016A.

Core, section, interval (cm)	Depth (mbsf)	C_1 (ppm)
167-1016A-		
1H-5, 0–5	6.03	113
2H-4, 0–5	12.13	16
3H-4, 0–5	21.63	12
4H-4, 0–5	31.13	6
5H-4, 0–5	40.63	10
6H-4, 0–5	50.13	5
7H-4, 0–5	59.63	9
8H-4, 0–5	69.13	9
9H-4, 0–5	78.63	11
10H-4, 0–5	88.13	10
11X-2, 0–5	94.63	7
12X-4, 0–5	100.83	9
13X-4, 0–5	110.53	9
14X-4, 0–5	120.13	12
15X-4, 0–5	129.73	14
16X-4, 0–5	139.33	15
17X-4, 0–5	148.93	11
18X-4, 0–5	158.53	10
19X-4, 0–5	168.13	14
20X-4, 0–5	177.73	6
21X-4, 0–5	187.33	8
22X-4, 0–5	197.03	9
23X-4, 0–5	206.63	7
24X-4, 0–5	216.23	6
25X-4, 0–5	225.83	6
26X-4, 0–5	235.43	7
27X-4, 0–5	245.13	6
28X-4, 0–5	254.73	4
29X-4, 0–5	264.33	4
30X-4, 0–5	274.03	4
31X-4, 0–5	283.73	5
32X-4, 0–5	293.33	4

below 200 mbsf, where the highest relative amount of biogenic opal was found, particularly in Subunit IIIB. The chert layer at the bottom of the hole is reflected by high density and resistivity values and low porosity values below 290 mbsf. Gamma-ray peaks are centered at 165 and 225 mbsf, coincident with intervals of highest clay content as described in the "Lithostratigraphy" section (this chapter).

Comparison of Core and Log Data

The core and log measurements of sediment bulk density are similar over their common interval, particularly below 230 mbsf, where the sediments are predominantly diatomites. Above 230 mbsf the core density data are lower than the log densities (Fig. 27). As observed at Hole 1014A, the core porosity data are significantly lower than the log (neutron) measurements because of elastic rebound caused by the release of lithostatic overburden during core recovery, and because the neutron log porosity data tend to overestimate porosity in clay- or opal-rich formations such as at Hole 1016A due to mineral-bound water. Comparison between the log natural gamma-ray activity and the core natural gamma-ray activity, between the log density and the core GRAPE density data, and between the log magnetic susceptibility and the core magnetic susceptibility data demonstrates that the logs can reliably reproduce first- and second-order features of the records generated from measurements of the sediments on the MST (Fig. 28). Detailed log-core comparison indicates that the log depth (mbsf) scale is offset from the core depth (mbsf) scale by ~2–3 m and that meter- and sub-meter-scale variations in the two sets of data are compressed or expanded relative to each other. Because log and core data appear highly correlated, the logs can be used to assess the degree of sediment elastic rebound and to quantify core gaps. For example, comparison of the log density record to the core GRAPE density splice record suggests that there is a 10%–27%

expansion of the sediment, and therefore of the mcd depth scale, relative to its true depth range on the mbsf scale (Fig. 29). In the core gap in the 150–175 mbsf section (see "Composite Depth and Sedimentation Rates" section, this chapter), 17% of the sedimentary sequence appears to be missing.

Discrete, high-resolution (every 4 cm) index property measurements of bulk density and porosity were made on Core 167-1016B-17H and compared with GRAPE bulk-density measurements and log density measurements from the same interval (Fig. 30). The discrete and GRAPE measurements clearly covary. The log data capture the main trends and variations measured in the discrete density and porosity measurements in the core, but the core is expanded relative to the log mbsf scale by approximately 15%. In addition, the high-frequency variations seen in the high-resolution log density record appear to correlate to the discrete, high-resolution core measurements, demonstrating that the log reliably records the variations measured in the sediments.

SUMMARY

Site 1016, the seaward site of the Conception transect, was intended to collect an almost complete Neogene sedimentary sequence while also providing paleoceanographic data near the core of the modern California Current. Late Miocene-age massive cherts encountered in the lower half of the sediment column prevented further drilling, however, and restricted our recovery to about the last 7.3 m.y. (Fig. 31). Four holes were drilled at the site to a maximum depth of 317 mbsf. Site 1016 was quadruple cored to 19 mbsf (~0.4 Ma), triple cored to 151 mbsf (~3.2 Ma), and double cored to 211 mbsf (~6.2 Ma). Continuous section could only be demonstrated to 154 mbsf, but this was the only core gap found throughout the double-cored section.

The sediment column is marked by the transition from silica-rich sediments at the Miocene/Pliocene boundary to a more calcium carbonate-rich Pliocene, similar to the sedimentary sequence at Site 1010. It also has a condensed lower Pliocene sediment column, similar to those at Sites 1012 and 1014. In addition, the Quaternary is typically much more rich in aluminosilicate and poor in calcium carbonate. This also is a typical feature of the other Leg 167 sites.

REFERENCES

Atwater, T., and Severinghaus, J., 1989. Tectonic map of the northeast Pacific Ocean. *In* Winterer, E.L., Hussong, D.M., and Decker, R.W. (Eds.) *The Eastern Pacific Ocean and Hawaii.* Geol. Soc. Am., Decade of North Am. Geol., Vol. N.

Barron, J.A., 1980. Upper Pliocene and Quaternary diatom biostratigraphy of Deep Sea Drilling Project Leg 54, tropical eastern Pacific. *In* Rosendahl, B.R., Hekinian, R., et al., *Init. Repts. DSDP,* 54: Washington (U.S. Govt. Printing Office), 455–485.

————, 1981. Late Cenozoic diatom biostratigraphy and paleoceanography of the middle-latitude eastern North Pacific, Deep Sea Drilling Project Leg 63. *In* Yeats, R.S., Haq, B.U., et al., *Init. Repts. DSDP,* 63: Washington (U.S. Govt. Printing Office), 507–538.

Barron, J.A., and Baldauf, J.G., 1986. Diatom stratigraphy of the lower Pliocene part of the Sisquoc Formation, Harris Grade section, California. *Micropaleontology,* 32:357–371.

Barron, J.A., and Gladenkov, A.Y., 1995. Early Miocene to Pleistocene diatom stratigraphy of Leg 145. *In* Rea, D.K., Basov, I.A., Scholl, D.W., and Allan, J.F. (Eds.), *Proc. ODP, Sci. Results,* 145: College Station, TX (Ocean Drilling Program), 3–19.

Bordovskiy, O.K., 1965. Accumulation and transformation of organic substances in marine sediment, 2. Sources of organic matter in marine basins. *Mar. Geol.,* 3:5–31.

Emerson, S., and Hedges, J.I., 1988. Processes controlling the organic carbon content of open ocean sediments. *Paleoceanography,* 3:621–634.

Ingle, J.C., Jr., 1973. Summary comments on Neogene biostratigraphy, physical stratigraphy, and paleo-oceanography in the marginal northeastern Pacific Ocean. *In* Kulm, L.D., von Huene, R., et al., *Init. Repts. DSDP,* 18: Washington (U.S. Govt. Printing Office), 949–960.

Koizumi, I., 1992. Diatom biostratigraphy of the Japan Sea: Leg 127. *In* Pisciotto, K.A., Ingle, J.C., Jr., von Breymann, M.T., Barron, J., et al., *Proc. ODP, Sci. Results,* 127/128 (Pt. 1): College Station, TX (Ocean Drilling Program), 249–289.

Lyle, M., Gallaway, P.J., Liberty, L.M., Mix, A., Stott, L., Hammond, D., Gardner, J., Dean, W., and the EW9504 Scientific Party, 1995a. Data submission. W9406 and EW9504 site surveys of the California margin proposed drillsites, Leg 167 (Vol. 1): site maps and descriptions. Boise State Univ., *CGISS Tech. Rep.,* 95–11.

————, 1995b. Data submission. W9406 and EW9504 site surveys of the California margin proposed drillsites, Leg 167 (Vol. 2): seismic profiles. Boise State Univ., *CGISS Tech. Rep.,* 95–12.

Mix, A.C., Rugh, W., Pisias, N.G., Veirs, S., Leg 138 Shipboard Sedimentologists (Hagelberg, T., Hovan, S., Kemp, A., Leinen, M., Levitan, M., Ravelo, C.), and Leg 138 Scientific Party, 1992. Color reflectance spectroscopy: a tool for rapid characterization of deep-sea sediments. *In* Mayer, L., Pisias, N., Janecek, T., et al., *Proc. ODP, Init. Repts.,* 138 (Pt. 1): College Station, TX (Ocean Drilling Program), 67–77.

Roessler, C.S., and Chelton, D.B., 1987. Zooplankton variability in the California Current, 1951–1982. *CalCOFI Rep.,* 28:59–96.

Ms 167IR-110

NOTE: For all sites drilled, core-description forms ("barrel sheets") and core photographs can be found in Section 3, beginning on page 499. Smear-slide data can be found in Section 4, beginning on page 1327. See Table of Contents for material contained on CD-ROM.

Table 16. Concentrations of inorganic carbon, calcium carbonate, total carbon, total organic carbon, total nitrogen, total sulfur in weight percent (wt%) in Hole 1016A.

Core, section, interval (cm)	Depth (mbsf)	Inorganic carbon (wt%)	$CaCO_3$ (wt%)	Total carbon (wt%)	Total organic carbon (wt%)	Total nitrogen (wt%)	Total organic carbon/total nitrogen (wt%)	Total sulfur (wt%)
167-1016A-								
1H-1, 115–116	1.15	0.38	3.17	1.61	1.23	0.23	5.35	0.77
1H-3, 29–30	2.79	0.13	1.08	1.35	1.22	0.22	5.55	0.34
1H-5, 29–30	4.79	0.46	3.83	1.74	1.28	0.36	3.56	0.53
2H-1, 28–29	7.88	0.81	6.75	1.83	1.02	0.22	4.64	0.41
2H-3, 28–29	10.88	0.12	1	1.19	1.07	0.24	4.46	0.55
2H-5, 28–29	13.88	0.36	3	1.45	1.09	0.21	5.19	0.52
2H-7, 28–29	16.88	0.12	1	0.98	0.86	0.19	4.53	0.46
3H-2, 29–30	18.89	0.27	2.25	1.21	0.94	0.21	4.48	0.68
3H-4, 29–30	21.89	1.53	12.74	2.23	0.7	0.16	4.37	0.35
3H-6, 29–30	24.89	0.59	4.91	1.39	0.8	0.18	4.44	0.26

Only part of this table is produced here. The entire table is on CD-ROM, back pocket, this volume.

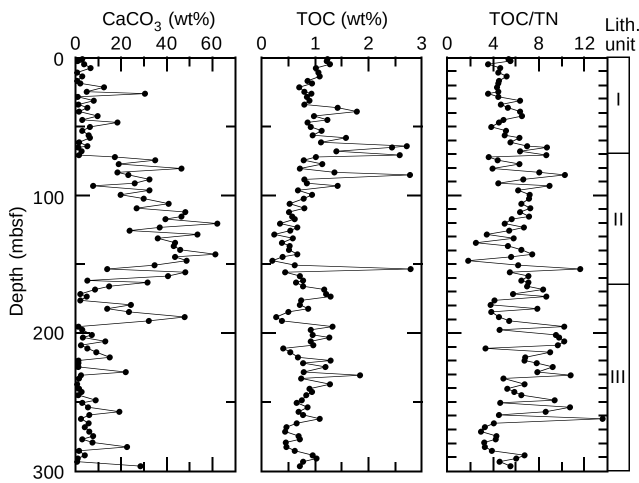

Figure 15. Depth variations of calcium carbonate, total organic carbon contents, and total organic carbon/total nitrogen ratio in sediments of Hole 1016A.

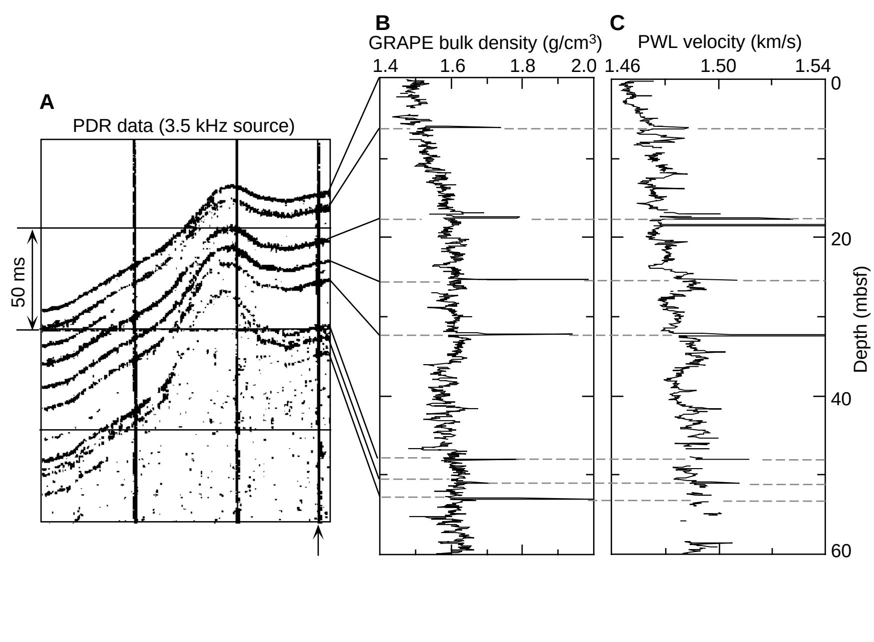

Figure 16. **A.** Shipboard 3.5-kHz PDR record acquired during the Site 1016 presite survey. The arrow marks the location where the beacon was dropped. Changes in (**B**) GRAPE bulk density and (**C**) PWL velocity from Hole 1016A mapped to seismic reflectors.

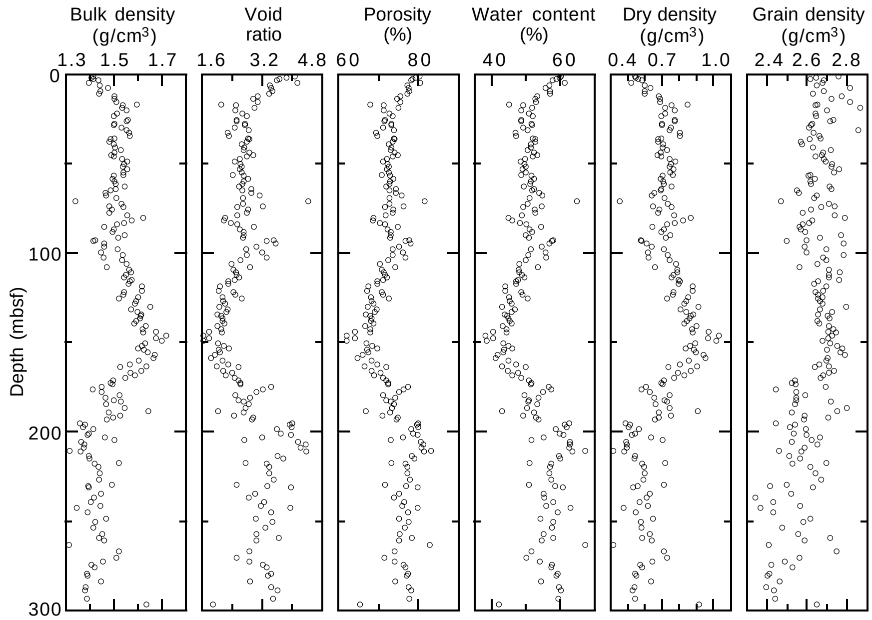

Figure 17. Index property data from Hole 1016A.

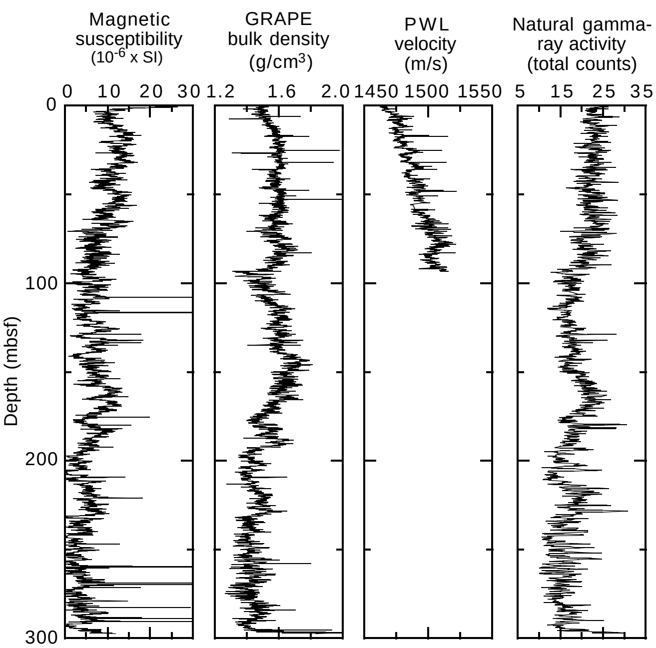

Figure 18. MST data from Hole 1016A.

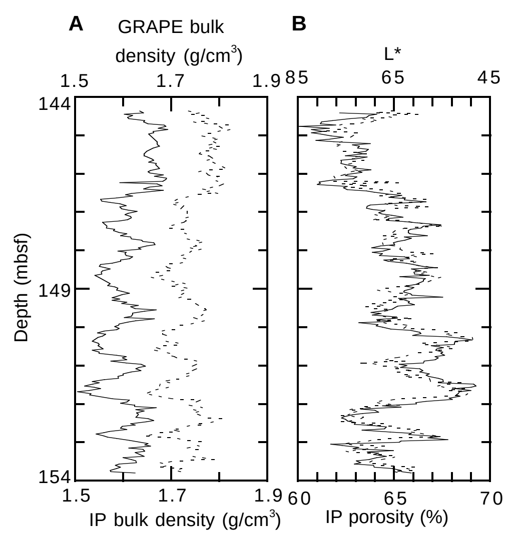

Figure 19. Correlation of index properties measured at 4-cm intervals in Core 167-1016B-17H. **A.** GRAPE bulk density (dashed line) with bulk density (solid line). **B.** Porosity (solid line) with intensity of color CIELAB L* (dashed line) smoothed over a 160-point running window.

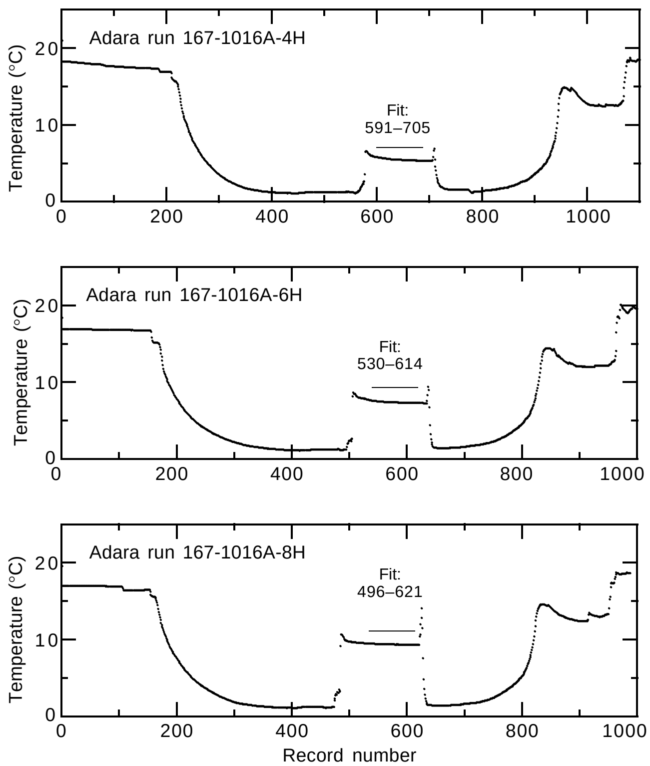

Figure 20. Hole 1016A downhole temperature vs. record number (5-s recording frequency) for each measurement run, showing the intervals fitted to determine the downhole temperature.

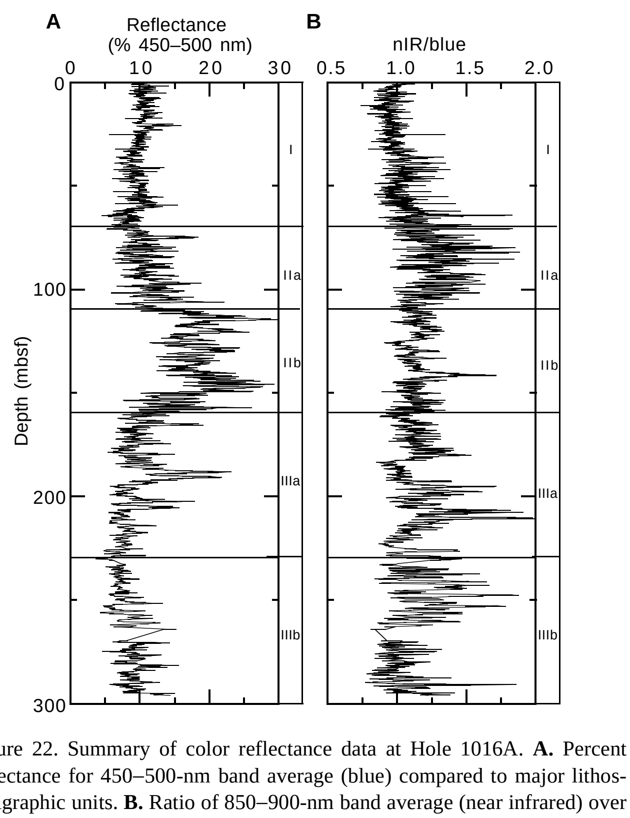

Figure 22. Summary of color reflectance data at Hole 1016A. **A.** Percent reflectance for 450–500-nm band average (blue) compared to major lithostratigraphic units. **B.** Ratio of 850–900-nm band average (near infrared) over 450–500 nm (blue).

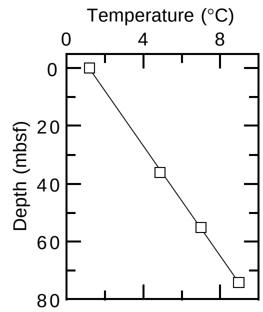

Figure 21. Downhole temperature gradient for Hole 1016A.

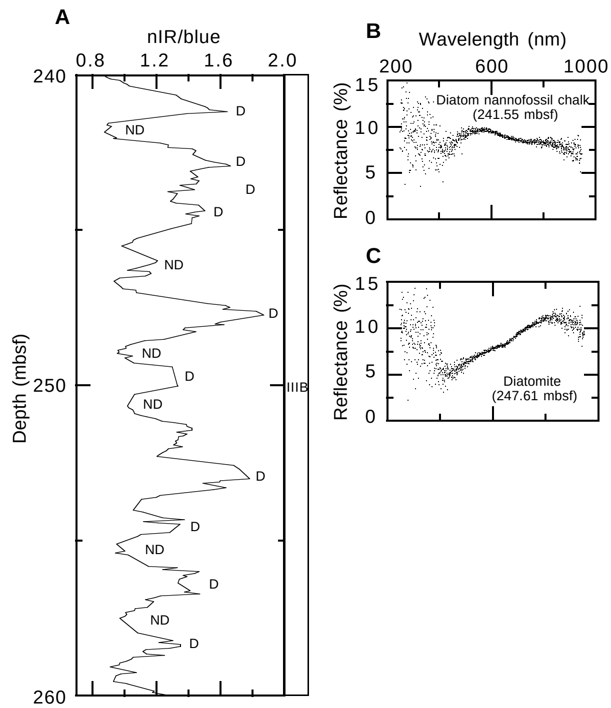

Figure 23. **A.** Ratio of near-infrared over blue reflectance from 240 to 260 mbsf compared to lithostratigraphic descriptions of Subunit IIIB. D = diatomite, ND = diatom nannofossil chalk. **B.** Spectra of diatom nannofossil chalk. **C.** Characteristic spectra of diatomite.

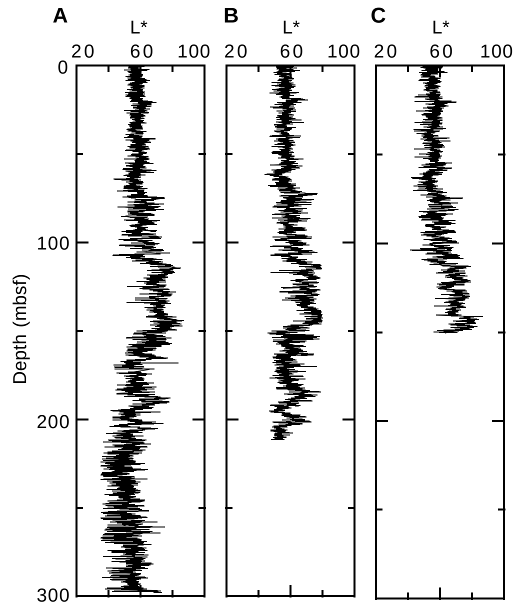

Figure 24. Intensity of color CIELAB L* from the digital color video data for Holes (**A**) 1016A, (**B**) 1016B, and (**C**) 1016D. Data were decimated at 2-cm intervals.

Table 20. Downhole measurements at Hole 1016A.

Date, time	Description
May 16, 1996	
1300	Set pipe at 77 mbsf, start wireline rig up, seas strong (3-m swell).
1400	Finish wireline rig up, RIH density-porosity combination tool string.
1600	At TD (317 mbsf), wireline heave compensator on, start density-porosity pass 1 (313–109 mbsf); 300 m/hr, stopped at base of pipe.
1700	At TD (317 mbsf), wireline heave compensator on, start density-porosity pass 2 (310–158), 300 m/hr; stopped because of temporary minitron failure.
1730	Begin pass 3 (195–70 mbsf), 300 m/hr, continue logging to mudline.
2000	POOH, rig down density-porosity, rig up and RIH with sonic-FMS toolstring.
2230	Begin sonic-FM pass 1 (292–75 mbsf) at 300 m/hr, wireline heave compensator on.
2330	End sonic-FM pass 1, POOH.
May 17, 1996	
0130	Rig up GHMT
0430	At TD with GHMT, begin pass 1 (285–65 mbsf) at 1000 m/hr.
0505	At TD with GHMT, begin pass 2 (282–47 mbsf) at 1000 m/hr.
0525	End GHMT pass 2, POOH GHMT, rig down.

Note: RIH = run in hole, TD = total depth, FMS = formation microscanner, POOH = pull out of hole, GHMT = geological high-sensitivity magnetic tool.

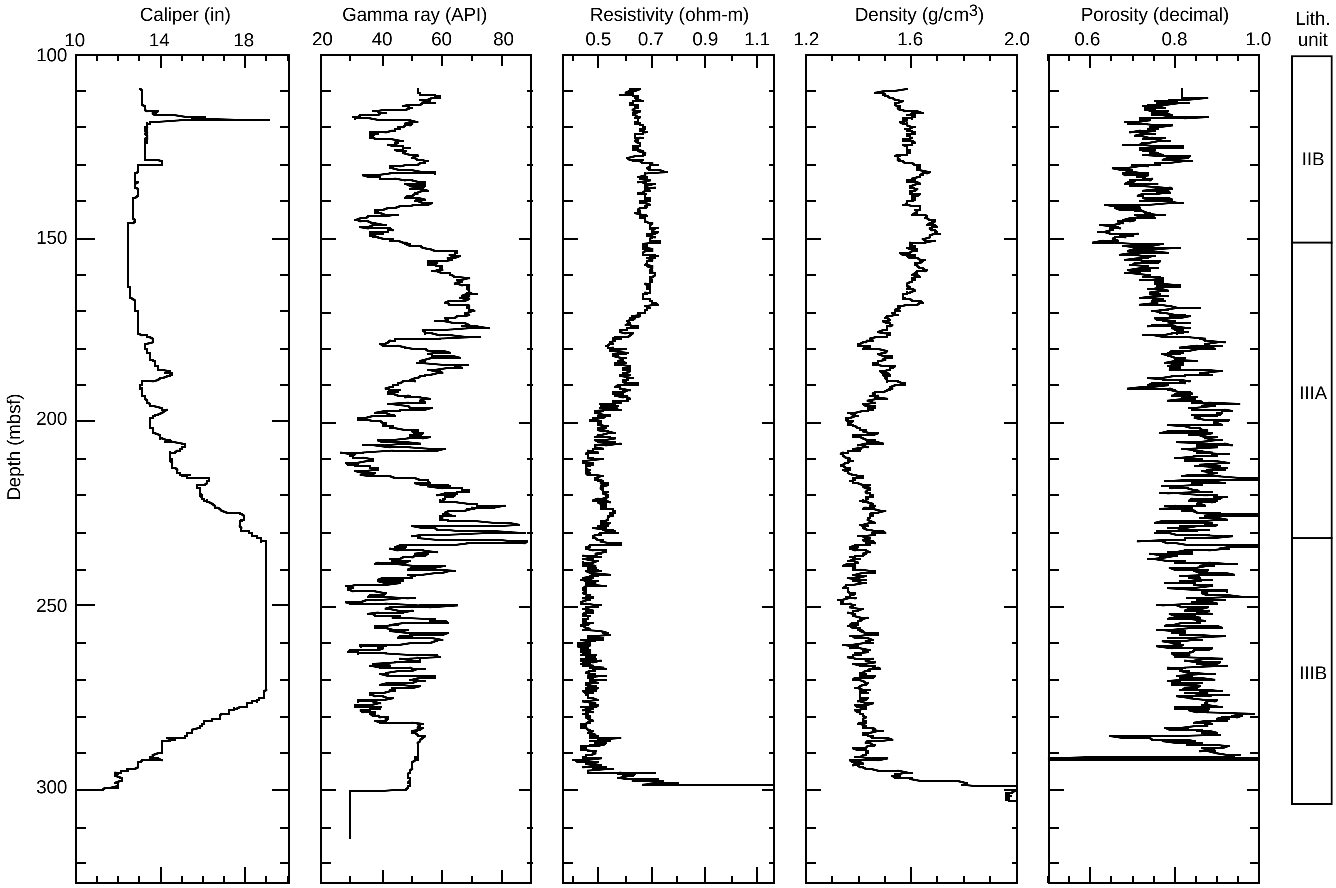

Figure 25. Downhole log data from the density-porosity tool string (pass 1) and a lithostratigraphic summary column at Hole 1016A (see "Lithostratigraphy" section, this chapter).

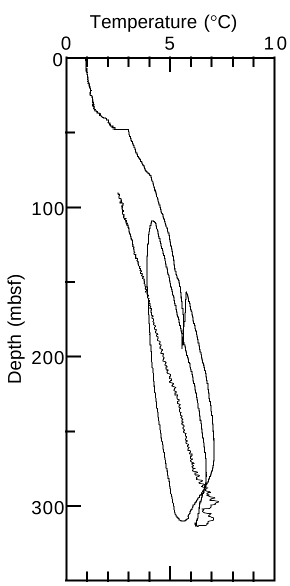

Figure 26. Borehole temperature measurements from the Lamont-Doherty temperature logging tool.

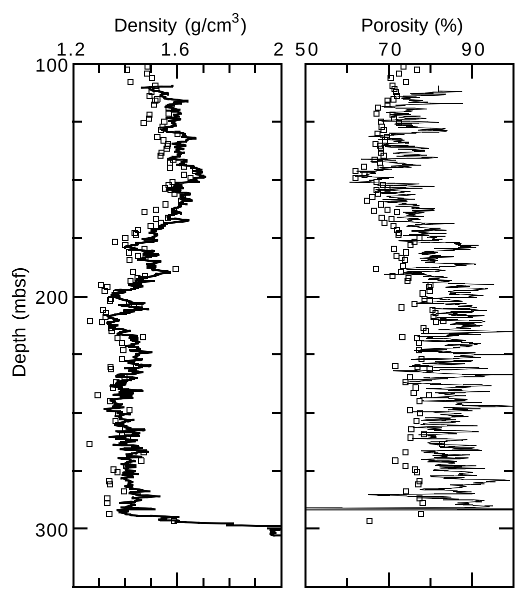

Figure 27. Density and neutron porosity log data for pass 1 (lines) compared to measured index properties (symbols).

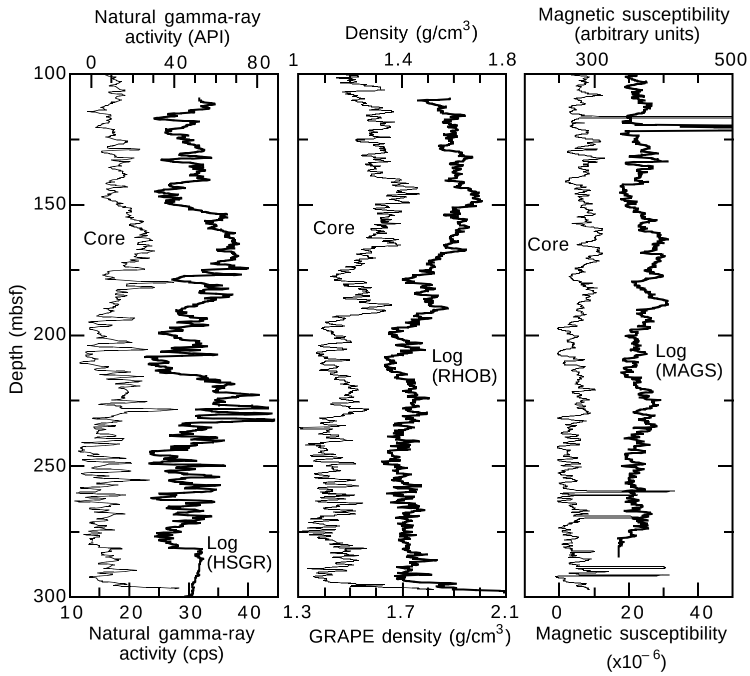

Figure 28. Comparison of core (MST) and log natural gamma ray, density, and magnetic susceptibility data at Hole 1016A using pass 1 of the density-porosity tool string and pass 1 of the GHMT tool string.

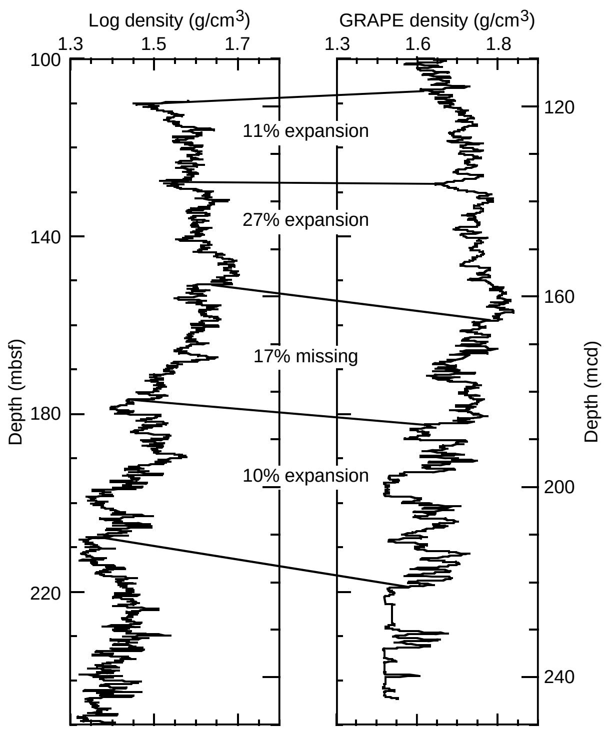

Figure 29. Comparison of the core GRAPE bulk density splice record and the log density record. Five tie points were made by matching major features found in both records, and the relative core expansion was calculated.

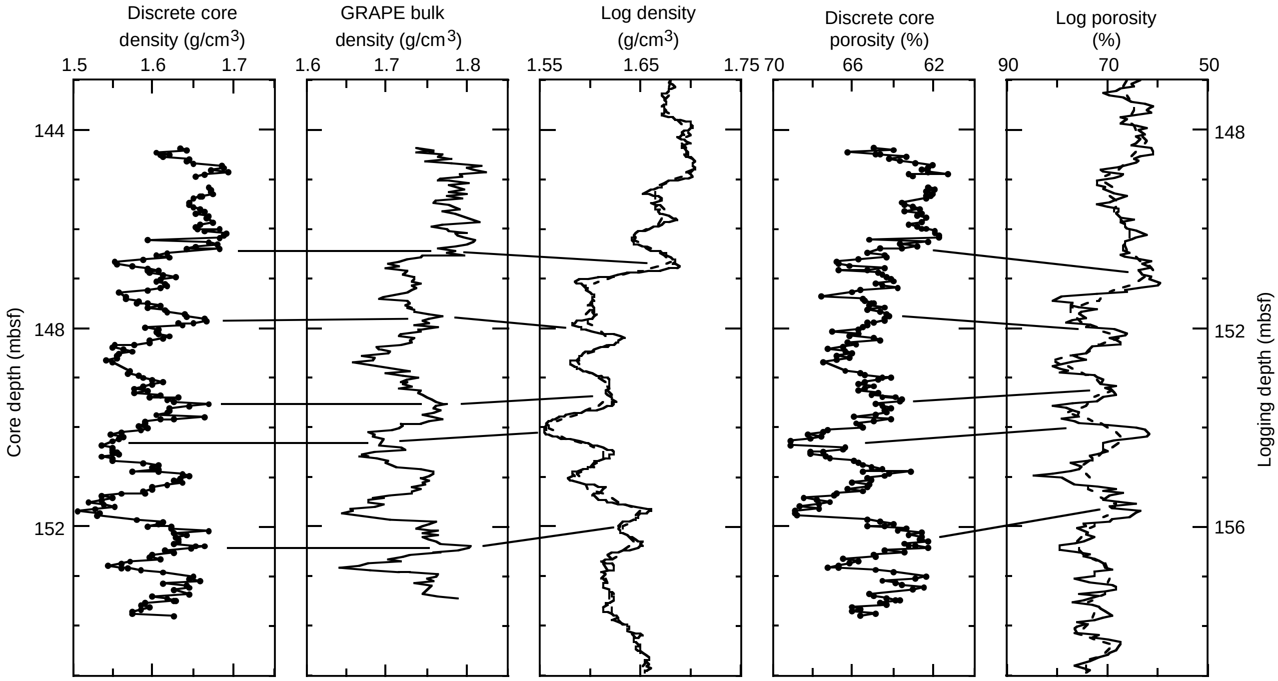

Figure 30. High-resolution index properties measurements of bulk density and porosity from Core 167-1016B-17H compared with GRAPE bulk density, log density, and porosity measurements.

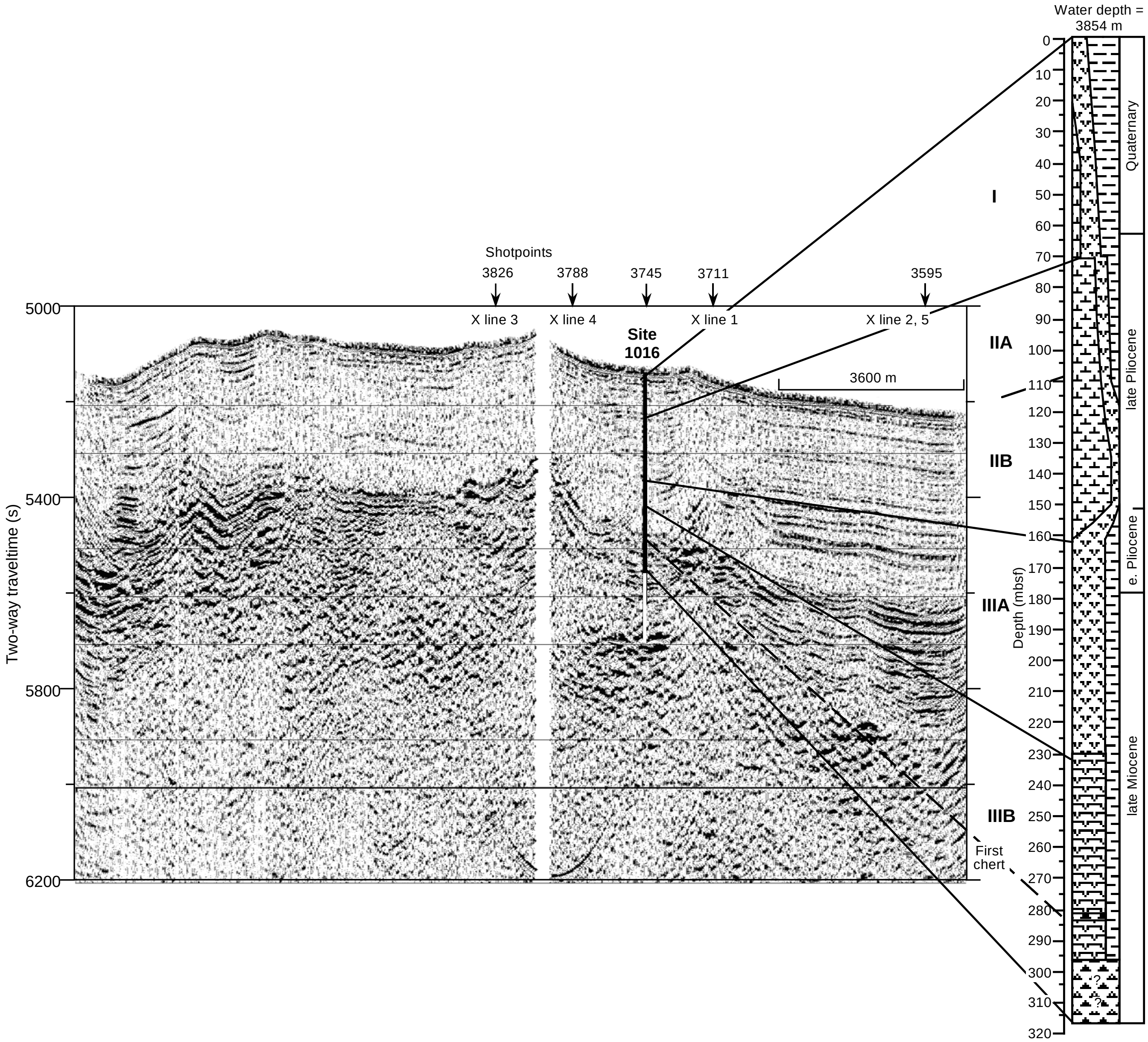

Figure 31. Comparison of the lithostratigraphic column at Site 1016 and a seismic profile through the site (Line EW9504 CA11-7; Lyle et al., 1995a, 1995b). Ties are calculated from shipboard velocity measurements (see "Physical Properties" section, this chapter). On y-axis, (s) = milliseconds.

SHORE-BASED LOG PROCESSING

HOLE 1016A

Bottom felt: 3845.4 mbrf (used for depth shift to seafloor)
Total penetration: 316.5 mbsf
Total core recovered: 303.7 m (95%)

Logging Runs

Logging string 1: DIT/HLDT/APS/HNGS (3 passes)
Logging string 2: FMS/GPIT/SDT/NGT
Logging string 3: GHMT/NGT (2 passes)

Wireline heave compensator was used to counter ship heave.

Bottom-Hole Assembly

The following bottom-hole assembly depths are as they appear on the logs after differential depth shift (see "Depth shift" section) and depth shift to the seafloor. As such, there might be a discrepancy with the original depths given by the drillers onboard. Possible reasons for depth discrepancies are ship heave, use of wireline heave compensator, and drill string and/or wireline stretch.

DIT/SDT/HLDT/APS/HNGS: Did not reach bottom-hole assembly (pass 1).

DIT/SDT/HLDT/APS/HNGS: Did not reach bottom-hole assembly (pass 2).

DIT/SDT/HLDT/APS/HNGS: Bottom-hole assembly at ~49.5 mbsf (pass 3).

FMS/GPIT/SDT/NGT: Did not reach bottom-hole assembly.

GHMT/NGT: Did not reach bottom-hole assembly (passes 1 and 2).

Processing

Depth shift: Original logs have been interactively depth shifted with reference to NGT from DIT/HLDT/APS/HNGS pass 1, and to the seafloor (–3845.4).

Gamma-ray and environmental corrections: Corrections for borehole size and type of drilling fluid were performed on the NGT data from the FMS/GPIT/SDT/NGT and GHMT/NGT tool strings. HNGS data from the DIT/HLDT/APS/HNGS tool string were corrected in real-time during the recording.

Acoustic data processing: The array sonic tool was operated in standard depth-derived, borehole compensated, long-spacing (8-10-10-12 ft) and short-spacing (3-5-5-7 ft) mode. Because of the poor quality of the transit times no processing has been performed.

Quality Control

Data recorded through bottom-hole assembly, such as the HNGS data above 50 mbsf (pass 3) should be used qualitatively only because of the attenuation on the incoming signal.

Hole diameter was recorded by the hydraulic caliper on the HLDT tool (CALI) and the caliper on the FMS string (C1 and C2).

Note: Details of standard shore-based processing procedures are found in the "Explanatory Notes" chapter, this volume. For further information about the logs, please contact:

Cristina Broglia
Phone: 914-365-8343
Fax: 914-365-3182
E-mail: chris@ldeo.columbia.edu

Amal Chakraborty
Phone: 914-365-6490
Fax: 914-365-3182
E-mail: amalc@ldeo.columbia.edu

Hole 1016A: Natural Gamma Ray-Density-Porosity Logging Data-Pass 1

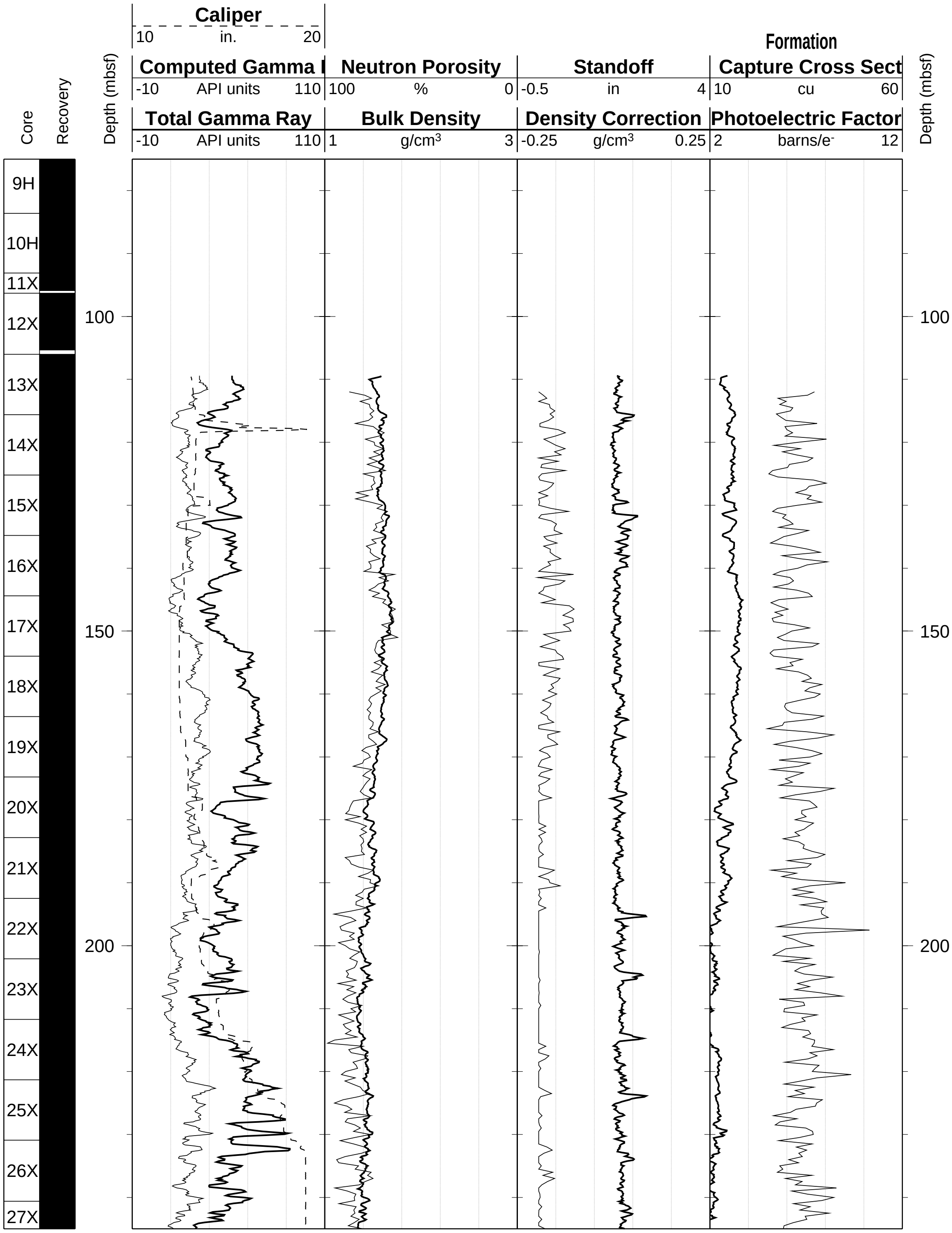

Hole 1016A: Natural Gamma Ray-Density-Porosity Logging Data-Pass 1 (cont.)

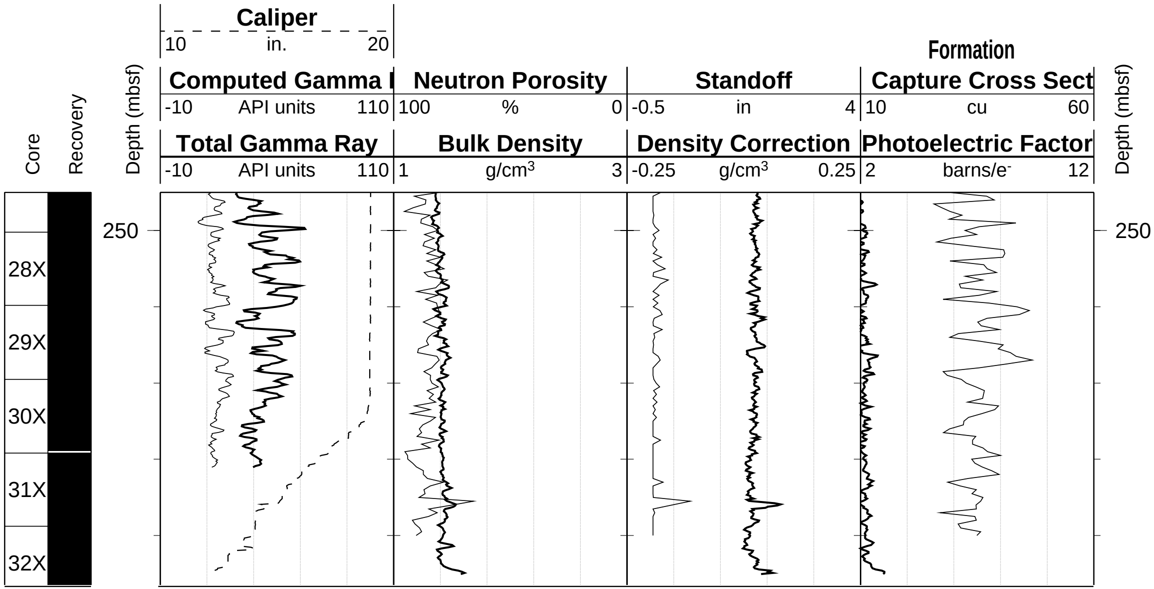

Hole 1016A: Natural Gamma Ray-Resistivity-Sonic Logging Data-Pass 1

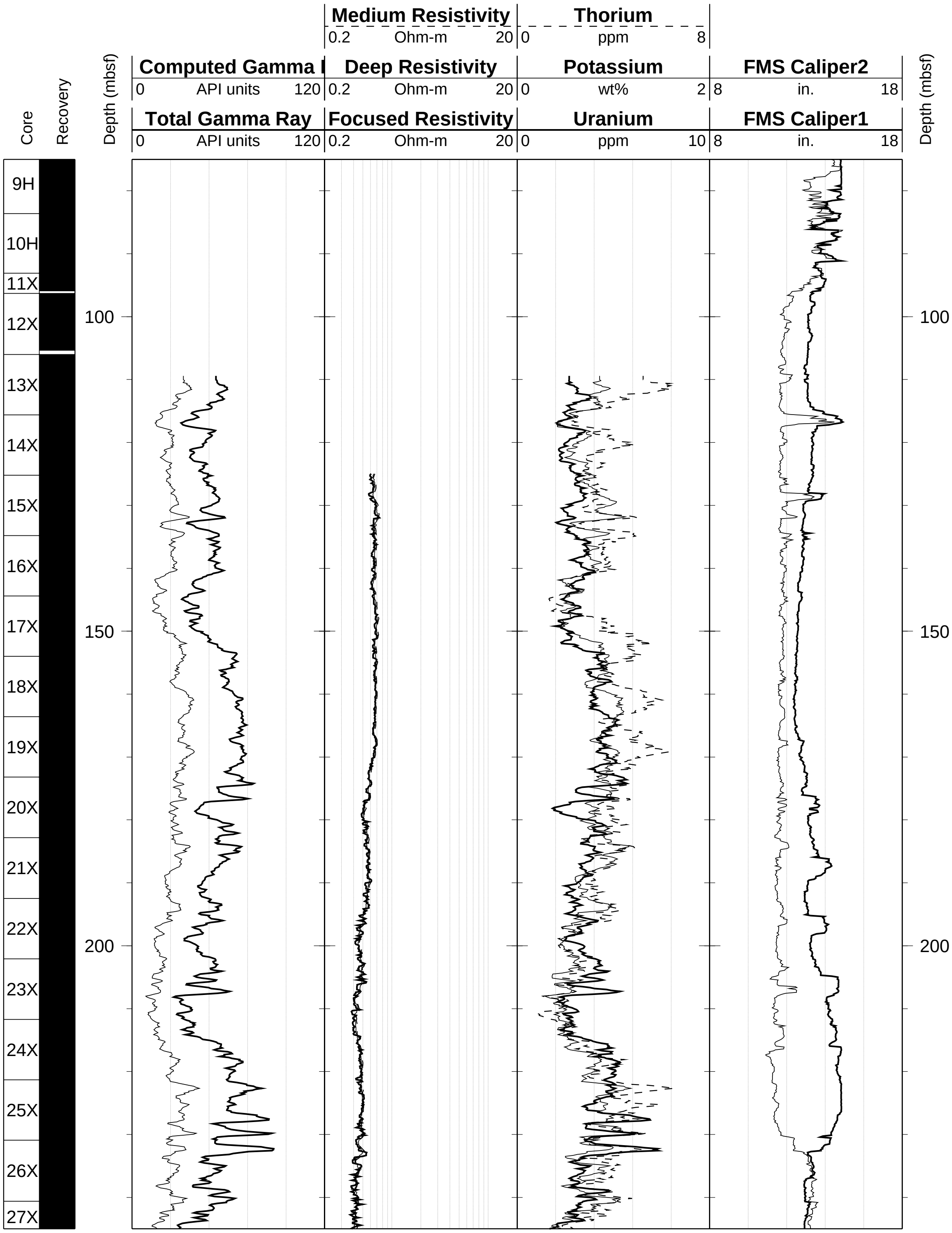

Hole 1016A: Natural Gamma Ray-Resistivity-Sonic Logging Data-Pass 1 (cont.)

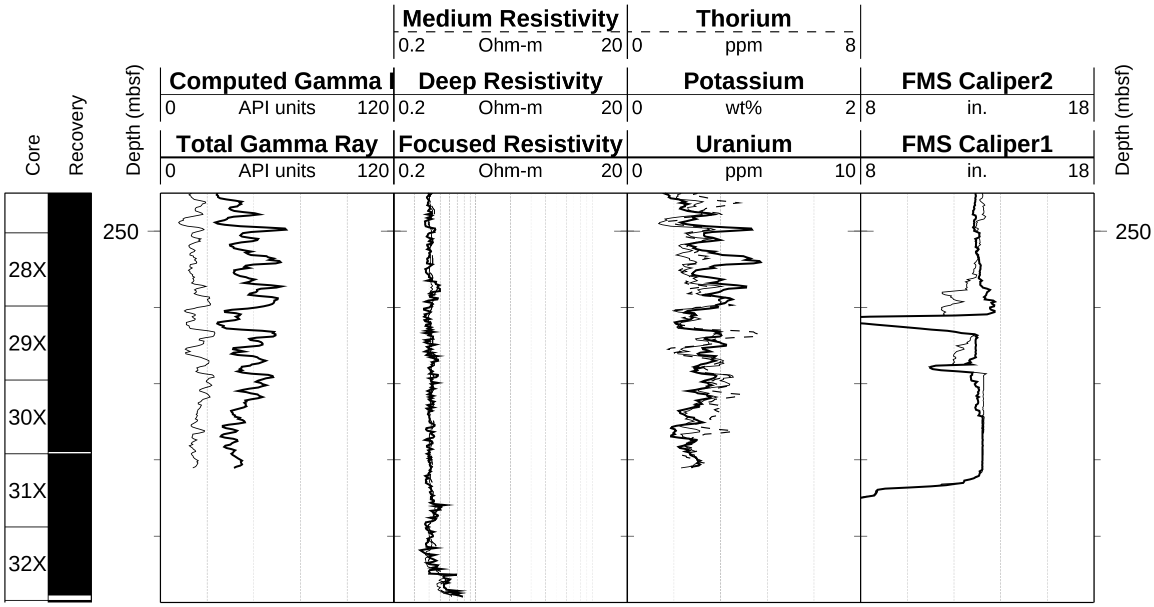

Hole 1016A: Natural Gamma Ray-Density-Porosity Logging Data-Pass 3

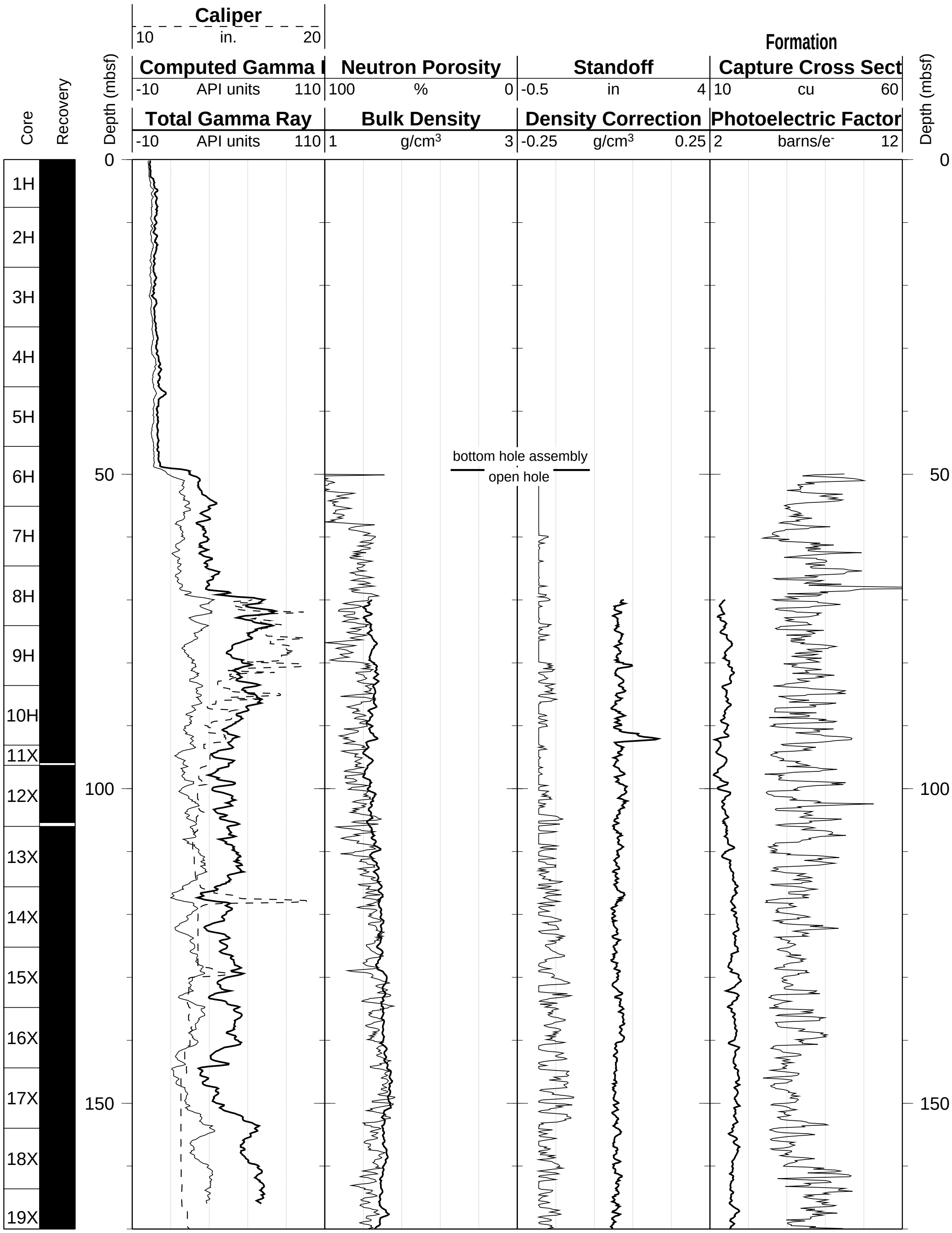

Hole 1016A: Natural Gamma Ray-Density-Porosity Logging Data-Pass 3 (cont.)

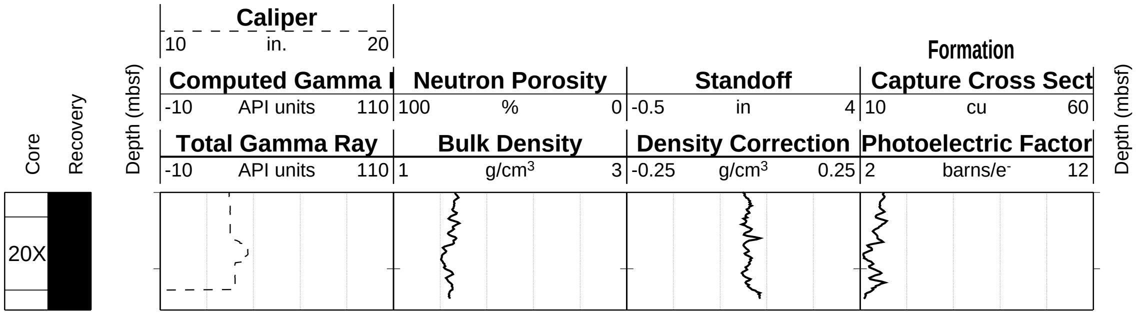

Hole 1016A: Natural Gamma Ray-Resistivity-Sonic Logging Data-Pass 3

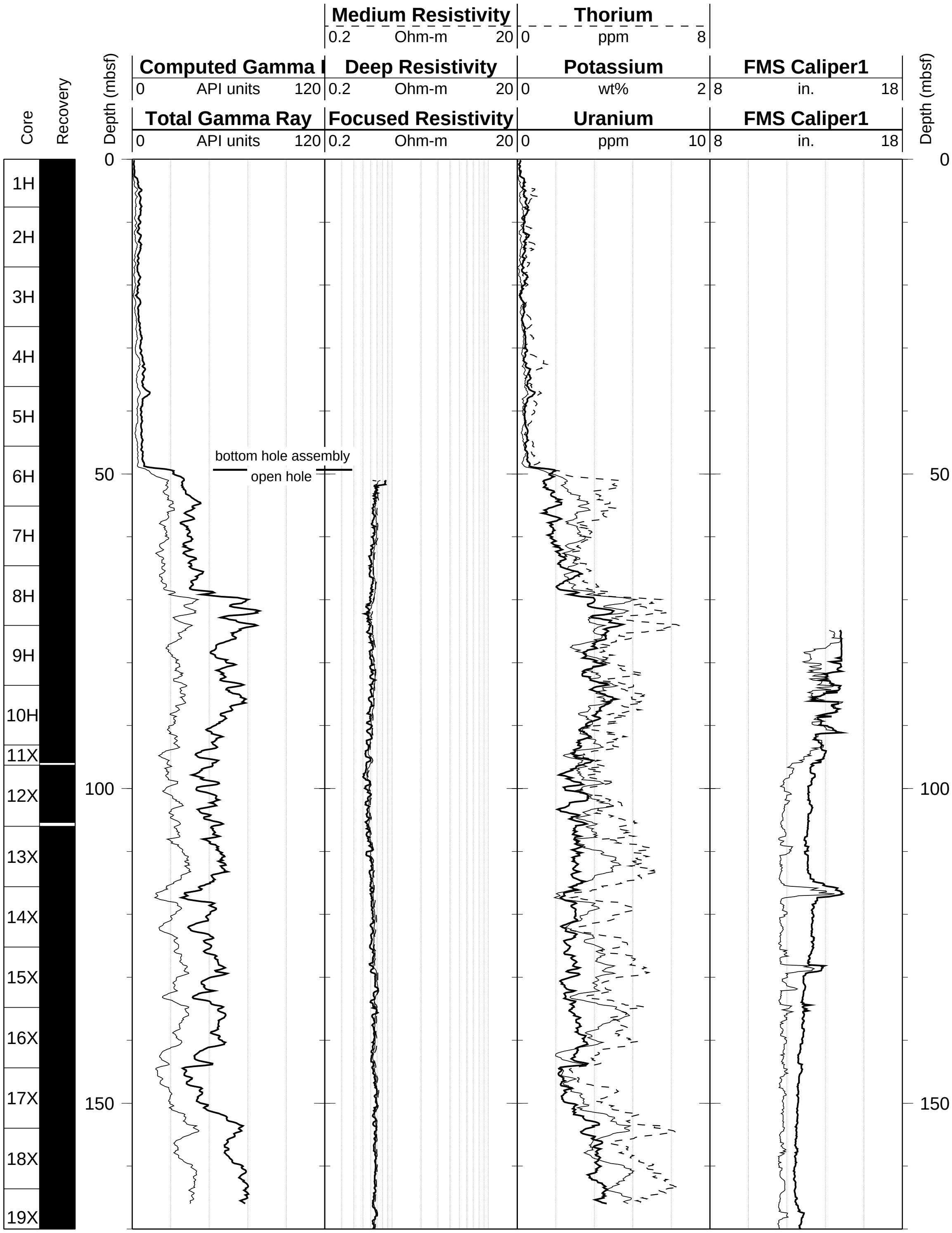

Hole 1016A: Natural Gamma Ray-Resistivity-Sonic Logging Data-Pass 3 (cont.)